Dissertation
submitted to the
Combined Faculty of Natural Sciences and Mathematics
of Heidelberg University, Germany
for the degree of
Doctor of Natural Sciences

Put forward by

Igor A. Valuev

born in Yekaterinburg, Russian Federation

Oral examination: November 23rd, 2022

Microscopic theory of nuclear-structure effects in atomic systems

Referees: PD Dr. Natalia S. Oreshkina
Prof. Dr. Maurits W. Haverkort

Zusammenfassung

In dieser Arbeit werden Kernstruktur-Effekte in atomaren Systemen aus mikroskopischer Sicht untersucht. Zu diesem Zweck wird eine detaillierte Beschreibung der Kerndynamik in die Berechnung der Kerngrößen- und Kernpolarisations-Korrekturen zu atomaren Energieniveaus und zum g-Faktor des gebundenen Elektrons integriert. Die Berechnungen werden für hochgeladene, wasserstoffartige Ionen und myonische Atome durchgeführt. Die Hartree-Fock Methode wird verwendet um die Ladungsverteilung des Kerngrundzustandes zu berechnen und die vollständigen Anregungsspektren werden mithilfe der Random-Phase-Approximation erhalten. Interaktionen zwischen Nukleonen werden durch eine effektive Skyrme Kraft beschrieben. Der Einfluss nuklearer Anregungen auf die Eigenschaften des Atoms werden Feld-Theoretisch behandelt und das vollständige Dirac-Spektrum des gebundenen Elektrons oder Myons wird durch Methoden der endlichen Basissätze einbezogen. Besonderer Fokus wird auf der Analyse der Abhängigkeit der Ergebnisse von dem gewählten Kernmodell liegen. Die Fehler der Berechnungen werden abgeschätzt und Unterdrückung der Kernstruktur-Effekte in verschiedenen gewichteten Differenzen wird diskutiert. Zuletzt werden die entwickelten Methoden auf das seit langem bestehende Problem der Feinstrukturanomalien in schweren myonischen Atomen angewandt.

Abstract

In this thesis, nuclear-structure effects in atomic systems are investigated from the microscopic point of view. To this end, a detailed description of nuclear dynamics is incorporated into calculations of the finite-nuclear-size and nuclear-polarization corrections to atomic energy levels and the bound-electron g factor. Hydrogen-like highly charged ions as well as muonic atoms are considered. Nuclear ground-state charge distributions are obtained within the Hartree-Fock method, while complete nuclear excitation spectra are computed by means of the random-phase approximation. The interaction between nucleons is modelled by the effective Skyrme force. The effects of nuclear excitations on atomic properties are described in a field-theoretical framework, where the full Dirac spectrum of a bound electron or muon is taken into account with the help of finite basis-set methods. Special attention is given to analyzing the nuclear model dependence, and the uncertainties of the calculations are estimated. In addition, the suppression of nuclear-structure effects in various weighted differences is discussed. Finally, the developed methods and computational codes are applied to the long-standing problem of the fine-structure anomalies in heavy muonic atoms.

In the course of this thesis, the following articles have been published in peer-reviewed journals:

- Igor A. Valuev, Zoltán Harman, Christoph H. Keitel, and Natalia S. Oreshkina
  Skyrme-type nuclear interaction as a tool for calculating the finite-nuclear-size correction to atomic energy levels and the bound-electron g factor
  Phys. Rev. A **101**, 062502 (2020) (Ref. [1])
- Igor A. Valuev, Gianluca Colò, Xavier Roca-Maza, Christoph H. Keitel, and Natalia S. Oreshkina
  Evidence Against Nuclear Polarization as Source of Fine-Structure Anomalies in Muonic Atoms
  Phys. Rev. Lett. **128**, 203001 (2022) (Ref. [2])
- A. Schneider, B. Sikora, S. Dickopf, M. Müller, N. S. Oreshkina, A. Rischka, I. A. Valuev, S. Ulmer, J. Walz, Z. Harman, C. H. Keitel, A. Mooser, and K. Blaum
  Direct measurement of the $^3He^+$ magnetic moments
  Nature, **606**, 878–883 (2022) (Ref. [3])

The following articles have been submitted to peer-reviewed journals:

- H. Cakir, N. S. Oreshkina, I. A. Valuev, V. Debierre, V. A. Yerokhin, C. H. Keitel, and Z. Harman
  Improved access to the fine-structure constant with the simplest atomic systems
  arXiv:2006.14261 (Ref. [4])
- V. Debierre, N. S. Oreshkina, I. A. Valuev, Z. Harman, and C. H. Keitel
  Testing Standard Model extensions with few-electron ions
  arXiv:2207.04868 (Ref. [5])

Contents

Introduction **1**
Highly charged ions . . . 2
Muonic atoms . . . 3
Outline of the thesis . . . 5
Units and notation . . . 6

1. Relativistic theory of atomic systems **7**
1.1. QED in the Furry picture . . . 7
1.2. Two-time Green's function . . . 10
1.3. Dirac equation in central potentials . . . 13
1.3.1. Separation of variables . . . 13
1.3.2. Numerical solution with B-spline basis sets . . . 16
1.4. Bound-electron g factor . . . 18

2. Microscopic description of nuclear structure **21**
2.1. Skyrme-Hartree-Fock mean field . . . 21
2.2. Random-phase approximation . . . 24

3. Finite-nuclear-size effect **27**
3.1. Nuclear charge distributions . . . 27
3.2. Choice of Skyrme parametrization . . . 29
3.3. Atomic energy levels and nuclear radii . . . 31
3.4. g factor and specific differences . . . 33

4. Nuclear-polarization effect **37**
4.1. Atomic energy levels . . . 37
4.1.1. Modified photon propagator . . . 37
4.1.2. Effective self-energy . . . 40
4.1.3. Feynman gauge . . . 45
4.1.4. Longitudinal approximation . . . 50
4.2. Muonic fine-structure anomalies . . . 55
4.3. g factor of hydrogenlike ions . . . 62
4.4. Reduced g factor . . . 68

Summary and Outlook **73**

A. Atomic reduced matrix elements **77**

B. Nuclear reduced matrix elements **79**

C. Nuclear polarization in the Coulomb gauge **83**

Bibliography **85**

Acknowledgments **95**

Introduction

At first glance, the role of a nucleus in an atomic system should be very simple. Being several orders of magnitude smaller than the typical size of atomic orbitals and comprising most of the atom's mass, a nucleus can be considered to a very good level of approximation as a point-like and infinitely heavy source of a classical electromagnetic field. While this still holds true for some applications, such a simplified view quickly becomes no longer adequate in high-precision atomic experiments. In fact, as early as in 1931, the measurements by Schüler and Keyston [6] on the hyperfine structure of the thallium isotopes ^{203}Tl and ^{205}Tl revealed variations between the two spectra, which the authors hypothesized to be caused by some differences in the nuclear fields of the isotopes. Ever since, the experimental precision has been continuously pushed forward, which in turn requires an increasingly more detailed description of nuclear structure in the context of atomic properties.

In addition to the advancements at the high-precision frontier, there is another way by which nuclear-structure effects can become more pronounced. It can be easily seen by considering the well-known formula for the Bohr radius for a single fermion of mass m_f bound to a point-like nucleus with a charge number Z (see, for instance, Ref. [7]):

$$r_\mathrm{B} = \frac{\hbar}{m_\mathrm{f} c_0 Z \alpha} \,,$$

where $\hbar$ is the Planck's constant, α is the fine-structure constant, and c_0 is the speed of light in vacuum. Thus, the larger the values of Z and m_f, the higher the overlap between the fermionic and nuclear wave functions, resulting in a higher sensitivity to the actual nuclear structure. The first option is realized in experiments on highly charged ions (HCIs), while the second possibility is found in exotic atomic systems, such as muonic atoms for which $m_\mu \approx 207 m_\mathrm{e}$ [8]. In the following sections, we briefly get acquainted with these two types of systems, as both of them will be of interest in this thesis.

Highly charged ions

Stripping all but a few electrons from heavy elements leads to one of the simplest and, at the same time, one of the most profound physical systems. HCIs provide an extremely rich scope of opportunities for fundamental research, ranging from stringent tests of quantum electrodynamics (QED) [9] to interpretation of astrophysical spectra [10]. A prominent characteristic of HCIs is that their bound electrons are subjected to the strongest electromagnetic fields currently accessible to experimental investigation. For instance, the electric field strength experienced by the $1s$ electron in the heaviest HCIs, such as H-like lead or uranium, amounts to around $10^{16}\ \mathrm{V\,cm^{-1}}$ [11], which is hardly achievable by any other means in laboratory environments. Together with high-precision measurement techniques, this makes HCIs the most suitable objects to probe the validity of QED in such extreme regimes. For example, combined experimental [12] and theoretical [13, 14] studies of the $1s$ Lamb shift in $^{238}U^{91+}$ confirmed QED predictions at the level of 2% in truly staggering conditions, where the rest mass of the electron is only four times larger than its binding energy to the nucleus. Remarkably, out of the total Lamb shift of around 460 eV, the finite-nuclear-size contribution amounts to almost 200 eV in this case.

In a similar spirit, nuclei with non-zero spin enable tests of QED in extreme magnetic fields, reaching up to 30 000 T for the $1s$ electron in $^{209}Bi^{82+}$, which is three orders of magnitude larger than the field produced by the strongest superconducting magnet [9]. In addition, because of the narrow width of the transitions between the resulting ground-state hyperfine sublevels in H-like ions, it has been proposed to use them for atomic clocks, which would be sensitive to hypothetical drifts of fundamental constants [15]. Despite the significant progress in both experimental measurements and theoretical understanding of the hyperfine structure, a high-precision description of such systems is still considerably limited by the uncertainties in nuclear-structure effects, in particular the nuclear magnetization distribution correction [16]. In order to circumvent this problem and suppress the nuclear effects, a weighted difference of the ground-state hyperfine splittings in Li- and H-like ions was introduced [17]. However, even with this approach, we are still quite far from truly precise tests of QED with the hyperfine structure.

In contrast, the most extraordinary level of precision for HCIs was achieved in the studies of the bound-electron g factor, a dimensionless quantity that characterizes the strength of the interaction between a bound electron and an external magnetic field. State-of-the-art Penning-trap measurements of the g factor together with comparably precise theoretical calculations represent to date the most stringent tests of bound-state QED. The g factor has been measured and calculated for H-like $^{12}C^{5+}$ [18, 19], $^{16}O^{7+}$ [20] and $^{28}Si^{13+}$ [21, 22] as well as for Li-like $^{28}Si^{11+}$ [23] and $^{40,48}Ca^{17+}$ [24] with relative uncertainties on the scale of 10^{-9} to 10^{-11}. Recently, a

similar level of experimental precision has been achieved for the first time for B-like $^{40}Ar^{13+}$ at the newly commissioned ALPHATRAP double Penning-trap setup at the Max Planck Institute for Nuclear Physics in Heidelberg, Germany [25]. This experiment also aims at measuring the bound-electron g factor in the high-Z regime, up to H-like $^{208}Pb^{81+}$, on the level of 10^{-11} or better [26]. Beyond probing bound-state QED, such a high precision can also be employed for measuring fundamental physical constants. A prominent example is the improvement of the 2010 CODATA value of the electron's mass by a factor of 13, which was enabled by the g-factor measurement in H-like $^{12}C^{5+}$ and the correspondingly precise theoretical calculation [19]. Another promising application of such studies in the high-Z regime would be determination of the fine-structure constant [4, 27, 28] or even search of its hypothetical variation [29–33]. Moreover, comparison between the experimental and theoretical results can also be used to test theories beyond the Standard Model by setting bounds on parameters of hypothetical new forces [5, 34].

As the experimental precision is being advanced even further, all the aforementioned applications are becoming more and more limited from the theoretical side by the ability to accurately calculate nuclear-structure effects. Even though various weighted differences have been introduced to cancel out nuclear contributions and thus alleviate this difficulty [4, 17, 27, 35], an improved understanding of nuclear structure is still desirable even in those approaches in order to reliably determine the degree of such a cancellation.

Muonic atoms

According to the principle of lepton universality, the only fundamental difference between the electron and its second-generation cousin, the muon, is their mass, namely $m_\mu \approx 207 m_\mathrm{e}$ [8]. This property, however, immediately leads to one more difference, i.e., the fact that the muon is unstable and decays via the weak interaction into an electron and two neutrinos in about 2.2 μs [36]:

$$\mu^- \to e^- + \bar{\nu}_e + \nu_\mu \,.$$

Nevertheless, this timescale turns out to be long enough for the muon to form bound states with nuclei, resulting in exotic atomic systems [37]. To produce such atoms, a muon beam is directed onto a target material, where the muons undergo kinetic-energy losses by their interactions with outer atomic electrons until being captured into high atomic orbits. Then a given muon cascades through the electron cloud all the way down to the ground state, emitting electromagnetic radiation in the X-ray range. The capture and cascade processes take place in a time frame of around $10^{-12} - 10^{-9}$ s, which is several orders of magnitude shorter than the average

lifetime of the muon. This holds true even in the case of heavy nuclei, where the overlap between the muonic and nuclear wave functions is so large that the nuclear-capture channel becomes dominant, thereby reducing the muonic lifetime to about 10^{-7} s [38, 39]:

$$\mu^- + p \rightarrow n + \nu_\mu \,.$$

Due to their extremely close proximity to the nucleus, muonic orbitals are highly sensitive to the nuclear structure. Indeed, in the case of high-Z elements, the muon in its ground state even spends most of its time inside the nucleus. This makes the muon an excellent probe to study essential nuclear properties, such as charge radii [40] or quadrupole moments [41, 42]. In fact, the earliest application of the muonic spectroscopy in 1953 constituted the first accurate measurement of nuclear size [43]. Since then, charge radii of the majority of stable nuclei have been obtained by this method [40]. An experiment of this kind that received particular attention in the last decade involved a measurement of the charge radius of the proton [44]. The resulting disagreement of 7 standard deviations between the values obtained by muonic and electronic probes became known as the *proton radius puzzle* [45]. More recent experimental results based on electronic hydrogen [46] as well as a reanalysis of the older data [47] support the new muonic value, suggesting that the proton might actually be about 5% smaller than it was believed in the 1990s and 2000s.

There has been another tantalizing puzzle in the realm of muonic atoms, which has persisted for more than 40 years and is still unresolved. Initially, it came from very poor fits of theoretical muonic transition energies to experimental data in an attempt to extract the charge radius of the ^{208}Pb nucleus [48, 49]. The main source of the discrepancies was identified to lie in the $\Delta 2p$ and $\Delta 3p$ fine-structure splittings, and anomalies of the same kind were later found also for the $\Delta 2p$ splittings in the case of ^{90}Zr [50] and a number of isotopes of Sn [51]. The anomalies were assumed to be rooted in the theoretical predictions of the so-called nuclear-polarization correction, which accounts for the dynamic interplay between muonic and nuclear degrees of freedom. The reason for such a choice of the main suspect is that nuclear polarization is by far the most uncertain and challenging effect to evaluate, as it requires detailed knowledge of the entire nuclear excitation spectrum. Thus, this example alone leaves no doubt that there is still a strong need for an improved understanding of nuclear-structure effects in muonic atoms.

It is also worth mentioning that in recent years there has been a revival of the muonic X-ray spectroscopy in the high-Z regime. The MuX collaboration at the Paul Scherrer Institute (Switzerland) has developed a technique to examine materials that are available only in microgram quantities. This enabled the first measurements with the radioactive targets ^{248}Cm and ^{226}Ra in 2019, with the analysis of the data currently ongoing [39].

Outline of the thesis

The aim of this thesis is to bring together state-of-the-art techniques from both atomic and nuclear physics by incorporating a detailed microscopic nuclear description into high-precision atomic calculations. Apart from providing a more accurate account of nuclear-structure effects in atomic systems, such a first-principles approach is also expected to give a better sense of the current limitations in the field.

The thesis is organized as follows. First, the basic ingredients for the combined calculations are presented in Chapters 1 and 2. Chapter 1 contains an overview of the necessary tools from relativistic atomic theory. After introducing the basics of bound-state QED in the Furry picture, the two-time Green's function formalism [52] for perturbative evaluation of atomic energy shifts is outlined. The Dirac equation in central potentials is discussed next, including the numerical techniques based on B-spline basis sets and the dual-kinetic-balance approach [53]. The chapter is concluded by a brief introduction of the bound-electron g factor. Chapter 2, on the other hand, describes computational methods from the nuclear physics side. It begins by introducing the effective Skyrme force, which is used in this work to model nucleon-nucleon interactions. A short discussion on the Hartree-Fock mean field immediately follows, providing a description of the nuclear ground state. Next, in order to demonstrate how to go beyond ground-state properties and compute a nuclear excitation spectrum, the random-phase approximation is briefly presented before concluding the chapter.

In Chapter 3, the nuclear ground-state charge distributions obtained from the Skyrme-Hartree-Fock procedure are used to calculate the finite-nuclear-size correction to atomic energy levels and the bound-electron g factor. The uncertainties and the limitations of the calculations are also discussed. The experience gained in Chapter 3 serves rather as a stepping stone to computations of the more challenging nuclear-polarization effect, which is the subject of Chapter 4. There, detailed derivations of the NP formalism within the field-theoretical framework are presented. This method is then applied to the long-standing problem of the fine-structure anomalies in muonic atoms, where special attention is given to the analysis of the dominant nuclear model uncertainty. Next, the formalism is further extended to evaluate the NP correction to the bound-electron g factor. Both Chapter 3 and Chapter 4 end with a discussion on the suppression of the corresponding nuclear-structure effects in various weighted differences involving the g factor. Finally, the main findings of the thesis are briefly summarized, and the outlook is given.

Units and notation

The relativistic unit system is used throughout the thesis such that

$$\hbar = c_0 = 1.$$

Furthermore, the Lorentz-Heaviside units of electromagnetism are employed, where the vacuum permittivity ε_0 and the vacuum permeability μ_0 are set to unity:

$$\varepsilon_0 = \mu_0 = 1.$$

In these units, the expression for the fine-structure constant is given by

$$\alpha = \frac{e^2}{4\pi},$$

where e is the elementary electric charge, which is denoted as $|e|$ throughout the thesis in order to avoid any confusion regarding its sign.

Four-vectors (x) and their components (x^μ) are represented by regular typeface, with four-tensor indices denoted by Greek letters running from 0 to 3. Bold upright letters are used for three-vectors ($\mathbf{x}$), whose lengths are denoted by non-bold upright letters ($|\mathbf{x}| \coloneqq \mathrm{x}$). Upper indices of three-vector components are displayed in italics to avoid confusion with exponentiation, i.e., $\mathbf{x} = (x^{\mathit{1}}, x^{\mathit{2}}, x^{\mathit{3}})$.

The signature of the metric tensor $\eta_{\mu\nu}$ is $(+---)$, and the Einstein summation convention is employed such that repeated indices are automatically summed over.

For the sake of simplicity, Fourier-transformed functions are denoted by the same letters as the original ones, and the distinction between different versions is made by explicitly indicating their functional dependence.

The Dirac representation of the gamma matrices is used:

$$\gamma^0 = \begin{pmatrix} \mathbb{1}_2 & 0 \\ 0 & -\mathbb{1}_2 \end{pmatrix}, \quad \gamma^i = \begin{pmatrix} 0 & \sigma^i \\ -\sigma^i & 0 \end{pmatrix}, \; i = 1, 2, 3,$$

where $\mathbb{1}_2$ is the 2×2 unit matrix, and σ^i are the Pauli matrices:

$$\sigma^{\mathit{1}} = \begin{pmatrix} 0 & 1 \\ 1 & 0 \end{pmatrix}, \quad \sigma^{\mathit{2}} = \begin{pmatrix} 0 & -i \\ i & 0 \end{pmatrix}, \quad \sigma^{\mathit{3}} = \begin{pmatrix} 1 & 0 \\ 0 & -1 \end{pmatrix},$$

The Dirac adjoint for a Dirac spinor ψ is defined in the usual way as $\bar{\psi} \coloneqq \psi^\dagger \gamma^0$.

1. Relativistic theory of atomic systems

The first relativistic description of a free electron was obtained in 1928 by Paul Dirac in an attempt to bring together quantum mechanics and the special theory of relativity [54]. His famous result was a first-order, Lorentz-covariant generalization of the Schrödinger equation:

$$(i\gamma^\mu \partial_\mu - m_\mathrm{e})\,\psi(x) = 0, \tag{1.1}$$

where m_e is the electron mass, and γ^μ denotes a set of the 4×4 Dirac matrices satisfying the anti-commutation relations $\{\gamma^\mu, \gamma^\nu\} = 2\eta^{\mu\nu}\mathbb{1}_4$, which also makes the electron wave function $\psi(x)$ a four-component spinor. Although Eq. (1.1) was originally formulated for a single electron, one soon realizes that single-particle quantum mechanics leads to catastrophic inconsistencies when faced with special relativity. For instance, one even obtains a non-zero probability of finding a particle outside of its forward light cone [55]! With energies high enough for phenomena like pair production, relativistic quantum mechanics has to be a many-body theory, almost by definition. Therefore, Eq. (1.1) must be rather understood as an equation for an *operator-valued field* $\hat{\psi}(x)$. To make matters even more complicated, the electromagnetic field $\hat{A}^\mu(x)$ also has to be brought into play, if one wishes to go beyond free particles and describe interactions. The corresponding interacting field theory is known as quantum electrodynamics (QED), and, to this day, it is the most successful physical theory in terms of agreement with experiments [56–60]. In the following section, we start with a brief overview of QED in the context of atomic systems.

1.1. QED in the Furry picture

Before considering the interaction between electrons and an atomic nucleus, we first recall the standard Lagrangian formulation of QED, which can be found in numerous textbooks, for example, in Refs. [61, 62]. The Lagrangian density for the free Dirac field corresponding to Eq. (1.1) can be written as

$$\mathcal{L}_\mathrm{D}^\mathrm{free} = \bar{\hat{\psi}}\,(i\gamma^\mu \partial_\mu - m_\mathrm{e})\,\hat{\psi}, \tag{1.2}$$

whereas the expression for the free electromagnetic field takes the following form:

$$\mathcal{L}_\mathrm{EM}^\mathrm{free} = -\frac{1}{4}\hat{F}_{\mu\nu}\hat{F}^{\mu\nu} - \frac{1}{2\xi}\left(\partial_\sigma \hat{A}^\sigma\right)^2, \tag{1.3}$$

where $\hat{F}^{\mu\nu}(x) = \partial^\mu \hat{A}^\nu(x) - \partial^\nu \hat{A}^\mu(x)$, and the second part is the gauge-fixing term corresponding to the Lorenz condition. The value of the parameter ξ determines the gauge choice. This extra term is essential for enabling canonical quantization of the photon field, and the free equation of motion for the four-potential $\hat{A}^\mu(x)$ reads

$$\partial^2 \hat{A}^\mu(x) - \left(1 - \frac{1}{\xi}\right) \partial^\mu \left(\partial_\sigma \hat{A}^\sigma(x)\right) = 0. \tag{1.4}$$

The interaction between the two fields is described by

$$\mathcal{L}_{\text{int}} = |e| \bar{\hat{\psi}} \gamma^\mu \hat{\psi} \hat{A}_\mu. \tag{1.5}$$

It should be noted that, for the sake of simplicity, the complicated issue of renormalization will be omitted in this brief overview. Therefore, solely on a formal level, no distinction between bare and physical quantities m_e and e will be made.

The Lagrangian density from Eq. (1.5) together with the standard machinery of Wick's theorem and Feynman diagrams can be used for perturbative calculations of various QED processes. However, such an approach breaks down in an attempt to describe bound states, for instance, in something as simple as the hydrogen atom. As demonstrated in Ref. [63], the existence of the hydrogen ground state implies the presence of a pole in the electron-proton scattering amplitude at around $E = m_\text{e} + m_\text{p} - 13.6\,\text{eV}$, where E is the center-of-mass energy. Since no term in the perturbation series has such a pole, it can only arise in the full sum over all the diagrams, thus necessitating a non-perturbative treatment for this class of problems. This is achieved in the following way. First, it can be shown that the interaction between electrons (or muons) and a heavy charged particle (i.e., an atomic nucleus) can be taken into account by simply introducing an additional term in the QED Lagrangian given by [63]

$$\mathcal{L}_{\text{ext}} = |e| \bar{\hat{\psi}} \gamma^\mu \hat{\psi} \mathcal{A}_\mu, \tag{1.6}$$

with $\mathcal{A}^\mu(x)$ being a classical electromagnetic four-potential generated by the nucleus. In this approach, known as the external-field approximation, the total Lagrangian can then be written in the form

$$\mathcal{L}_{\text{QED+ext}} = -\frac{1}{4} \hat{F}_{\mu\nu} \hat{F}^{\mu\nu} - \frac{1}{2\xi} \left(\partial_\sigma \hat{A}^\sigma\right)^2 + \bar{\hat{\psi}} \left(i\gamma^\mu \partial_\mu - m_\text{e} + |e| \gamma^\mu \mathcal{A}_\mu\right) \hat{\psi} + |e| \bar{\hat{\psi}} \gamma^\mu \hat{\psi} \hat{A}_\mu, \tag{1.7}$$

where the new term from Eq. (1.6) is now embedded into the Dirac part of the Lagrangian

$$\mathcal{L}_\text{D}^\text{ext} = \bar{\hat{\psi}} \left(i\gamma^\mu \partial_\mu - m_\text{e} + |e| \gamma^\mu \mathcal{A}_\mu\right) \hat{\psi}. \tag{1.8}$$

Thus, neglecting in the zeroth-order approximation the interaction with the second-quantized field $\hat{A}^\mu(x)$, one takes as the starting point the Dirac field satisfying the following equation of motion:

$$[i\gamma^\mu\partial_\mu - m_\mathrm{e} + |e|\gamma^\mu\mathcal{A}_\mu(x)]\,\hat{\psi}(x) = 0. \tag{1.9}$$

In the case of a static external field $\mathcal{A}^\mu(\mathbf{x})$, it can be taken into account non-perturbatively by means of the following expansion (using the discrete notation for simplicity) [64]:

$$\hat{\psi}(x) = \sum_n^{\varepsilon_n>0} \hat{a}_n\psi_n(\mathbf{x})e^{-i\varepsilon_n t} + \sum_n^{\varepsilon_n<0} \hat{b}_n^\dagger\psi_n(\mathbf{x})e^{-i\varepsilon_n t}, \tag{1.10}$$

with $\psi_n(\mathbf{x})$ and ε_n being the complete sets of the eigenstates and the eigenvalues of the stationary ("single-particle") Dirac equation, respectively:

$$\Big\{\boldsymbol{\alpha}\cdot[-i\nabla + |e|\boldsymbol{\mathcal{A}}(\mathbf{x})] + \beta m_\mathrm{e} - |e|\mathcal{A}_0(\mathbf{x})\Big\}\psi_n(\mathbf{x}) = \varepsilon_n\psi_n(\mathbf{x}), \tag{1.11}$$

where the $\boldsymbol{\alpha}$ and β Dirac matrices are related to the γ^μ ones as $\beta = \gamma^0$ and $\alpha^i = \gamma^0\gamma^i$ ($i = 1, 2, 3$). The index n collectively denotes all quantum numbers necessary to characterize the eigenstates, while $\hat{a}_n^\dagger$ ($\hat{a}_n$) and $\hat{b}_n^\dagger$ ($\hat{b}_n$) in Eq. (1.10) are the creation (annihilation) operators for electrons and positrons in such states, respectively. The non-vanishing anti-commutation relations for these operators are

$$\left\{\hat{a}_n, \hat{a}_{n'}^\dagger\right\} = \left\{\hat{b}_n, \hat{b}_{n'}^\dagger\right\} = \delta_{nn'}. \tag{1.12}$$

The representation in Eq. (1.10) is referred to as the Furry picture of QED [65], which is in a certain sense intermediate between the Heisenberg and interaction representations. It is worth noting that for the electromagnetic operator $\hat{A}^\mu(x)$ the Furry and interaction pictures coincide.

In terms of practical calculations, the main consequence of passing to the Furry picture is the modification of the electron propagator, which is defined as

$$S(x_1, x_2) \coloneqq -i\left\langle 0\middle|\, T\left[\hat{\psi}(x_1)\bar{\hat{\psi}}(x_2)\right]\middle|\, 0\right\rangle, \tag{1.13}$$

where T denotes the time-ordering prescription, and $|0\rangle$ is the "vacuum" state in the presence of the external field $\mathcal{A}^\mu(\mathbf{x})$. Using the expansion from Eq. (1.10), anti-commutation relations from Eq. (1.12) as well as the integral representation of the Heaviside step function, one readily obtains the so-called dressed electron propagator

$$S(x_1, x_2) = \int_{-\infty}^{+\infty}\frac{d\omega}{2\pi}\sum_n \frac{\psi_n(\mathbf{x}_1)\bar{\psi}_n(\mathbf{x}_2)}{\omega - \varepsilon_n(1 - i0^+)}\,e^{-i\omega(x_1^0 - x_2^0)}, \tag{1.14}$$

or, due to the homogeneity in time, its Fourier-transformed version

$$S(\omega, \mathbf{x}_1, \mathbf{x}_2) = \sum_n \frac{\psi_n(\mathbf{x}_1)\bar{\psi}_n(\mathbf{x}_2)}{\omega - \varepsilon_n(1 - i0^+)}. \tag{1.15}$$

It can be immediately seen that, contrary to the free electron propagator

$$S_0(x_1, x_2) = \int \frac{d^4p}{(2\pi)^4} \frac{\gamma^\mu p_\mu + m_\mathrm{e}}{p^2 - m_\mathrm{e}^2 + i0^+} \, e^{-ip\cdot(x_1 - x_2)}, \tag{1.16}$$

the expression in Eq. (1.14) has poles corresponding to the unperturbed electronic bound states obtained from Eq. (1.11). With the dressed electron propagator at our disposal, we are now in a position to take into account the interaction term from Eq. (1.5) and calculate radiative corrections to these zeroth-order states.

1.2. Two-time Green's function

In this section, we summarize the main results of the formalism presented in Ref. [52]. First, we recall that, due to the LSZ reduction theorem [62, 66], the complete information about an atomic system of N electrons is contained in the $2N$-point Green's (correlation) function given by

$$G(x_1', \ldots, x_N'; x_1, \ldots, x_N) = \left\langle 0 \middle| T\left[\hat{\psi}_\mathrm{H}(x_1') \cdots \hat{\psi}_\mathrm{H}(x_N')\bar{\hat{\psi}}_\mathrm{H}(x_N) \cdots \bar{\hat{\psi}}_\mathrm{H}(x_1)\right] \middle| 0 \right\rangle, \tag{1.17}$$

with the field operators being in the Heisenberg representation. On the one hand, the function G can be evaluated pertubatively by expressing it in terms of the asymptotic in-fields (in the Furry picture) as

$$\begin{aligned} &G(x_1', \ldots, x_N'; x_1, \ldots, x_N) \qquad (1.18)\\ &= \frac{\left\langle 0 \middle| T\left[\hat{\psi}_\mathrm{in}(x_1') \cdots \hat{\psi}_\mathrm{in}(x_N')\bar{\hat{\psi}}_\mathrm{in}(x_N) \cdots \bar{\hat{\psi}}_\mathrm{in}(x_1) \exp\left\{-i\int d^4z\, \mathcal{H}_\mathrm{int}(z)\right\}\right] \middle| 0 \right\rangle}{\left\langle 0 \middle| T\exp\left\{-i\int d^4z\, \mathcal{H}_\mathrm{int}(z)\right\} \middle| 0 \right\rangle} \end{aligned}$$

and then expanding the exponents (where $\mathcal{H}_\mathrm{int} = -\mathcal{L}_\mathrm{int}$) and applying Wick's theorem at each order of the expansion.

On the other hand, it turns out that the two-time Green's function defined as

$$\widetilde{G}(t', \mathbf{x}_1', \ldots, \mathbf{x}_N'; t, \mathbf{x}_1, \ldots, \mathbf{x}_N) \coloneqq G((t', \mathbf{x}_1'), \ldots, (t', \mathbf{x}_N'); (t, \mathbf{x}_1), \ldots, (t, \mathbf{x}_N)) \tag{1.19}$$

also contains the complete information about the system's energy levels, which can be shown by considering its spectral representation. This fact allows for a much

simpler procedure to extract the energy levels from $\widetilde{G}$. For this purpose, another Green's function, denoted as $g_{ii}(E)$, is introduced for a given unperturbed atomic state $\Psi_i(\mathbf{x}_1, \ldots, \mathbf{x}_N)$:

$$\begin{aligned} g_{ii}(E)\delta(E-E') = \frac{2\pi}{i}\frac{1}{N!}\int dE_1 \ldots dE_N dE'_1 \ldots dE'_N \\ \times \delta(E - E_1 - \cdots - E_N)\delta(E' - E'_1 - \cdots - E'_N) \\ \times \langle i|G(E'_1, \ldots, E'_N; E_1, \ldots, E_N)\gamma_1^0 \ldots \gamma_N^0|i\rangle, \end{aligned} \tag{1.20}$$

where

$$\begin{aligned} &\langle i|G(E'_1, \ldots, E'_N; E_1, \ldots, E_N)\gamma_1^0 \ldots \gamma_N^0|i\rangle \\ &:= \int d^3x_1 \ldots d^3x_N d^3x'_1 \ldots d^3x'_N \, \Psi_i^\dagger(\mathbf{x}'_1, \ldots, \mathbf{x}'_N) \\ &\times G((E'_1, \mathbf{x}'_1), \ldots, (E'_N, \mathbf{x}'_N); (E_1, \mathbf{x}_1), \ldots, (E_N, \mathbf{x}_N))\gamma_1^0 \ldots \gamma_N^0 \Psi_i(\mathbf{x}_1, \ldots, \mathbf{x}_N), \end{aligned} \tag{1.21}$$

and the Green's function G has been Fourier-transformed with respect to the time variables. In the above expressions, a gamma matrix γ_k^0 acts on the kth particle. In the simplest case of only one bound electron, Eq. (1.20) reduces to

$$g_{ii}(E)\delta(E-E') = \frac{2\pi}{i}\langle i|G(E'; E)\gamma^0|i\rangle. \tag{1.22}$$

The unperturbed wave function $\Psi_i(\mathbf{x}_1, \ldots, \mathbf{x}_N)$ is in general a linear combination of Slater determinants, and the corresponding zeroth-order energy is the sum of the single-electron contributions: $E_i^{(0)} = \varepsilon_{i_1} + \cdots + \varepsilon_{i_N}$.

It can be shown that the spectral representation of the function $g_{ii}(E)$ yields

$$g_{ii}(E) = \frac{A_i}{E - E_i} + \text{ terms that are regular at } E \sim E_i, \tag{1.23}$$

where E_i is the energy level corresponding to the full interacting theory, and the explicit expression for the residue A_i, although known, will not be needed in what follows. Barring some (surmountable) subtleties with regard to isolating the pole at E_i, Eq. (1.23) provides a simple and systematic way of evaluating the energy shift $\Delta E_i = E_i - E_i^{(0)}$. Thus, by choosing a small contour Γ in the complex E-plane surrounding the pole at E_i but excluding all other singularities, we have

$$\frac{1}{2\pi i}\oint_\Gamma dE\, g_{ii}(E) = A_i, \tag{1.24}$$

$$\frac{1}{2\pi i}\oint_\Gamma dE\, E g_{ii}(E) = E_i A_i. \tag{1.25}$$

Then, after obtaining the zeroth-order approximation for the function $g_{ii}(E)$:

$$g_{ii}^{(0)}(E) = \frac{1}{E - E_i^{(0)}}, \tag{1.26}$$

and defining the difference

$$\Delta g_{ii}(E) \coloneqq g_{ii}(E) - g_{ii}^{(0)}(E), \tag{1.27}$$

one can easily verify that the energy shift ΔE_i is expressed, independent of A_i, by the following formula:

$$\Delta E_i = \frac{\dfrac{1}{2\pi i}\oint_\Gamma dE\, \Delta E \Delta g_{ii}(E)}{1 + \dfrac{1}{2\pi i}\oint_\Gamma dE\, \Delta g_{ii}(E)}, \tag{1.28}$$

where $\Delta E = E - E_i^{(0)}$. Finally, $\Delta g_{ii}(E)$ and ΔE_i are expanded in a perturbation series in the fine-structure constant α:

$$\Delta g_{ii}(E) = \Delta g_{ii}^{(1)}(E) + \Delta g_{ii}^{(2)}(E) + \cdots, \tag{1.29}$$

$$\Delta E_i = \Delta E_i^{(1)} + \Delta E_i^{(2)} + \cdots, \tag{1.30}$$

such that Eq. (1.28) yields the following expressions for the first two terms:

$$\Delta E_i^{(1)} = \frac{1}{2\pi i}\oint_\Gamma dE\, \Delta E \Delta g_{ii}^{(1)}(E), \tag{1.31}$$

$$\Delta E_i^{(2)} = \frac{1}{2\pi i}\oint_\Gamma dE\, \Delta E \Delta g_{ii}^{(2)}(E) - \Delta E_i^{(1)} \frac{1}{2\pi i}\oint_\Gamma dE\, \Delta g_{ii}^{(1)}(E). \tag{1.32}$$

We conclude this section by listing below in Fig. 1.1 the Feynman rules that will be used in this thesis. An explicit expression of the photon propagator $D_{\mu\nu}$ depends on the gauge choice, and it will be discussed later in Chapter 4.

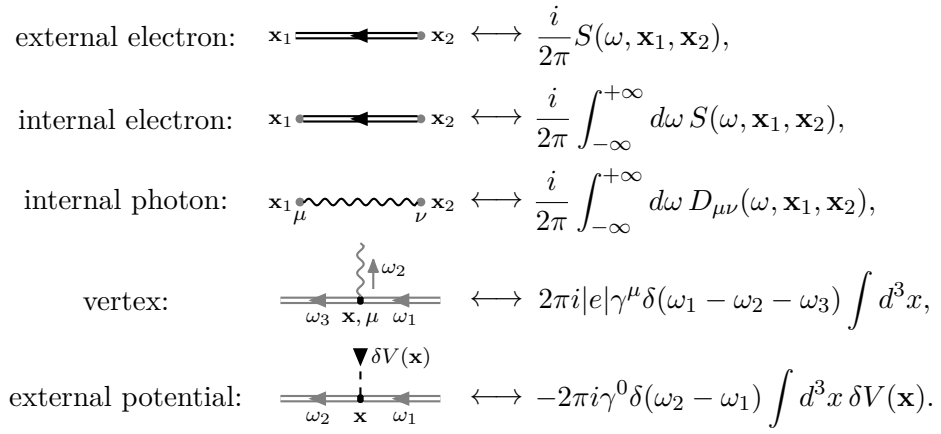

Figure 1.1.: Some of the Feynman rules for perturbative evaluation of the Green's function $G((E_1', \mathbf{x}_1'), \ldots, (E_N', \mathbf{x}_N'); (E_1, \mathbf{x}_1), \ldots, (E_N, \mathbf{x}_N))$.

1.3. Dirac equation in central potentials

Even though single-particle quantum mechanics is, strictly speaking, incompatible with special relativity, one still has to solve the single-particle Dirac equation (1.11) in order to compute the dressed electron propagator given by Eq. (1.14). In this section, we consider an important special case of this equation, where the only non-vanishing component of the external field is $\mathcal{A}_0$, corresponding to the electrostatic potential of an atomic nucleus. In addition, we assume this potential to be spherically symmetric, which serves as a good first approximation, while possible nuclear deformations can be treated later as perturbations, if necessary. Thus, with $V(\mathrm{x}) \coloneqq -|e|\mathcal{A}_0(\mathrm{x})$ denoting the potential energy, Eq. (1.11) becomes

$$[-i\boldsymbol{\alpha}\cdot\nabla + \beta m_\mathrm{e} + V(\mathrm{x})]\,\psi(\mathbf{x}) = \varepsilon\psi(\mathbf{x}). \tag{1.33}$$

1.3.1. Separation of variables

As in the case of the Schrödinger equation, spherical symmetry enables separation of the radial (x) and angular ($\Omega_\mathbf{x}$) variables [67, 68]. In order to carry out such a separation, we first note that, in the relativistic case, the orbital ($\hat{\mathbf{L}}$) and spin ($\hat{\mathbf{S}}$) angular momenta are not separately conserved. In fact, it was exactly non-conservation of the orbital angular momentum that guided P. Dirac [54] towards inferring the form of the spin contribution and constructing the conserved total angular momentum as $\hat{\mathbf{J}} = \hat{\mathbf{L}} + \hat{\mathbf{S}}$. Therefore, one needs to consider eigenfunctions of $\hat{\mathbf{J}}$, known as spherical spinors $\Omega_{jlm}(\Omega_\mathbf{x})$, which are obtained by combining the spherical harmonics $Y_{lm}(\Omega_\mathbf{x})$ with the spin 1/2 eigenfunctions χ_σ:

$$\Omega_{jlm}(\Omega_\mathbf{x}) = \sum_\sigma C^{jm}_{l(m-\sigma),\frac{1}{2}\sigma} Y_{l(m-\sigma)}(\Omega_\mathbf{x})\chi_\sigma, \tag{1.34}$$

where $C^{j_3m_3}_{j_1m_1,j_2m_2}$ denotes the Clebsch-Gordan coefficients for adding two angular momenta j_1 and j_2 into j_3, and the following eigenvalue equations hold:

$$\begin{cases} \hat{\mathbf{L}}^2 Y_{lm}(\Omega_\mathbf{x}) = l(l+1)Y_{lm}(\Omega_\mathbf{x}) \\ \hat{L}^3 Y_{lm}(\Omega_\mathbf{x}) = mY_{lm}(\Omega_\mathbf{x}), \end{cases} \qquad \begin{cases} \hat{\mathbf{S}}^2\chi_\sigma = \frac{3}{4}\chi_\sigma \\ \hat{S}^3\chi_\sigma = \sigma\chi_\sigma, \end{cases} \tag{1.35}$$

$$\begin{cases} \hat{\mathbf{J}}^2\Omega_{jlm}(\Omega_\mathbf{x}) = j(j+1)\Omega_{jlm}(\Omega_\mathbf{x}) \\ \hat{J}^3\Omega_{jlm}(\Omega_\mathbf{x}) = m\Omega_{jlm}(\Omega_\mathbf{x}). \end{cases} \tag{1.36}$$

The two-component spin eigenfunctions (or spinors) for $\sigma = \pm 1/2$ are given by

$$\chi_{1/2} = \begin{pmatrix} 1 \\ 0 \end{pmatrix}, \quad \chi_{-1/2} = \begin{pmatrix} 0 \\ 1 \end{pmatrix}, \tag{1.37}$$

and the expressions for the spherical harmonics can be found, e.g., in Ref. [68]. The explicit forms of the spherical spinors for the two possible values of the total angular momentum $j = l \pm 1/2$ are readily obtained as

$$\Omega_{(l+1/2)lm}(\Omega_{\mathbf{x}}) = \begin{pmatrix} \sqrt{\frac{l+m+1/2}{2l+1}} Y_{l(m-1/2)}(\Omega_{\mathbf{x}}) \\ \sqrt{\frac{l-m+1/2}{2l+1}} Y_{l(m+1/2)}(\Omega_{\mathbf{x}}) \end{pmatrix}, \tag{1.38}$$

$$\Omega_{(l-1/2)lm}(\Omega_{\mathbf{x}}) = \begin{pmatrix} -\sqrt{\frac{l-m+1/2}{2l+1}} Y_{l(m-1/2)}(\Omega_{\mathbf{x}}) \\ \sqrt{\frac{l+m+1/2}{2l+1}} Y_{l(m+1/2)}(\Omega_{\mathbf{x}}) \end{pmatrix}. \tag{1.39}$$

With the spherical spinors at hand, we can now separate the variables and build a four-component ansatz for a solution of Eq. (1.33) that has a definite total angular momentum j:

$$\psi_{jm}(\mathbf{x}) = \begin{pmatrix} g(\mathrm{x})\Omega_{jlm}(\Omega_{\mathbf{x}}) \\ if(\mathrm{x})\Omega_{jl'm}(\Omega_{\mathbf{x}}) \end{pmatrix}, \tag{1.40}$$

where the factor of i is introduced solely for later convenience. In order to determine the relation between the orbital quantum numbers l and l', we now turn our attention to the property of parity. Under the usual parity operation $\hat{P}_0$ that maps $\mathbf{x} \to -\mathbf{x}$, the spherical harmonics transform as

$$\hat{P}_0 Y_{lm}(\Omega_{\mathbf{x}}) = (-1)^l Y_{lm}(\Omega_{\mathbf{x}}), \tag{1.41}$$

from which follows that, although the orbital angular momentum l is not conserved, it still defines the parity of a spherical spinor $\Omega_{jlm}(\Omega_{\mathbf{x}})$ as $(-1)^l$. On the other hand, the action of the parity transformation on a four-component spinor $\psi(\mathbf{x})$ is a bit more complicated and is given by the operator [67]

$$\hat{P} = e^{i\phi}\gamma^0 \hat{P}_0, \tag{1.42}$$

where the phase factor $e^{i\phi}$ can be defined in two possible ways. If an application of two successive space inversions is interpreted as a rotation of angle 0, then the original spinor is reproduced, and $e^{i\phi} = \pm 1$. However, if two inversions are understood as a rotation by 2π, the spinor changes sign, and we have instead $e^{i\phi} = \pm i$. It should be noted that the only difference between the two definitions would occur for Majorana spinors for which only the second interpretation would be consistent with the condition of neutrality [69].

Since the operator $\hat{P}$ commutes with the Dirac Hamiltonian, the wave function $\psi_{jm}(\mathbf{x})$ must have a "good parity" p:

$$\begin{aligned} \hat{P}\psi_{jm}(\mathbf{x}) &= p\psi_{jm}(\mathbf{x}) \\ &= e^{i\phi} \begin{pmatrix} \mathbb{1}_2 & 0 \\ 0 & -\mathbb{1}_2 \end{pmatrix} \begin{pmatrix} g(\mathrm{x})\hat{P}_0\Omega_{jlm}(\Omega_{\mathbf{x}}) \\ if(\mathrm{x})\hat{P}_0\Omega_{jl'm}(\Omega_{\mathbf{x}}) \end{pmatrix} = e^{i\phi} \begin{pmatrix} (-1)^l g(\mathrm{x})\Omega_{jlm}(\Omega_{\mathbf{x}}) \\ (-1)^{l'+1} if(\mathrm{x})\Omega_{jl'm}(\Omega_{\mathbf{x}}) \end{pmatrix}, \end{aligned} \tag{1.43}$$

which shows that the spherical spinors $\Omega_{jlm}(\Omega_{\mathbf{x}})$ and $\Omega_{jl'm}(\Omega_{\mathbf{x}})$ must have opposite parities. It is conventional to define the parity of the state $\psi_{jm}(\mathbf{x})$ as the parity of its upper spherical spinor $\Omega_{jlm}(\Omega_{\mathbf{x}})$.

In addition, it is convenient to introduce the so-called relativistic angular momentum quantum number κ corresponding to the eigenvalues of the operator

$$\hat{K} = -1 - 2\hat{\mathbf{L}} \cdot \hat{\mathbf{S}}, \tag{1.44}$$

$$\hat{K}\,\Omega_{jlm}(\Omega_{\mathbf{x}}) = \kappa \Omega_{jlm}(\Omega_{\mathbf{x}}), \tag{1.45}$$

where $\kappa = \pm(j + 1/2)$ for $l = j \pm 1/2$, which can be summarized in one relation as

$$\kappa(j, l) = (-1)^{j+l+\frac{1}{2}} \left(j + \frac{1}{2}\right), \tag{1.46}$$

and, conversely, each pair (j, l) is uniquely specified by the single quantum number κ:

$$\begin{cases} j(\kappa) = |\kappa| - 1/2 \\ l(\kappa) = |\kappa + 1/2| - 1/2. \end{cases} \tag{1.47}$$

As a result, a more compact notation $\Omega_{\kappa m} \equiv \Omega_{jlm}$ can be used, and Eq. (1.40) becomes

$$\psi_{\kappa m}(\mathbf{x}) = \frac{1}{\mathrm{x}} \begin{pmatrix} G(\mathrm{x})\Omega_{\kappa m}(\Omega_{\mathbf{x}}) \\ iF(\mathrm{x})\Omega_{-\kappa m}(\Omega_{\mathbf{x}}) \end{pmatrix}, \tag{1.48}$$

where we also defined $G(\mathrm{x}) = \mathrm{x}g(\mathrm{x})$ and $F(\mathrm{x}) = \mathrm{x}f(\mathrm{x})$ for later convenience.

After separating the variables, one can easily reduce Eq. (1.33) to a system of coupled ordinary differential equations for the radial functions $G(\mathrm{x})$ and $F(\mathrm{x})$ [67]:

$$\hat{H}_\kappa \begin{pmatrix} G(\mathrm{x}) \\ F(\mathrm{x}) \end{pmatrix} \coloneqq \begin{pmatrix} V(\mathrm{x}) + m_\mathrm{e} & \frac{\kappa}{\mathrm{x}} - \frac{d}{d\mathrm{x}} \\ \frac{\kappa}{\mathrm{x}} + \frac{d}{d\mathrm{x}} & V(\mathrm{x}) - m_\mathrm{e} \end{pmatrix} \begin{pmatrix} G(\mathrm{x}) \\ F(\mathrm{x}) \end{pmatrix} = \varepsilon \begin{pmatrix} G(\mathrm{x}) \\ F(\mathrm{x}) \end{pmatrix}. \tag{1.49}$$

The resulting spectrum consists of discrete bound states for $0 < \varepsilon < m_e$ as well as two continua in the regions $\varepsilon \leq -m_\mathrm{e}$ and $\varepsilon \geq m_\mathrm{e}$. The bound states are labeled by an additional (principal) quantum number n, while the continuum states are characterized by the corresponding real-valued eigenvalues of ε.

In the case of the Coulomb potential of a point-like nucleus:

$$V_\mathrm{point}(\mathrm{x}) = -\frac{Z\alpha}{\mathrm{x}}, \tag{1.50}$$

Eq. (1.49) can be solved analytically (see, e.g., Ref. [67] for the expressions of the radial wave functions), resulting in the famous formula

$$\varepsilon_\mathrm{point}[n\kappa] = m_\mathrm{e} \left[1 + \frac{(Z\alpha)^2}{\left(n - |\kappa| + \sqrt{\kappa^2 - (Z\alpha)^2}\right)^2}\right]^{-1/2}. \tag{1.51}$$

However, for extended nuclei, one has to resort to numerical methods.

1.3.2. Numerical solution with *B*-spline basis sets

In order to evaluate the dressed electron propagator from Eq. (1.14), it is necessary to perform summation and integration over the entire Dirac spectrum. With an infinite number of bound states as well as positive- and negative-energy continua, this task poses an obvious challenge. Namely, direct calculations are difficult to implement with high accuracy, as they inevitably involve estimations of remainders of the sum over the bound states and the integrals over the continua. According to Refs. [70, 71], this challenge can be effectively dealt with in two steps. First, by confining the system to a spherical cavity of a finite (but large) radius R_{cav} and imposing appropriate boundary conditions, the continuous part of the spectrum is made discrete; however, it still remains infinite. Therefore, in the second step, this finite-cavity spectrum (*not* the original one) is further approximated by expanding the radial wave functions within a finite basis set of $2N$ functions $u_i(\mathrm{x})$:

$$\begin{pmatrix} G(\mathrm{x}) \\ F(\mathrm{x}) \end{pmatrix} = \sum_{i=1}^{2N} c_i u_i(\mathrm{x}). \tag{1.52}$$

This way, via the variational principle, the problem of finding the radial wave functions is reduced to a $2N \times 2N$ generalized eigenvalue equation

$$\mathbf{A} \cdot \mathbf{c} = \varepsilon \mathbf{B} \cdot \mathbf{c}, \tag{1.53}$$

where the matrices $\mathbf{A}$ and $\mathbf{B}$ are given by

$$A_{ij} = \frac{\langle u_i | \hat{H}_\kappa | u_j \rangle + \langle u_j | \hat{H}_\kappa | u_i \rangle}{2}, \quad B_{ij} = \langle u_i | u_j \rangle. \tag{1.54}$$

By solving Eq. (1.53) for a given κ, one obtains $2N$ discrete energy levels $\varepsilon_{n\kappa}$ as well as $2N$ sets of coefficients $\mathbf{c}(n\kappa)$. One half of these states approximate the negative continuum, while the other half corresponds to both the bound states and the positive continuum. With this representation, any computation involving the radial wave functions $G(\mathrm{x})$ and $F(\mathrm{x})$ can now be translated to operations on the coefficients $\mathbf{c}(n\kappa)$ and the basis functions $u_i(\mathrm{x})$.

An important practical aspect of such calculations is the selection of a suitable basis set. One of the computationally most efficient choices is to approximate the functions $G(\mathrm{x})$ and $F(\mathrm{x})$ by piecewise polynomials. This can be done in a systematic way by means of B-splines defined on a division of the interval $[0, R_{\mathrm{cav}}]$ into segments. A B-spline of order K is a piecewise polynomial of degree $K-1$, and the endpoints of the subintervals are given by a knot sequence $\{t_i\}$, $i = 1, 2, \ldots, N+K$, where N is the number of B-splines. The knots at the points $\mathrm{x} = 0$ and $\mathrm{x} = R_{\mathrm{cav}}$ are chosen to have K-fold multiplicity, meaning that $t_1 = t_2 = \cdots = t_K = 0$ and $t_{N+1} = t_{N+2} = \cdots = t_{N+K} = R_{\mathrm{cav}}$, while the knots $t_{K+1}, t_{K+2}, \ldots, t_N$ are distributed between 0

and R_{cav} in a way that best fits a particular application. On this knot sequence $\{t_i\}$, the B-splines $B_{i,K}(\mathrm{x})$ of order K are defined recursively as follows:

$$B_{i,1}(\mathrm{x}) = \begin{cases} 1, t_i \leq \mathrm{x} < t_{i+1}, \\ 0, \text{ otherwise}, \end{cases} \tag{1.55}$$

$$B_{i,K}(\mathrm{x}) = \frac{\mathrm{x} - t_i}{t_{i+K-1} - t_i} B_{i,K-1}(\mathrm{x}) + \frac{t_{i+K} - \mathrm{x}}{t_{i+K} - t_{i+1}} B_{i+1,K-1}(\mathrm{x}). \tag{1.56}$$

It follows that the function $B_{i,K}(\mathrm{x}) \neq 0$ for $t_i \leq \mathrm{x} < t_{i+K}$ and vanishes outside this interval. In the case of knots with multiplicity greater than 1, limiting forms of the above relations must be used. For atomic calculations, the order $K = 9$ was found to be accurate enough for most purposes [70].

Going back to the basis functions $u_i(\mathrm{x})$, it was proved in Ref. [53] that the most obvious choice:

$$u_i(\mathrm{x}) = \begin{pmatrix} B_{i,K}(\mathrm{x}) \\ 0 \end{pmatrix} \text{ for } i = 1, \ldots, N, \tag{1.57}$$

$$u_i(\mathrm{x}) = \begin{pmatrix} 0 \\ B_{i-N,K}(\mathrm{x}) \end{pmatrix} \text{ for } i = N+1, \ldots, 2N, \tag{1.58}$$

results in the occurrence of spurious states for $\kappa > 0$ as the lowest bound states with non-physical energies. Although the corresponding wave functions oscillate rapidly and therefore can be simply disregarded in practical calculations, they still disturb the rest of the numerical spectrum. In order to eliminate the spurious states in a natural manner and thereby improve the convergence properties of the basis-set calculations, it was proposed in Ref. [53] to use the functions $u_i(\mathrm{x})$ in the following form:

$$u_i(\mathrm{x}) = \begin{pmatrix} B_{i,K}(\mathrm{x}) \\ \frac{1}{2m_{\mathrm{e}}} \left(\frac{d}{d\mathrm{x}} + \frac{\kappa}{\mathrm{x}} \right) B_{i,K}(\mathrm{x}) \end{pmatrix} \text{ for } i = 1, \ldots, N, \tag{1.59}$$

$$u_i(\mathrm{x}) = \begin{pmatrix} \frac{1}{2m_{\mathrm{e}}} \left(\frac{d}{d\mathrm{x}} - \frac{\kappa}{\mathrm{x}} \right) B_{i-N,K}(\mathrm{x}) \\ B_{i-N,K}(\mathrm{x}) \end{pmatrix} \text{ for } i = N+1, \ldots, 2N, \tag{1.60}$$

which was termed as the dual-kinetic-balance basis.

For the atomic calculations in this thesis, we employ finite basis-set expansions in terms of B-splines within the dual-kinetic-balance approach based on the numerical implementation by Halil Cakir [72]. Thereby, the computations are reduced to finite sums with no remainders to evaluate. The convergence of the results is readily controlled by increasing the size of the cavity and the number of the B-splines such that the results are independent of R_{cav} and N.

1.4. Bound-electron g factor

Besides atomic energy levels, another important quantity, known as the bound-electron g factor, will be of interest in this thesis. Originally, a g factor is defined as the proportionality coefficient that relates the electron's magnetic moment $\hat{\boldsymbol{\mu}}$ (in units of the Bohr magneton $\mu_\mathrm{B} = |e|/2m_\mathrm{e}$) to its angular momentum $\hat{\mathbf{M}}$:

$$\frac{\hat{\boldsymbol{\mu}}}{\mu_\mathrm{B}} = -g\hat{\mathbf{M}}, \text{ e.g., } \frac{\hat{\boldsymbol{\mu}}_\mathrm{S}}{\mu_\mathrm{B}} = -g_\mathrm{S}\hat{\mathbf{S}} \text{ and } \frac{\hat{\boldsymbol{\mu}}_\mathrm{L}}{\mu_\mathrm{B}} = -g_\mathrm{L}\hat{\mathbf{L}}. \tag{1.61}$$

For a free electron in the Dirac theory, i.e., without taking into account radiative corrections, $g_\mathrm{S} = 2$ [54, 63]. At a higher level of accuracy, this value receives various QED contributions, with the first-order result being $g_\mathrm{S} = 2[1 + \alpha/(2\pi)]$, which was first calculated by Julian Schwinger [73, 74]. At present, the so-called electron's anomalous magnetic moment $a = (g_\mathrm{S} - 2)/2$ has been calculated up to the order $(\alpha/\pi)^5$ [58–60] as well as measured at a comparable level of precision [56, 57]. Together with an independently determined value of α [75, 76], the free-electron g factor provides the most stringent test of QED in the absence of a strong external electromagnetic field.

In the case of a bound atomic electron, an additional magnetic moment arises due to its orbital motion. Assuming an infinitely heavy nucleus, the associated factor g_L is exactly equal to 1, analogous to the case of the classical gyromagnetic ratio [77]. For a finite nuclear mass M_nucl, the effective value of $g_\mathrm{L} = 1 - m_\mathrm{e}/M_\mathrm{nucl}$ applies [78].

As for the total magnetic moment $\hat{\boldsymbol{\mu}}_\mathrm{total} = -\mu_\mathrm{B}(g_\mathrm{L}\hat{\mathbf{L}} + g_\mathrm{S}\hat{\mathbf{S}})$, it is not collinear with the total angular momentum $\hat{\mathbf{J}} = \hat{\mathbf{L}} + \hat{\mathbf{S}}$ because of the different values of g_S and g_L. However, due to the projection theorem [79], the component of $\hat{\boldsymbol{\mu}}_\mathrm{total}$ perpendicular to $\hat{\mathbf{J}}$ does not contribute to the expectation value $\langle jm|\hat{\boldsymbol{\mu}}_\mathrm{total}|jm\rangle$, which makes $\hat{\boldsymbol{\mu}}_\mathrm{total}$ *effectively* lie on the direction of $\hat{\mathbf{J}}$. Consequently, similar to Eq. (1.61), one can define in terms of matrix elements:

$$\frac{\langle jm|\hat{\boldsymbol{\mu}}_\mathrm{total}|jm\rangle}{\mu_\mathrm{B}} = -g_\mathrm{J}\langle jm|\hat{\mathbf{J}}|jm\rangle, \tag{1.62}$$

where it can be easily shown that

$$g_\mathrm{J} = g_\mathrm{L}\frac{j(j+1) - s(s+1) + l(l+1)}{2j(j+1)} + g_\mathrm{S}\frac{j(j+1) + s(s+1) - l(l+1)}{2j(j+1)}. \tag{1.63}$$

Eqs. (1.62) and (1.63) allow to describe the so-called anomalous Zeeman splitting of atomic energy levels in a weak external magnetic field $\mathbf{B} = (0, 0, B^3)$. Thus, for the interaction term from the non-relativistic Pauli equation:

$$\hat{H}_\mathrm{mag} = -\hat{\boldsymbol{\mu}}_\mathrm{total} \cdot \mathbf{B}, \tag{1.64}$$

it immediately follows that

$$\Delta E_{jm} = \langle jm| - \hat{\boldsymbol{\mu}}_{\text{total}} \cdot \mathbf{B}|jm\rangle = g_{\text{J}} \mu_{\text{B}} B^{\mathcal{Z}} m. \tag{1.65}$$

The coefficient g_{J} is called the Landé g factor, named after Alfred Landé, who was able to provide an empirical analysis of the anomalous Zeeman effect in 1921 [80], well before Dirac's theory of the electron.

Finally, a more general relativistic definition of a g factor as a measure of the response to an external magnetic field can be obtained directly from the stationary Dirac equation (1.33). According to the minimal coupling prescription, the interaction of an electron with the external magnetic field is given by

$$\delta V(\mathbf{x}) = |e| \boldsymbol{\alpha} \cdot \mathbf{A}(\mathbf{x}), \tag{1.66}$$

where the vector potential can be chosen in the form $\mathbf{A}(\mathbf{x}) = [\mathbf{B} \times \mathbf{x}]/2$. The first-order Zeeman splitting is then expressed as

$$\Delta E^{(1)}_{n\kappa m} = \frac{|e|}{2} \langle n\kappa m| \boldsymbol{\alpha} \cdot [\mathbf{B} \times \mathbf{x}]|n\kappa m\rangle = \frac{|e|}{2} B^{\mathcal{Z}} \langle n\kappa m|[\mathbf{x} \times \boldsymbol{\alpha}]^{\mathcal{Z}}|n\kappa m\rangle. \tag{1.67}$$

Following the calculation of the angular part of $\langle n\kappa m|[\mathbf{x} \times \boldsymbol{\alpha}]^{\mathcal{Z}}|n\kappa m\rangle$ from Ref. [81], it can be shown that the energy shift can be again written in the form

$$\Delta E^{(1)}_{n\kappa m} = g \mu_{\text{B}} B^{\mathcal{Z}} m, \tag{1.68}$$

with

$$g = \frac{2\kappa m_{\text{e}}}{j(j+1)} \int_0^\infty G_{n\kappa}(\text{x}) F_{n\kappa}(\text{x}) \text{x}\, \text{dx}. \tag{1.69}$$

It is this generalized g factor that will be considered in this thesis.

To conclude this section, we also mention the important special case of a point-like nucleus, where Eq. (1.69) can be evaluated analytically such that the expression for the g factor reduces to [82]

$$g_{\text{point}}[n\kappa] = \frac{\kappa}{j(j+1)} \left(\kappa \frac{E_{\text{point}}[n\kappa]}{m_{\text{e}}} - \frac{1}{2} \right). \tag{1.70}$$

2. Microscopic description of nuclear structure

In Chapter 1, we saw that for atomic QED calculations one needs to take into account the entire Dirac spectrum of a bound electron. Therefore, it can be already guessed that a similar summation would have to be carried out with respect to the nuclear spectrum if the atomic nucleus were to come into play in its full glory. This will indeed turn out to be the case in Chapter 4 for the nuclear-polarization effect. Contrary to the dynamics of electrons, a truly *ab initio* description is extremely challenging even for very light nuclei and simply unfeasible for heavy ones. Nevertheless, effective models of nucleon-nucleon interactions together with sophisticated particle-hole theories have proven to be successful at describing a rich variety of nuclear excitations. In this chapter, we briefly review such an approach to tackle this formidable task.

2.1. Skyrme-Hartree-Fock mean field

The starting point of any effective microscopic nuclear model is the construction of an interaction potential $\hat{V}$ between nucleons. Given the short range of the nuclear force, the simplest possible radial dependence of such a potential for two nucleons with coordinates $\mathbf{r}_1$ and $\mathbf{r}_2$ would be of the form

$$\hat{V}_{\text{contact}}(\mathbf{r}_1, \mathbf{r}_2) \propto \delta(\mathbf{r}_1 - \mathbf{r}_2). \tag{2.1}$$

In that case, the matrix element of $\hat{V}(\mathbf{r})$ with $\mathbf{r} = \mathbf{r}_1 - \mathbf{r}_2$ in momentum space:

$$\langle \mathbf{p}|\hat{V}|\mathbf{p}'\rangle \propto \int d^3r\, e^{-i(\mathbf{p}-\mathbf{p}')\mathbf{r}}\, \hat{V}(\mathbf{r}), \tag{2.2}$$

would be a constant, i.e., momentum independent. Unfortunately, this simple zero-range interaction is not adequate for most applications, except perhaps for some qualitative computations. It is clear from Eq. (2.2) that a more realistic description with any finite range leads to a momentum dependence of $\langle \mathbf{p}|\hat{V}|\mathbf{p}'\rangle$. The lowest-order rotationally invariant expression has the form [83]

$$\langle \mathbf{p}|\hat{V}_{\text{short-range}}|\mathbf{p}'\rangle = \tilde{v}_0 + \tilde{v}_1 \left(\mathbf{p}^2 + \mathbf{p}'^2\right) + \tilde{v}_2 \mathbf{p}\cdot\mathbf{p}', \tag{2.3}$$

which corresponds to the following interaction potential in the coordinate space:

$$\hat{V}_{\text{short-range}}(\mathbf{r}) = v_0\delta(\mathbf{r}) + v_1\left(\hat{\mathbf{p}}^2\delta(\mathbf{r}) + \delta(\mathbf{r})\hat{\mathbf{p}}^2\right) + v_2\hat{\mathbf{p}}\cdot\delta(\mathbf{r})\hat{\mathbf{p}}, \tag{2.4}$$

where $\hat{\mathbf{p}} = -i\nabla$ is the momentum operator.

Despite its simplicity, the short-range expansion in Eq. (2.4) lays the foundation for one of the most successful and widely used effective interactions in microscopic nuclear theory. In 1956, Tony Skyrme used this approximation to study nuclear surface properties [84], and a couple of years later he proposed to supplement the effective potential with a three-body contact term

$$\hat{V}_{\text{3-body}}(\mathbf{r}_1, \mathbf{r}_2, \mathbf{r}_3) \propto \delta(\mathbf{r}_1 - \mathbf{r}_2)\delta(\mathbf{r}_2 - \mathbf{r}_3), \tag{2.5}$$

in order to account for the influence of other nucleons on two-body interactions [85]. Within the mean-field framework, it can be shown that for spin-saturated even-even nuclei this term is equivalent to a density-dependent two-body potential [86]

$$\hat{V}_\rho(\mathbf{r}_1, \mathbf{r}_2) \propto (1 + \hat{P}_\sigma)\delta(\mathbf{r}_1 - \mathbf{r}_2)\rho\left((\mathbf{r}_1 + \mathbf{r}_2)/2\right), \tag{2.6}$$

where ρ is the total nucleon density and $\hat{P}_\sigma$ is the spin-exchange operator:

$$\hat{P}_\sigma = \frac{1}{2}\left(1 + \boldsymbol{\sigma}_1\cdot\boldsymbol{\sigma}_2\right), \tag{2.7}$$

where $\boldsymbol{\sigma}_1$ and $\boldsymbol{\sigma}_2$ are the Pauli matrices acting on the spin variables of the nucleons 1 and 2, respectively. Finally, with the inclusion of the two-body spin-orbit term in the short range limit [87]:

$$\hat{V}_{\text{s.o.}} = iW_0\left(\boldsymbol{\sigma}_1 + \boldsymbol{\sigma}_2\right)\cdot\left[\hat{\mathbf{P}}^\dagger \times \delta(\mathbf{r})\hat{\mathbf{P}}\right], \tag{2.8}$$

the standard form of the Skyrme-type interaction is written as [88]

$$\begin{aligned}\hat{V}_{\text{Skyrme}}(\mathbf{r}_1, \mathbf{r}_2) = {} & t_0\left(1 + x_0\hat{P}_\sigma\right)\delta(\mathbf{r}) \\ & + \frac{1}{2}t_1\left(1 + x_1\hat{P}_\sigma\right)\left[\hat{\mathbf{P}}^{\dagger 2}\delta(\mathbf{r}) + \delta(\mathbf{r})\hat{\mathbf{P}}^2\right] \\ & + t_2\left(1 + x_2\hat{P}_\sigma\right)\hat{\mathbf{P}}^\dagger\cdot\delta(\mathbf{r})\hat{\mathbf{P}} \\ & + \frac{1}{6}t_3\left(1 + x_3\hat{P}_\sigma\right)\rho^\lambda(\mathbf{R})\delta(\mathbf{r}) \\ & + iW_0\left(\boldsymbol{\sigma}_1 + \boldsymbol{\sigma}_2\right)\cdot\left[\hat{\mathbf{P}}^\dagger \times \delta(\mathbf{r})\hat{\mathbf{P}}\right],\end{aligned} \tag{2.9}$$

where $\mathbf{r} = \mathbf{r}_1 - \mathbf{r}_2$, $\mathbf{R} = \frac{1}{2}\left(\mathbf{r}_1 + \mathbf{r}_2\right)$, and $\hat{\mathbf{P}} = \frac{1}{2i}\left(\nabla_1 - \nabla_2\right)$, with $\hat{\mathbf{P}}^\dagger$ acting on the left. The parameters of the Skyrme force t_j, x_j ($j \in \{0, 1, 2, 3\}$), W_0 and λ are adjusted to reproduce the experimental ground-state properties. A more general power dependence on the nucleon density ρ^λ is allowed in order to improve the

description of the compressibility properties of the nuclear matter. Furthermore, an additional parameter W_0' is sometimes also introduced to weight differently neutron and proton effects on the last spin-orbit term [89].

Even though the presence of the δ-functions in Eq. (2.9) simplifies all types of computations enormously, further approximations are still needed in order to make a microscopic nuclear description feasible. A hint comes from the observation of the so-called "magic numbers" of nucleons associated with especially stable nuclei, similar to the case of closed shells in inert gases. Hence, in analogy to multi-electron atomic systems, this motivates the assumption that a given nucleon moves independently in an average potential generated by all other nucleons. A well-established approach for extracting such a single-particle potential from a two-body interaction is the Hartree-Fock method. In this approximation, the ground-state many-body wave function Φ_{HF} is assumed to be a Slater determinant built out of the single-nucleon occupied states $\{\varphi_i(\mathbf{r})\}$. The Skyrme-Hartree-Fock equations are then obtained via the variational principle by requiring that the total energy functional

$$E\left[\Phi_{\mathrm{HF}}\right] = \left\langle \Phi_{\mathrm{HF}} \left| \sum_i \frac{\hat{\mathbf{p}}_i^2}{2M} + \sum_{i<j} \hat{V}_{\mathrm{Skyrme}}(i,j) + \sum_{i<j}^{\mathrm{protons}} V_{\mathrm{Coulomb}}(i,j) \right| \Phi_{\mathrm{HF}} \right\rangle \tag{2.10}$$

must be stationary with respect to norm-conserving variations of the single-nucleon functions:

$$\frac{\delta}{\delta\varphi_i}\left(E\left[\{\varphi_j\}\right] - \sum_j \epsilon_j \int |\varphi_j(\mathbf{r})|^2 \, d^3r \right) = 0, \tag{2.11}$$

where ϵ_i are the Lagrange multipliers. In the above expressions, the summations run over all nucleons (unless specified otherwise), and M is the nucleon mass. The condition (2.11) leads to the following set of non-linear equations [86, 90, 91]:

$$\hat{h}_q\Big(\mathbf{r}, \{\varphi_j(\mathbf{r})\}\Big)\varphi_i^q(\mathbf{r}) = \epsilon_i \varphi_i^q(\mathbf{r}), \tag{2.12}$$

with

$$\begin{aligned} \hat{h}_q\Big(\mathbf{r}, \{\varphi_j(\mathbf{r})\}\Big) = \Bigg[&- \nabla \cdot \frac{1}{2m_q^*(\{\varphi_j(\mathbf{r})\})} \nabla + U_q\left(\{\varphi_j(\mathbf{r})\}\right) \\ &+ \delta_{q\mathrm{p}} V_{\mathrm{C}}(\mathbf{r}, \{\varphi_j^{\mathrm{p}}(\mathbf{r})\}) - i\mathbf{W}_q(\{\varphi_j(\mathbf{r})\}) \cdot (\nabla \times \boldsymbol{\sigma}) \Bigg], \end{aligned} \tag{2.13}$$

where the additional label q is used to distinguish between protons ($q = \mathrm{p}$) and neutrons ($q = \mathrm{n}$). The derivation of the operators $\hat{h}_q$ as well as the explicit expressions for the effective masses m_q^*, central potentials U_q, spin-orbit potentials $\mathbf{W}_q$ and Coulomb potential V_{C} in the Slater approximation can be found in Refs. [86, 90].

The key point is that all these quantities depend on $\{\varphi_i\}$ and therefore can be calculated only when all the occupied states are known. Consequently, the procedure of obtaining the single-nucleon functions necessitates an initial guess, and then the Skyrme-Hartree-Fock equations are solved iteratively until self-consistency to a desired precision is achieved. As usual, in the case of spherical symmetry the problem simplifies greatly due to the fact that the single-particle wave functions can be factorized as

$$\varphi_i(\mathbf{r}) = R_{njl}(\mathrm{r})\Omega_{jlm}(\Omega_{\mathbf{r}}), \tag{2.14}$$

such that Eqs. (2.12) are reduced to one-dimensional differential equations on the radial functions $R_{njl}(\mathrm{r})$, which can be found in Ref. [86]. Analogously to Subsection 1.3.1, the nucleon states are characterized by the principal quantum number n, total angular momentum j (with projection m) and the parity $(-1)^l$.

Once convergence is reached, Eqs. (2.12) can determine not only the occupied orbitals but also the unoccupied ones. Thus, at this point, nuclear excited states can be modeled as individual particle-hole excitations. However, in addition to these elementary processes, there are many experimentally observed phenomena, such as giant resonances with much larger electromagnetic transition probabilities, that cannot be adequately reproduced in such a simplified view. It turns out that these resonances can only be explained by considering coherent participation of many nucleons. In the next section, following Refs. [91, 92], we will introduce a method that enables an accurate description of such collective motions inside a nucleus.

2.2. Random-phase approximation

The simplest possible microscopic treatment of nuclear excitations leading to collective behaviour is obtained by diagonalizing the Hamiltonian in a finite space of particle-hole configurations while keeping the Hartree-Fock description of the ground state. This procedure is known as the Tamm-Dancoff approximation (TDA), and it is a major step forward in explaining the structure of experimental nuclear spectra. However, the main drawback of the Tamm-Dancoff method is the fact that nucleon correlations are built only into the excited states while being completely neglected in the ground state. Formally, this can be expressed by the relations

$$|\nu\rangle_{\mathrm{TDA}} = Q^{\dagger}_{\mathrm{TDA},\,\nu}\,|0\rangle_{\mathrm{HF}} \quad \text{and} \quad Q_{\mathrm{TDA},\,\nu}\,|0\rangle_{\mathrm{HF}} = 0 \;\forall\; \nu, \tag{2.15}$$

where the "vacuum" $|0\rangle_{\mathrm{HF}}$ corresponds to the Hartree-Fock ground state, and the creation operator $Q^{\dagger}_{\mathrm{TDA},\,\nu}$ for an excited state $|\nu\rangle_{\mathrm{TDA}}$:

$$Q^{\dagger}_{\mathrm{TDA},\,\nu} = \sum_{mi} C^{(\nu)}_{mi} a^{\dagger}_m a_i, \tag{2.16}$$

is given in terms of the single-particle creation (annihilation) operators $a_m^\dagger$ (a_i) and the expansion coefficients $C_{mi}^{(\nu)}$. In this section, the indices i, j refer to the occupied states, while m, n correspond to the unoccupied ones.

A simple but highly successful generalization of the Tamm-Dancoff approach is called the random-phase approximation (RPA). Historically, this formalism takes its origin from the theory of Bohm and Pines of plasma oscillations of an electron gas, where the term "random-phase approximation" corresponded to the neglect of the coupling between collective vibrations of different momenta [93]. The modern and more elegant formulation of the RPA resembles little of the original derivation, and in the context of nuclear physics it can be ultimately understood as the following generalization of Eq. (2.16):

$$Q_{\mathrm{RPA},\,\nu}^\dagger = \sum_{mi} X_{mi}^{(\nu)} a_m^\dagger a_i - \sum_{mi} Y_{mi}^{(\nu)} a_i^\dagger a_m. \tag{2.17}$$

The inclusion of the second term in Eq. (2.17) has a very clear physical meaning: the operator $Q_{\mathrm{RPA},\,\nu}^\dagger$ can not only create a particle-hole pair but also destroy one. In analogy to Eqs. (2.15), the RPA ground and excited states are defined as

$$|\nu\rangle_{\mathrm{RPA}} = Q_{\mathrm{RPA},\,\nu}^\dagger\,|0\rangle_{\mathrm{RPA}} \quad \text{and} \quad Q_{\mathrm{RPA},\,\nu}\,|0\rangle_{\mathrm{RPA}} = 0\ \forall\ \nu, \tag{2.18}$$

where the second relation implies that the combinations $a_i^\dagger a_m$ in $Q_{\mathrm{RPA},\,\nu}^\dagger$ lead to particle-hole admixtures in $|0\rangle_{\mathrm{RPA}}$, which are exactly the ground-state correlations that were omitted in the TDA method.

In the case of spherical nuclei, the excited states have a good angular momentum J and a good parity π. For practical calculations, it is advantageous to exploit this symmetry and find the RPA states separately for each J^π mode. To this end, one introduces the creation operators for particle-hole pairs coupled to the total angular momentum:

$$\mathcal{A}_{mi}^\dagger(JM) = \sum_{m_m, m_i} C_{j_m m_m, j_i(-m_i)}^{JM} a_{j_m m_m}^\dagger (-1)^{j_i - m_i} a_{j_i m_i}. \tag{2.19}$$

In terms of $\mathcal{A}_{mi}^\dagger(JM)$, the operator $Q_{\mathrm{RPA},\,\nu}^\dagger$ is then redefined as

$$Q_{\mathrm{RPA},\,\nu}^\dagger = \sum_{mi} X_{mi}^{(\nu)} \mathcal{A}_{mi}^\dagger(JM) - \sum_{mi} Y_{mi}^{(\nu)} \mathcal{A}_{mi}(\widetilde{JM}), \tag{2.20}$$

where

$$\mathcal{A}_{mi}(\widetilde{JM}) = (-1)^{J+M} \mathcal{A}_{mi}(J(-M)). \tag{2.21}$$

The information about a given excitation $|\nu\rangle_{\mathrm{RPA}}$ is contained in the so-called RPA amplitudes $X_{mi}^{(\nu)}$ and $Y_{mi}^{(\nu)}$, which can be shown to satisfy the matrix equation

$$\begin{pmatrix} \mathbf{A} & \mathbf{B} \\ -\mathbf{B} & -\mathbf{A} \end{pmatrix} \begin{pmatrix} \mathbf{X}^{(\nu)} \\ \mathbf{Y}^{(\nu)} \end{pmatrix} = E_\nu \begin{pmatrix} \mathbf{X}^{(\nu)} \\ \mathbf{Y}^{(\nu)} \end{pmatrix}, \tag{2.22}$$

where E_ν are the corresponding excitation energies, and the matrices $\mathbf{A}$ and $\mathbf{B}$ are built out of the matrix elements of the residual interaction as follows:

$$A_{mi,nj} = (\epsilon_m - \epsilon_i)\delta_{mn}\delta_{ij} + \overbrace{\langle m\underbrace{j|\hat{V}_{\rm res}|i}n\rangle}^{J}_{J}, \tag{2.23}$$

$$B_{mi,nj} = \overbrace{\langle mn|\hat{V}_{\rm res}|\underbrace{ij}\rangle}^{J}_{J}, \tag{2.24}$$

where

$$\overbrace{\langle \underbrace{ab}|\hat{V}_{\rm res}|cd\rangle}^{J}_{J} \coloneqq \sum_{\text{all } m} (-1)^{j_b - m_b + j_c - m_c} C^{JM}_{j_a m_a, j_c(-m_c)} C^{JM}_{j_d m_d, j_b(-m_b)} \times \langle j_a m_a, j_b m_b|\hat{V}_{\rm res}|j_c m_c, j_d m_d\rangle. \tag{2.25}$$

The term "residual interaction" refers to the difference between the full two-body potential and the mean-field approximation, and it can be in general expressed as a functional derivative of the Hartree-Fock energy functional E with respect to the nucleon densities:

$$\hat{V}^{qq'}_{\rm res} = \frac{\delta^2 E}{\delta\rho_q \delta\rho_{q'}}, \tag{2.26}$$

where (explicitly indicating the spin variable σ)

$$\rho_{\rm p}(\mathbf{r}) = \sum_{i,\sigma} |\varphi^{\rm p}_i(\mathbf{r},\sigma)|^2, \quad \rho_{\rm n}(\mathbf{r}) = \sum_{i,\sigma} |\varphi^{\rm n}_i(\mathbf{r},\sigma)|^2. \tag{2.27}$$

The complete formulas for the matrix elements of $\hat{V}_{\rm res}$ are rather cumbersome and can be found in Ref. [91]. We note that it is important to use in the RPA description exactly the same pieces of the residual interaction that have been used in the underlying Hartree-Fock calculation, without approximations (see, e.g., Ref. [94]). In this thesis, we employ the numerical implementation of the Hartree-Fock-based RPA from Ref. [91] with a full self-consistency between the Hartree-Fock mean field and the RPA excitations, which allows fulfilment of the proper conservation laws.

Once the RPA equation (2.22) is solved for a given excitation mode J^π, the obtained amplitudes $\mathbf{X}^{(\nu)}$ and $\mathbf{Y}^{(\nu)}$ can be used to calculate various quantities of interest. For example, a reduced transition matrix element of a Hermitian one-body spherical tensor operator $\hat{O}_{JM}$ is given by [92]

$${}_{\rm RPA}\langle \nu, J||\hat{O}_J||0\rangle_{\rm RPA} = \sum_{mi} \left[X^{(\nu)}_{mi}\langle m||\hat{O}_J||i\rangle + (-1)^J Y^{(\nu)}_{mi}\langle m||\hat{O}_J||i\rangle^* \right], \tag{2.28}$$

where the particle-hole matrix elements $\langle m||\hat{O}_J||i\rangle$ can be evaluated by using the Hartree-Fock single-nucleon wave functions.

3. Finite-nuclear-size effect

In this chapter, the microscopic description of a nuclear ground state is applied to calculations of the finite-nuclear-size (FNS) correction to atomic energy levels and the bound-electron g factor in hydrogenlike ions. First, we introduce different models of nuclear charge distributions as well as experimental model-independent expansions. Then, before comparing the microscopic approach to simpler models and experimental data, we discuss the question of the ambiguity in the choice of a Skyrme parametrization. The main discussion of the numerical results follows next, where the uncertainties of the calculations are also estimated. In addition, the suppression of the FNS effect in the specific differences of g factors is demonstrated. The work described in this chapter was published in Ref. [1].

3.1. Nuclear charge distributions

The single-particle wave functions obtained from the Skyrme-Hartree-Fock calculations (2.12) can be used to construct point nucleon densities, in particular the proton density

$$\rho_{\rm p}(\mathbf{r}) = \sum_{i,\sigma} |\varphi_i^{\rm p}(\mathbf{r},\sigma)|^2, \tag{3.1}$$

where the spin variable σ is indicated explicitly. In order to obtain the corresponding nuclear charge distribution, the proton density is then folded with the proton form factor $f_{\rm p}(r)$ to account for the finite extent of the proton [86]:

$$f_{\rm p}(r) = \frac{1}{(r_0\sqrt{\pi})^3} e^{-r^2/r_0^2}\ ,\ r_0 = 0.65\ \text{fm}, \tag{3.2}$$

$$\rho_{\rm c}(\mathbf{r}) = \int f_{\rm p}(\mathbf{r}-\mathbf{r}')\rho_{\rm p}(\mathbf{r}')\, d^3r'. \tag{3.3}$$

In this chapter, we assume spherical symmetry of nuclear charge distributions. In this case, the following simpler models for $\rho_{\rm c}(r)$ are widely used:

• the homogeneously-charged-sphere approximation ("sphere"):

$$\rho_{\rm c}(r) = \begin{cases} \rho_0^{\rm sphere} & \text{for } 0 \le r \le \sqrt{\frac{5}{3}\langle r^2\rangle}, \\ 0 & \text{otherwise,} \end{cases} \tag{3.4}$$

where $\sqrt{\langle \mathrm{r}^2 \rangle}$ is the root-mean-square (RMS) charge radius of the nucleus;
• Fermi distribution ("Fermi"):

$$\rho_{\mathrm{c}}(\mathrm{r}) = \frac{\rho_0^{\mathrm{Fermi}}}{1 + e^{(\mathrm{r}-c)/a}}, \tag{3.5}$$

with the half-density radius c and the standard value of the diffuseness parameter $a = 2.3/[4\ln(3)]$ fm [95].

From the experimental side, nuclear charge distributions can be obtained in a model-independent way by expanding $\rho_{\mathrm{c}}(\mathrm{r})$ in a sufficiently large set of functions and fitting the expansion coefficients to electron scattering data [96]. The majority of such experiments are analyzed by means of two different approaches:
• expansion into a sum of spherical Bessel functions j_0 of order zero ("Bessel"):

$$\rho_{\mathrm{c}}(\mathrm{r}) = \begin{cases} \sum\limits_{\nu} a_\nu j_0\left(\nu\pi \mathrm{r}/R\right) & \text{for } 0 < \mathrm{r} \le R, \\ 0 & \text{otherwise}, \end{cases} \tag{3.6}$$

with a cutoff radius R;
• expansion into a sum of Gaussians ("Gauss"):

$$\rho_{\mathrm{c}}(\mathrm{r}) = \sum_i A_i \left(e^{-[(\mathrm{r}-R_i)/\gamma]^2} + e^{-[(\mathrm{r}+R_i)/\gamma]^2} \right), \tag{3.7}$$

$$A_i = Q_i \left[2\pi^{3/2}\gamma^3 \left(1 + 2R_i^2/\gamma^2\right) \right]^{-1}, \quad \sum_i Q_i = 1,$$

where R_i and Q_i are the positions and the amplitudes of the Gaussians, respectively, and the parameter γ is related to the root-mean-square radius R_{G} of the Gaussians as follows: $R_{\mathrm{G}} = \gamma\sqrt{3/2}$.

For a given charge distribution $\rho_{\mathrm{c}}(\mathrm{r})$, the corresponding potential of an extended nucleus is given by

$$V(\mathrm{r}) = -4\pi\alpha Z \int_0^\infty \frac{\rho_{\mathrm{c}}(\mathrm{r}')\mathrm{r}'^2}{\max(\mathrm{r}, \mathrm{r}')}\, d\mathrm{r}', \tag{3.8}$$

where the following normalization condition is adopted:

$$4\pi \int_0^\infty \rho_{\mathrm{c}}(\mathrm{r})\mathrm{r}^2\, d\mathrm{r} = 1. \tag{3.9}$$

The potential (3.8) enters the Dirac equation (1.33), which can be solved numerically in order to determine the energy levels and the wave functions of an electron bound to a finite-size nucleus. The bound-electron g factor is then readily obtained by plugging the numerical solutions for the radial functions into Eq. (1.69). Finally, the corresponding FNS corrections for a given state with the quantum numbers $n\kappa$

are defined as the differences between the numerical values for the potential (3.8) and the analytical solutions for a point-like nucleus (see Eqs. (1.51) and (1.70)):

$$\Delta E_{\mathrm{FNS}}[n\kappa] = E_{\mathrm{ext}}[n\kappa] - E_{\mathrm{point}}[n\kappa], \tag{3.10}$$

$$\Delta g_{\mathrm{FNS}}[n\kappa] = g_{\mathrm{ext}}[n\kappa] - g_{\mathrm{point}}[n\kappa]. \tag{3.11}$$

3.2. Choice of Skyrme parametrization

Since the effective Skyrme interaction (2.9) depends on various parameters, we first discuss their influence on the computational results. For this purpose, we consider the FNS correction to the ground-state ($1s_{1/2}$) energy and the g factor in hydrogenlike lead $^{208}_{82}\mathrm{Pb}^{81+}$. To illustrate the breadth of the parameter space, three widely used Skyrme forces, namely LNS [97], SLy5 [90] and SkP [98], are compared in Table 3.1, where the vast differences between these models are most evident from the values of the three selected parameters t_1, x_0 and x_3. The next column demonstrates the corresponding large variations in the values of the RMS nuclear charge radius obtained by using each of these parametrizations. As a result, the FNS corrections $\Delta E_{\mathrm{FNS}}[1s_{1/2}]$ and $\Delta g_{\mathrm{FNS}}[1s_{1/2}]$ also vary significantly in such a way that the results may turn out to be larger or smaller than the ones obtained in the homogeneously-charged-sphere approximation (using the tabulated value of $\sqrt{\langle \mathrm{r}^2 \rangle} = 5.5012$ fm [99]).

Table 3.1.: Comparison between the parameters t_1, x_0, and x_3 from the LNS, SLy5, and SkP Skyrme parametrizations as well as the corresponding values of the RMS nuclear charge radius of the $^{208}_{82}\mathrm{Pb}$ nucleus. The FNS corrections to the ground-state energy $\Delta E_{\mathrm{FNS}}[1s_{1/2}]$ (in units of the electron rest energy) and the g factor $\Delta g_{\mathrm{FNS}}[1s_{1/2}]$ for hydrogenlike lead $^{208}_{82}\mathrm{Pb}^{81+}$ are presented in the last two columns. For comparison, the results for the homogeneously-charged-sphere approximation are also included in the last row.

Model	t_1	x_0	x_3	$\sqrt{\langle \mathrm{r}^2 \rangle}$, fm	$\Delta E_{\mathrm{FNS}}[1s_{1/2}]$ $\times 10^4$	$\Delta g_{\mathrm{FNS}}[1s_{1/2}]$ $\times 10^4$
LNS	266.735	0.06277	-0.03413	5.3238	1.2483	4.3014
SLy5	483.13	0.778	1.267	5.5072	1.3169	4.5369
SkP	320.62	0.29215	0.18103	5.5242	1.3234	4.5590
Sphere	–	–	–	5.5012 [99]	1.3172	4.5380

However, since it is known that the magnitude of the FNS correction is highly influenced by the value of the RMS nuclear radius [100, 101], it would be natural to somehow adjust Skyrme parameters and reproduce the tabulated value of $\sqrt{\langle r^2 \rangle}$ beforehand, similar to how it is done in the case of other models. We found that nuclear radii are most sensitive to varying the Skyrme parameter t_0, and the results of such adjustments in order to obtain $\sqrt{\langle r^2 \rangle} = 5.5012$ fm for $^{208}_{82}$Pb are shown in Table 3.2. It can be seen that, once the value of the RMS nuclear radius is fixed, the magnitudes of the FNS corrections indeed become stable, despite the significant differences between the parameter sets. We tested this procedure on a wide range of nuclei and parametrizations, and we found that a similarly strong suppression of the ambiguity in the choice of a parameter set takes place in all cases. It is important to emphasize that these minor adjustments of $\sqrt{\langle r^2 \rangle}$ do not affect the overall shape of the microscopic charge distributions. On a similar note, while such modifications undoubtedly affect other predictions of the Skyrme model (e.g., nuclear binding energies), one can expect these effects to be reasonably small for most applications, as long as the adjustments lie within the radius tolerance of the Skyrme-force fitting protocol (e.g., 0.02 fm for SLy5 [90]).

In light of the findings of this section, all the "Skyrme" FNS corrections in the following discussion were obtained by using only the SLy5 interaction (which is one of the most widely used parametrizations of the Skyrme force), and the parameter t_0 was adjusted to reproduce the experimental values of RMS nuclear radii in each particular case.

Table 3.2.: Adjustments of the t_0 Skyrme parameter within the LNS, SLy5, and SkP parametrizations (in order to reproduce $\sqrt{\langle r^2 \rangle} = 5.5012$ fm) and the corresponding FNS corrections to the ground-state energy $\Delta E_{\mathrm{FNS}}[1s_{1/2}]$ (in units of the electron rest energy) and the g factor $\Delta g_{\mathrm{FNS}}[1s_{1/2}]$ for hydrogenlike lead $^{208}_{82}\mathrm{Pb}^{81+}$.

Parameter set	Change in t_0	$\Delta E_{\mathrm{FNS}}[1s_{1/2}]$ $\times 10^4$	$\Delta g_{\mathrm{FNS}}[1s_{1/2}]$ $\times 10^4$
LNS	-2484.97 → -2454.60 (1.22%)	1.3148	4.5296
SLy5	-2484.88 → -2486.12 (0.05%)	1.3147	4.5291
SkP	-2931.70 → -2935.95 (0.15%)	1.3147	4.5291

3.3. Atomic energy levels and nuclear radii

In Table 3.3 we present the FNS corrections $\Delta E_{\rm FNS}[1s_{1/2}]$, $\Delta E_{\rm FNS}[2s_{1/2}]$, and $\Delta E_{\rm FNS}[2p_{1/2}]$ calculated by using different nuclear charge distributions for three hydrogenlike ions: ${}^{40}_{20}\mathrm{Ca}^{19+}$, ${}^{116}_{50}\mathrm{Sn}^{49+}$, and ${}^{208}_{82}\mathrm{Pb}^{81+}$. The expansion coefficients for the "Bessel" and "Gauss" experimental charge densities were taken from Ref. [96], while the parameters of all the theoretical models were adjusted to yield the following tabulated values of the RMS nuclear radii: $\sqrt{\langle \mathrm{r}^2 \rangle} = 3.4776(19)$, 4.6250(19), and 5.5012(13) fm for ${}^{40}_{20}\mathrm{Ca}^{19+}$, ${}^{116}_{50}\mathrm{Sn}^{49+}$, and ${}^{208}_{82}\mathrm{Pb}^{81+}$, respectively [99]. We note that there are two different sets of the "Bessel" coefficients for the ${}^{208}_{82}\mathrm{Pb}$ nucleus in the literature [102, 103], and the results only for the parameters from Ref. [103] are presented in Table 3.3 for the sake of simplicity.

One peculiar feature of these FNS corrections is immediately conspicuous: the values from the "Fermi" and "Skyrme" models agree with each other much better than with the results from the experimental "Bessel" and "Gauss" charge distributions. At first glance, this observation might seem surprising, especially when the charge densities themselves are compared side by side. An example of such a comparison for the ${}^{40}_{20}\mathrm{Ca}$ nucleus is shown in Fig. 3.1. It can be seen that the shapes of the "Skyrme" and the experimental charge distributions are in excellent agreement with each other, and yet the difference in the corresponding FNS corrections is larger than even between the "Skyrme" and the "sphere" values. The explanation for this observation comes from the fact that the "Gauss" charge density in Fig. 3.1 yields $\sqrt{\langle \mathrm{r}^2 \rangle} = 3.4797$ fm instead of the tabulated value of 3.4776 fm employed in the theoretical models. Thus, the value of the RMS nuclear radius turns out to be such a crucial input parameter that it can be even more important than the shape of a charge distribution.

This conclusion suggests a straightforward way to estimate the calculation uncertainties for the FNS corrections. Since the main source of uncertainty comes from $\sqrt{\langle \mathrm{r}^2 \rangle}$, one can simply vary its value within the experimental error bars, i.e., by varying the t_0 parameter in the "Skyrme" model, and calculate the corresponding variation in $\Delta E_{\rm FNS}$ or $\Delta g_{\rm FNS}$. The calculation uncertainties obtained in such a manner are presented in Tables 3.3 and 3.4. The results demonstrate that the "Skyrme" and the "Fermi" FNS corrections agree with each other within the current uncertainties in the values of nuclear radii. However, it is clear that the "Skyrme" model provides a more realistic and thus more reliable description of nuclear charge distributions, which will become increasingly important in the future when the values of nuclear radii are known to a higher level of precision.

Table 3.3.: FNS corrections (in units of the electron rest energy) to the energies of the states $1s_{1/2}$, $2s_{1/2}$, and $2p_{1/2}$ for hydrogenlike $^{40}_{20}\mathrm{Ca}^{19+}$, $^{116}_{50}\mathrm{Sn}^{49+}$, and $^{208}_{82}\mathrm{Pb}^{81+}$. Different models of the nuclear charge distribution as well as experimental distributions were used in the calculations. The presented calculation uncertainties correspond to the error bars of the RMS nuclear radii [99].

$^{40}_{20}\mathrm{Ca}^{19+}$		$\Delta E_{\mathrm{FNS}}[1s_{1/2}]$ $\times 10^8$	$\Delta E_{\mathrm{FNS}}[2s_{1/2}]$ $\times 10^9$	$\Delta E_{\mathrm{FNS}}[2p_{1/2}]$ $\times 10^{11}$
	Sphere	2.8514	3.6319	1.4696
	Fermi	2.8502	3.6304	1.4692
	Skyrme	2.8502	3.6303	1.4690
	Bessel	2.8057	3.5737	1.4461
	Gauss	2.8535	3.6345	1.4708
	Skyrme (+rad. unc.)	2.850(3)	3.630(4)	1.469(2)
$^{116}_{50}\mathrm{Sn}^{49+}$		$\Delta E_{\mathrm{FNS}}[1s_{1/2}]$ $\times 10^6$	$\Delta E_{\mathrm{FNS}}[2s_{1/2}]$ $\times 10^7$	$\Delta E_{\mathrm{FNS}}[2p_{1/2}]$ $\times 10^8$
	Sphere	3.7906	5.3366	1.4456
	Fermi	3.7859	5.3299	1.4439
	Skyrme	3.7860	5.3301	1.4439
	Gauss	3.7884	5.3334	1.4448
	Skyrme (+rad. unc.)	3.786(3)	5.330(4)	1.444(1)
$^{208}_{82}\mathrm{Pb}^{81+}$		$\Delta E_{\mathrm{FNS}}[1s_{1/2}]$ $\times 10^4$	$\Delta E_{\mathrm{FNS}}[2s_{1/2}]$ $\times 10^5$	$\Delta E_{\mathrm{FNS}}[2p_{1/2}]$ $\times 10^6$
	Sphere	1.3172	2.2871	1.9590
	Fermi	1.3147	2.2827	1.9554
	Skyrme	1.3147	2.2827	1.9554
	Bessel	1.3155	2.2842	1.9566
	Gauss	1.3155	2.2842	1.9566
	Skyrme (+rad. unc.)	1.3147(4)	2.2827(9)	1.9554(7)

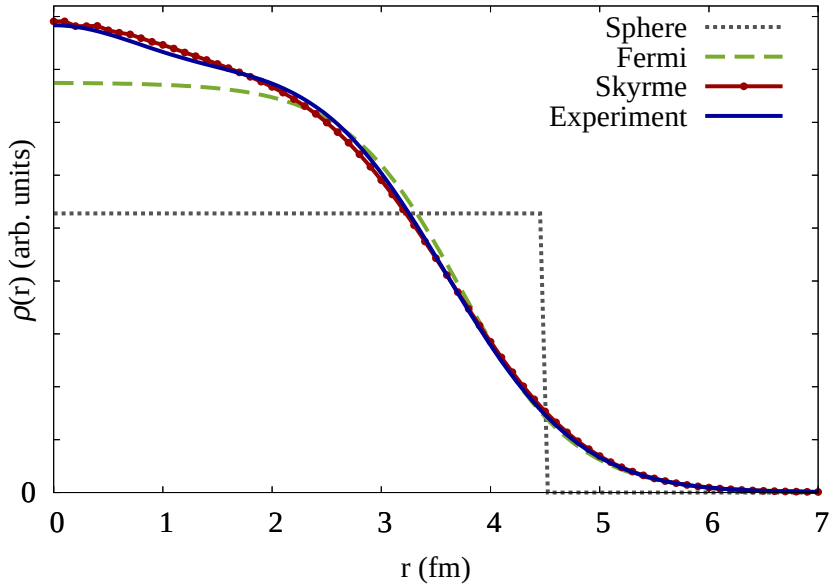

Figure 3.1.: Comparison between an experimental charge distribution ("Gauss") and different models for the $^{40}_{20}$Ca nucleus.

3.4. g factor and specific differences

In general, the same trends as described above for the energy levels hold true also in the case of the FNS corrections to the bound-electron g factor. In this last section we additionally consider the specific differences of the g factors in the $1s_{1/2}$ and $2s_{1/2}$ states as well as in the $1s_{1/2}$ and $2p_{1/2}$ states. These quantities were introduced in Refs. [27, 35] with the aim of suppressing the FNS effect; therefore, they are expected to have more stable values with respect to the choice of a nuclear charge distribution. The specific differences are defined as follows:

$$g'_s = g[2s_{1/2}] - \xi_s g[1s_{1/2}], \quad \xi_s = \frac{\Delta g_{\rm FNS}[2s_{1/2}]}{\Delta g_{\rm FNS}[1s_{1/2}]}, \tag{3.12}$$

$$g'_p = g[2p_{1/2}] - \xi_p g[1s_{1/2}], \quad \xi_p = \frac{\Delta g_{\rm FNS}[2p_{1/2}]}{\Delta g_{\rm FNS}[1s_{1/2}]}. \tag{3.13}$$

Expressions for the weights ξ_s and ξ_p can be obtained by means of the analytical formula for $\Delta g_{\rm FNS}$ that was derived in Ref. [101] within the second-order perturbation

theory. The corresponding expansions in powers of $(Z\alpha)$ read as follows:

$$\xi_s = \frac{1}{8} + 0.110081(Z\alpha)^2 + 0.0615871(Z\alpha)^4 + 0.0302009(Z\alpha)^6 + 0.0148406(Z\alpha)^8 + \{\text{h.o.}\}, \tag{3.14}$$

$$\xi_p = \frac{3}{128}(Z\alpha)^2 + 0.0333355(Z\alpha)^4 + 0.0312421(Z\alpha)^6 + 0.0257139(Z\alpha)^8 + \{\text{h.o.}\}. \tag{3.15}$$

The calculated values of $\Delta g'_{\rm FNS} = g'_{\rm ext} - g'_{\rm point}$ for the weights (3.14) and (3.15), together with the FNS corrections to the g factors in the states $1s_{1/2}$, $2s_{1/2}$, and $2p_{1/2}$ for ${}^{40}_{20}\mathrm{Ca}^{19+}$, ${}^{116}_{50}\mathrm{Sn}^{49+}$, and ${}^{208}_{82}\mathrm{Pb}^{81+}$, are shown in Table 3.4. It can be seen that for the specific differences g'_s and g'_p the FNS effect is indeed suppressed by several orders of magnitude. However, we also found that a much stronger suppression can be achieved by evaluating ξ_s and ξ_p numerically, e.g., within the homogeneously-charged-sphere approximation, and then using the obtained weights for other nuclear models. For instance, in this approach the corrections $\Delta g'_{s,\rm FNS}$ and $\Delta g'_{p,\rm FNS}$ for ${}^{208}_{82}\mathrm{Pb}^{81+}$ within the "Skyrme" model become only -1.1×10^{-9} and 5.4×10^{-10}, respectively, which is 2–3 orders of magnitude smaller than the corresponding values given in Table 3.4. This shows that in the case of heavy ions a direct numerical calculation of ξ_s and ξ_p should be preferred over using analytical perturbation-theory formulas.

Table 3.4.: FNS corrections to the g factors in the states $1s_{1/2}$, $2s_{1/2}$, and $2p_{1/2}$ for hydrogenlike $^{40}_{20}\mathrm{Ca}^{19+}$, $^{116}_{50}\mathrm{Sn}^{49+}$, and $^{208}_{82}\mathrm{Pb}^{81+}$. In the last two columns the magnitudes of the remaining FNS contributions to the specific differences g'_s and g'_p are presented (using the weights given by Eqs. (3.14) and (3.15)). Different models of the nuclear charge distribution as well as experimental distributions were used in the calculations. The presented calculation uncertainties correspond to the error bars of the RMS nuclear radii [99].

$^{40}_{20}\mathrm{Ca}^{19+}$		$\Delta g_{\mathrm{FNS}}[1s_{1/2}]$ $\times 10^7$	$\Delta g_{\mathrm{FNS}}[2s_{1/2}]$ $\times 10^8$	$\Delta g_{\mathrm{FNS}}[2p_{1/2}]$ $\times 10^{11}$	$\Delta g'_{s,\mathrm{FNS}}$ $\times 10^{13}$	$\Delta g'_{p,\mathrm{FNS}}$ $\times 10^{13}$
	Sphere	1.1316	1.4413	5.8293	-2.0	0.5
	Fermi	1.1311	1.4407	5.7672	-1.0	-5.4
	Skyrme	1.1311	1.4406	5.8504	-5.1	5.0
	Bessel	1.1134	1.4182	5.7560	1.5	2.5
	Gauss	1.1324	1.4423	5.8395	-2.0	1.2
	Skyrme (+rad. unc.)	1.131(1)	1.441(1)	5.85(2)	–	–
$^{116}_{50}\mathrm{Sn}^{49+}$		$\Delta g_{\mathrm{FNS}}[1s_{1/2}]$ $\times 10^5$	$\Delta g_{\mathrm{FNS}}[2s_{1/2}]$ $\times 10^6$	$\Delta g_{\mathrm{FNS}}[2p_{1/2}]$ $\times 10^8$	$\Delta g'_{s,\mathrm{FNS}}$ $\times 10^{10}$	$\Delta g'_{p,\mathrm{FNS}}$ $\times 10^{10}$
	Sphere	1.4426	2.0308	5.5116	-7.32	3.87
	Fermi	1.4407	2.0282	5.5050	-7.41	3.92
	Skyrme	1.4408	2.0282	5.5052	-7.40	3.91
	Gauss	1.4417	2.0295	5.5086	-7.41	3.92
	Skyrme (+rad. unc.)	1.411(1)	2.028(2)	5.505(5)	–	–
$^{208}_{82}\mathrm{Pb}^{81+}$		$\Delta g_{\mathrm{FNS}}[1s_{1/2}]$ $\times 10^4$	$\Delta g_{\mathrm{FNS}}[2s_{1/2}]$ $\times 10^5$	$\Delta g_{\mathrm{FNS}}[2p_{1/2}]$ $\times 10^6$	$\Delta g'_{s,\mathrm{FNS}}$ $\times 10^7$	$\Delta g'_{p,\mathrm{FNS}}$ $\times 10^7$
	Sphere	4.5380	7.8734	6.7814	-2.271	1.138
	Fermi	4.5292	7.8579	6.7687	-2.278	1.141
	Skyrme	4.5291	7.8579	6.7687	-2.278	1.141
	Bessel	4.5321	7.8630	6.7731	-2.280	1.142
	Gauss	4.5320	7.8629	6.7730	-2.280	1.142
	Skyrme (+rad. unc.)	4.529(2)	7.858(3)	6.769(2)	–	–

4. Nuclear-polarization effect

Perhaps, the most challenging nuclear effects in atomic systems to describe are those stemming from dynamic interactions between atomic and internal nuclear degrees of freedom. Such effects of nuclear excitations upon an atomic spectrum are known in the literature under two distinct names corresponding to different computational procedures required. If exact matrix diagonalizations must be carried out, as in the case of muonic atoms with deformed nuclei, the resulting mixed energy-level structure is referred to as dynamic hyperfine splitting. Otherwise, for a wide range of systems the dynamic effects can be treated in perturbation theory, and they are generally called nuclear polarization (NP). It is the latter that this final and main chapter is devoted to. Here, we consider not only the "ordinary" electrons as bound atomic particles but also their heavier cousins, the muons. For this reason, we collectively refer to them as bound fermions in general derivations.
The chapter is organized as follows. First, in Section 4.1, a field-theoretical framework for evaluating NP energy shifts of atomic energy levels is presented. Next, in Section 4.2, this approach is applied to the problem of the fine-structure anomalies in muonic atoms. Afterwards, in Section 4.3, the longitudinal approximation of the method is extended to evaluate the NP correction to the bound-electron g factor in H-like ions. Finally, in Section 4.4, the suppression of the NP effect is investigated for a newly proposed weighted difference named the reduced g factor.

4.1. Atomic energy levels

4.1.1. Modified photon propagator

The derivations in Section 4.1 follow, combine and extend the ideas presented in Refs. [104–107]. The starting point of a perturbative field-theoretical treatment of dynamic nuclear effects is to express the total nuclear four-current density as the following sum:

$$\hat{J}^{\mu}_{\mathrm{N,\,total}}(x) = J^{\mu}_{\mathrm{N,\,stat}}(\mathbf{x}) + \hat{J}^{\mu}_{\mathrm{N,\,fluc}}(x), \tag{4.1}$$

with the static part $J^{\mu}_{\mathrm{N,\,stat}}$ (c-number) corresponding to the nuclear ground state and the fluctuating part $\hat{J}^{\mu}_{\mathrm{N,\,fluc}}$ describing intrinsic nuclear dynamics due to external electromagnetic excitations. In a similar spirit to the external-field approximation

from Chapter 1, where $J^\mu_{\mathrm{N,\,stat}}$ is taken into account by introducing the corresponding classical field $\mathcal{A}^\mu_{\mathrm{stat}}$ and the Lagrangian term (1.6), we associate with the fluctuating current $\hat{J}^\mu_{\mathrm{N,\,fluc}}$ a second-quantized photon field $\hat{A}^\mu_{\mathrm{fluc}}$. In this view, the Dirac four-current $\hat{j}^\mu_{\mathrm{f}}$ of a bound fermion interacts with the total electromagnetic field

$$\hat{A}^\mu_{\mathrm{total}}(x) = \mathcal{A}^\mu_{\mathrm{stat}}(\mathbf{x}) + \hat{A}^\mu_{\mathrm{fluc}}(x) + \hat{A}^\mu_{\mathrm{free}}(x) \coloneqq \mathcal{A}^\mu_{\mathrm{stat}}(\mathbf{x}) + \hat{A}^\mu_{\mathrm{rad}}(x), \tag{4.2}$$

where the total quantum radiation field $\hat{A}^\mu_{\mathrm{rad}}$ is defined as the sum of the free photon field $\hat{A}^\mu_{\mathrm{free}}$ and the fluctuating part $\hat{A}^\mu_{\mathrm{fluc}}$ generated by $\hat{J}^\mu_{\mathrm{N,\,fluc}}$. The latter is described by the following equation of motion (where for simplicity we assume the gauge-fixing parameter $\xi = 1$):

$$\partial^2 \hat{A}^\mu_{\mathrm{fluc}}(x) = \hat{J}^\mu_{\mathrm{N,\,fluc}}(x). \tag{4.3}$$

As a consequence, one is lead to the modified photon propagator

$$\begin{aligned} i\mathcal{D}_{\mu\nu}(x,x') &= \langle 0|T[\hat{A}^{\mathrm{rad}}_\mu(x)\hat{A}^{\mathrm{rad}}_\nu(x')]|0\rangle \\ &= \langle 0|T[\hat{A}^{\mathrm{free}}_\mu(x)\hat{A}^{\mathrm{free}}_\nu(x')]|0\rangle \\ &+ \langle 0|T[\hat{A}^{\mathrm{free}}_\mu(x)\hat{A}^{\mathrm{fluc}}_\nu(x')]|0\rangle + \langle 0|T[\hat{A}^{\mathrm{fluc}}_\mu(x)\hat{A}^{\mathrm{free}}_\nu(x')]|0\rangle \\ &+ \langle 0|T[\hat{A}^{\mathrm{fluc}}_\mu(x)\hat{A}^{\mathrm{fluc}}_\nu(x')]|0\rangle, \end{aligned} \tag{4.4}$$

whereas the usual free photon propagator is given by

$$iD_{\mu\nu}(x-x') = \langle 0|T[\hat{A}^{\mathrm{free}}_\mu(x)\hat{A}^{\mathrm{free}}_\nu(x')]|0\rangle, \tag{4.5}$$

where $|0\rangle$ denotes the "vacuum" state in the presence of the external field $\mathcal{A}^\mu_{\mathrm{stat}}(\mathbf{x})$, which corresponds to the nucleus being in its ground state. The last term in Eq. (4.4) can be rewritten as

$$\begin{aligned} &\langle 0|T[\hat{A}^{\mathrm{fluc}}_\mu(x)\hat{A}^{\mathrm{fluc}}_\nu(x')]|0\rangle \\ &= \int d^4x_1\, d^4x_2\, \eta_{\mu\xi}\delta^{(4)}(x-x_1)\langle 0|T[\hat{A}^\xi_{\mathrm{fluc}}(x_1)\hat{A}^\zeta_{\mathrm{fluc}}(x_2)]|0\rangle\eta_{\zeta\nu}\delta^{(4)}(x_2-x') \\ &= \int d^4x_1\, d^4x_2\, \{\partial^2_{x_1} D_{\mu\xi}(x-x_1)\}\langle 0|T[\hat{A}^\xi_{\mathrm{fluc}}(x_1)\hat{A}^\zeta_{\mathrm{fluc}}(x_2)]|0\rangle\{\partial^2_{x_2} D_{\zeta\nu}(x_2-x')\} \\ &= \int d^4x_1\, d^4x_2\, D_{\mu\xi}(x-x_1)\langle 0|\partial^2_{x_2}\partial^2_{x_1} T[\hat{A}^\xi_{\mathrm{fluc}}(x_1)\hat{A}^\zeta_{\mathrm{fluc}}(x_2)]|0\rangle D_{\zeta\nu}(x_2-x'), \end{aligned} \tag{4.6}$$

where in the last step we have performed four integrations by parts with vanishing boundary terms, while in the step before we have used the fact that the free photon propagator is the Green's function of the free equation of motion

$$\partial^2 D_{\mu\nu}(x) = \eta_{\mu\nu}\delta^{(4)}(x). \tag{4.7}$$

It is important to bear in mind that the derivatives in the last line of Eq. (4.6) act not only on the fields $\hat{A}^{\mu}_{\text{fluc}}$ but also on the θ-functions from the time-ordered product:

$$\begin{aligned}
&\langle 0|T[\hat{A}^{\text{fluc}}_{\mu}(x)\hat{A}^{\text{fluc}}_{\nu}(x')]|0\rangle \\
&= \int d^4x_1\, d^4x_2\, D_{\mu\xi}(x-x_1)\langle 0|T[\{\partial^2_{x_1}\hat{A}^{\xi}_{\text{fluc}}(x_1)\}\{\partial^2_{x_2}\hat{A}^{\zeta}_{\text{fluc}}(x_2)\}]|0\rangle D_{\zeta\nu}(x_2-x') \\
&+ \text{additional terms} \\
&= \int d^4x_1\, d^4x_2\, D_{\mu\xi}(x-x_1)\langle 0|T[\hat{J}^{\xi}_{\text{N, fluc}}(x_1)\hat{J}^{\zeta}_{\text{N, fluc}}(x_2)]|0\rangle D_{\zeta\nu}(x_2-x') \\
&+ \text{additional terms,}
\end{aligned} \tag{4.8}$$

where the resulting two-point current correlation function defines the so-called nuclear-polarization tensor

$$i\Pi^{\xi\zeta}_{\text{N}}(x_1,x_2) \coloneqq \langle 0|T[\hat{J}^{\xi}_{\text{N, fluc}}(x_1)\hat{J}^{\zeta}_{\text{N, fluc}}(x_2)]|0\rangle. \tag{4.9}$$

It was pointed out by Kenneth Johnson in 1961 [108] that such a time-ordered product of two currents is in general not a covariant function. Thus, the role of the "additional terms" in Eq. (4.8) is to maintain the Lorentz covariance of the vacuum expectation value $\langle 0|T[\hat{A}^{\text{fluc}}_{\mu}(x)\hat{A}^{\text{fluc}}_{\nu}(x')]|0\rangle$ and the modified photon propagator as a whole. In principle, these terms can be obtained directly by taking the derivatives with respect to the θ-functions in Eq. (4.6) and then evaluating the resulting commutators in terms of the canonical variables in the Hamiltonian formalism [109]. Fortunately, there is a less tedious way of inferring the form of these contributions. According to the work of Lowell Brown [110], a proper two-point current correlation operator with the restored Lorentz covariance can be defined as the second-order response of a system to an external electromagnetic field. He also showed that, besides the time-ordered product (4.9), this operator contains only one additional term, which we will denote in our case as $iS^{\xi\zeta}_{\text{N}}(x_1,x_2)$. Moreover, the requirement of gauge invariance implies that [110]

$$\partial_{x_1,\xi}\left(i\Pi^{\xi\zeta}_{\text{N}}(x_1,x_2) + iS^{\xi\zeta}_{\text{N}}(x_1,x_2)\right) = 0, \tag{4.10}$$

which leads to

$$\begin{aligned}
&\langle 0|\delta(x^0_1-x^0_2)[\hat{J}^{0}_{\text{N, fluc}}(x_1),\hat{J}^{\zeta}_{\text{N, fluc}}(x_2)]|0\rangle \\
&+ \langle 0|T[\partial_{x_1,\xi}\hat{J}^{\xi}_{\text{N, fluc}}(x_1)\hat{J}^{\zeta}_{\text{N, fluc}}(x_2)]|0\rangle + i\partial_{x_1,\xi}S^{\xi\zeta}_{\text{N}}(x_1,x_2) = 0,
\end{aligned} \tag{4.11}$$

where the second term is equal to zero due to the continuity equation of nuclear charge conservation. While the equal-time commutator in Eq. (4.11) vanishes for $\zeta = 0$, it was shown by Julian Schwinger from fundamental principles of quantum

field theory that charge and current ($\zeta = 1, 2, 3$) densities cannot commute at a common time [111]. It follows from Eq. (4.11) that these non-vanishing commutators, known as the Schwinger terms, must be cancelled by the divergence of $iS_{\mathrm{N}}^{\xi\zeta}$, if gauge invariance is to be satisfied. The contribution $iS_{\mathrm{N}}^{\xi\zeta}$ is often called the "seagull" or "catastrophic" term, and this kind of cancellation is in fact a very general result in current-algebra theories [112].

At this point, it is clear that the expression of the seagull term depends on a specific definition of $\hat{J}^{\mu}_{\mathrm{N,\,fluc}}$. In this thesis, we employ the non-relativistic nuclear charge-current density operators (see Appendix B), and it can be shown that in this case the seagull term takes on the following form [107]:

$$S_{\mathrm{N}}^{\xi\zeta}(x_1, x_2) = \frac{|e|\langle 0|\hat{J}^{0}_{\mathrm{N,\,fluc}}(0, \mathbf{x}_1)|0\rangle}{M_{\mathrm{p}}} \delta^{\xi\zeta}\delta^{(4)}(x_1 - x_2), \tag{4.12}$$

where M_{p} is the proton mass, and $\delta^{\xi\zeta}$ is the Kronecker delta extended to four dimensions with $\delta^{00} = 0$. The contribution (4.12) describes the coupling of the electromagnetic currents at the same point, and its physical significance is to ensure gauge invariance of the calculated NP corrections.

Finally, going back to Eq. (4.4), it is clear that the mixed terms vanish:

$$\langle 0|T[\hat{A}^{\mathrm{fluc}}_{\mu}(x)\hat{A}^{\mathrm{free}}_{\nu}(x')]|0\rangle = \langle 0|T[\hat{A}^{\mathrm{free}}_{\mu}(x)\hat{A}^{\mathrm{fluc}}_{\nu}(x')]|0\rangle = 0, \tag{4.13}$$

such that the expression for the modified photon propagator can be written as

$$\mathcal{D}_{\mu\nu}(x, x') = D_{\mu\nu}(x - x') + D^{\mathrm{NP}}_{\mu\nu}(x, x'), \tag{4.14}$$

defining the NP correction $D^{\mathrm{NP}}_{\mu\nu}(x, x')$ to the free photon propagator as follows:

$$D^{\mathrm{NP}}_{\mu\nu}(x, x') \coloneqq \int d^4x_1\, d^4x_2\, D_{\mu\xi}(x - x_1) \left[\Pi_{\mathrm{N}}^{\xi\zeta}(x_1, x_2) + S_{\mathrm{N}}^{\xi\zeta}(x_1, x_2)\right] D_{\zeta\nu}(x_2 - x'). \tag{4.15}$$

4.1.2. Effective self-energy

The concept of the modified photon propagator as the simple sum in Eq. (4.14) allows a systematic treatment of the NP effect by putting it on the same footing as the usual QED corrections. In particular, the additional term $D^{\mathrm{NP}}_{\mu\nu}(x, x')$ in the context of the self-energy correction leads to the effective diagram shown in Fig. 4.1, where the sum $\left[\Pi_{\mathrm{N}}^{\xi\zeta}(x_1, x_2) + S_{\mathrm{N}}^{\xi\zeta}(x_1, x_2)\right]$ is represented by a shaded blob and called the NP insertion. This correction to the self-energy due to nuclear dynamics is sometimes referred to as the "ordinary NP correction", and it is the main focus of this chapter. In the following, only the $\hat{J}^{\mu}_{\mathrm{N,\,fluc}}$ part of the nuclear four-current density will be considered; therefore, the subscript "fluc" will be omitted for the sake of notational simplicity.

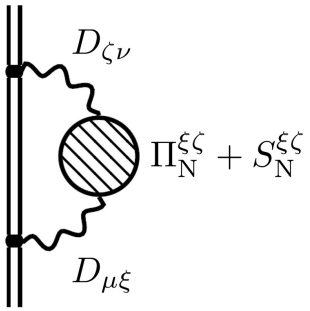

Figure 4.1.: NP as effective self-energy. A bound fermion and a photon are indicated by the double and wavy lines, respectively. The shaded blob represents the NP insertion.

In order to evaluate the effective self-energy diagram, we first want to express the NP tensor in terms of directly calculable quantities. For this purpose, we explicitly write out the time ordering in Eq. (4.9):

$$\begin{aligned}\langle 0|T[\hat{J}_{\mathrm{N}}^{\xi}(t_1,\mathbf{x}_1)\hat{J}_{\mathrm{N}}^{\zeta}(t_2,\mathbf{x}_2)]|0\rangle &= \theta(t_1-t_2)\langle 0|\hat{J}_{\mathrm{N}}^{\xi}(t_1,\mathbf{x}_1)\hat{J}_{\mathrm{N}}^{\zeta}(t_2,\mathbf{x}_2)|0\rangle \\ &\quad + \theta(t_2-t_1)\langle 0|\hat{J}_{\mathrm{N}}^{\zeta}(t_2,\mathbf{x}_2)\hat{J}_{\mathrm{N}}^{\xi}(t_1,\mathbf{x}_1)|0\rangle.\end{aligned} \tag{4.16}$$

From now on, we will denote the nuclear ground state as $|I\rangle$ and use the explicit notation $|0\rangle \equiv |I\rangle$. By assuming that the nuclear four-current density is evolved by a collective Hamiltonian $\hat{H}_{\mathrm{N}}$, inserting a complete set of nuclear excitations $|I'\rangle$ and employing the integral representation of the θ-function, we can rewrite the first term in Eq. (4.16) as follows:

$$\begin{aligned}&\theta(t_1-t_2)\langle I|\hat{J}_{\mathrm{N}}^{\xi}(t_1,\mathbf{x}_1)\hat{J}_{\mathrm{N}}^{\zeta}(t_2,\mathbf{x}_2)|I\rangle \\ &= \theta(t_1-t_2)\sum_{I'}\langle I|e^{i\hat{H}_{\mathrm{N}}t_1}\hat{J}_{\mathrm{N}}^{\xi}(0,\mathbf{x}_1)e^{-i\hat{H}_{\mathrm{N}}t_1}|I'\rangle\langle I'|e^{i\hat{H}_{\mathrm{N}}t_2}\hat{J}_{\mathrm{N}}^{\zeta}(0,\mathbf{x}_2)e^{-i\hat{H}_{\mathrm{N}}t_2}|I\rangle \\ &= \int\frac{ds}{2\pi i}\frac{e^{is(t_1-t_2)}}{s-i0}\sum_{I'}e^{-i(E_{I'}-E_I)(t_1-t_2)}\langle I|\hat{J}_{\mathrm{N}}^{\xi}(0,\mathbf{x}_1)|I'\rangle\langle I'|\hat{J}_{\mathrm{N}}^{\zeta}(0,\mathbf{x}_2)|I\rangle \\ &= \int\frac{d\omega}{2\pi i}e^{-i\omega(t_1-t_2)}\sum_{I'}\frac{\langle I|\hat{J}_{\mathrm{N}}^{\xi}(0,\mathbf{x}_1)|I'\rangle\langle I'|\hat{J}_{\mathrm{N}}^{\zeta}(0,\mathbf{x}_2)|I\rangle}{\omega_{\mathrm{N}}-\omega-i0},\end{aligned} \tag{4.17}$$

where $\omega_{\mathrm{N}} = E_{I'} - E_I$, and the substitution $\omega = \omega_{\mathrm{N}} - s$ is performed in the last step. In what follows, the time-independent four-current densities $\hat{J}_{\mathrm{N}}^{\xi}(0,\mathbf{x})$ will be written simply as $\hat{J}_{\mathrm{N}}^{\xi}(\mathbf{x})$ for brevity purposes. After performing analogous steps for the second term in Eq. (4.16), one obtains the following expression for the NP tensor, which becomes homogeneous in time:

$$\Pi_{\mathrm{N}}^{\xi\zeta}(t_1-t_2,\mathbf{x}_1,\mathbf{x}_2) = \int\frac{d\omega}{2\pi}\,e^{-i\omega(t_1-t_2)}\,\Pi_{\mathrm{N}}^{\xi\zeta}(\omega,\mathbf{x}_1,\mathbf{x}_2), \tag{4.18}$$

where

$$\Pi_{\mathrm{N}}^{\xi\zeta}(\omega,\mathbf{x}_1,\mathbf{x}_2)=\sum_{I'}\left(\frac{\langle I|\hat{J}_{\mathrm{N}}^{\xi}(\mathbf{x}_1)|I'\rangle\langle I'|\hat{J}_{\mathrm{N}}^{\zeta}(\mathbf{x}_2)|I\rangle}{\omega-\omega_{\mathrm{N}}+i0}-\frac{\langle I'|\hat{J}_{\mathrm{N}}^{\xi}(\mathbf{x}_1)|I\rangle\langle I|\hat{J}_{\mathrm{N}}^{\zeta}(\mathbf{x}_2)|I'\rangle}{\omega+\omega_{\mathrm{N}}-i0}\right). \tag{4.19}$$

Similarly, the Fourier-transformed version of the seagull term reads

$$S_{\mathrm{N}}^{\xi\zeta}(\omega,\mathbf{x}_1,\mathbf{x}_2)=\frac{|e|\langle I|\hat{\rho}_{\mathrm{N}}(\mathbf{x}_1)|I\rangle}{M_{\mathrm{p}}}\delta^{\xi\zeta}\delta^{(3)}(\mathbf{x}_1-\mathbf{x}_2). \tag{4.20}$$

Next, before making use of the two-time Green's function method, we need an expression of the NP correction to the photon propagator in the energy representation. By using Eq. (4.18) together with the relation

$$D_{\mu\xi}(x-x_1)=\int\frac{d\omega'}{2\pi}\,e^{-i\omega'(t-t_1)}D_{\mu\xi}(\omega',\mathbf{x}-\mathbf{x}_1), \tag{4.21}$$

one readily obtains for $D_{\mu\nu}^{\mathrm{NP}}(x,x')$ the following:

$$\begin{aligned}D_{\mu\nu}^{\mathrm{NP}}(x,x')&=\int d^3x_1d^3x_2dt_1dt_2\frac{d\omega'}{2\pi}e^{-i\omega'(t-t_1)}\frac{d\omega}{2\pi}e^{-i\omega(t_1-t_2)}\frac{d\omega''}{2\pi}e^{-i\omega''(t_2-t')}\\&\times D_{\mu\xi}(\omega',\mathbf{x}-\mathbf{x}_1)\left[\Pi_{\mathrm{N}}^{\xi\zeta}(\omega,\mathbf{x}_1,\mathbf{x}_2)+S_{\mathrm{N}}^{\xi\zeta}(\omega,\mathbf{x}_1,\mathbf{x}_2)\right]D_{\zeta\nu}(\omega'',\mathbf{x}_2-\mathbf{x}')\\&=\int\frac{d\omega}{2\pi}e^{-i\omega(t-t')}D_{\mu\nu}^{\mathrm{NP}}(\omega,\mathbf{x},\mathbf{x}'),\end{aligned} \tag{4.22}$$

such that the desired expression is given by

$$\begin{aligned}D_{\mu\nu}^{\mathrm{NP}}(\omega,\mathbf{x},\mathbf{x}')\coloneqq\int d^3x_1d^3x_2D_{\mu\xi}(\omega,\mathbf{x}-\mathbf{x}_1)\left[\Pi_{\mathrm{N}}^{\xi\zeta}(\omega,\mathbf{x}_1,\mathbf{x}_2)+S_{\mathrm{N}}^{\xi\zeta}(\omega,\mathbf{x}_1,\mathbf{x}_2)\right]\\\times D_{\zeta\nu}(\omega,\mathbf{x}_2-\mathbf{x}').\end{aligned} \tag{4.23}$$

The corresponding Feynman rule for the Green's function $G(\{E',\mathbf{x}'\};\{E,\mathbf{x}\})$ is depicted in Fig. 4.2. With this new prescription, we can write for the effective self-energy diagram:

$$\begin{aligned}G((E',\mathbf{x}');(E,\mathbf{x}))=\int d^3x_1d^3x_2d\eta d\omega\,&\frac{i}{2\pi}S(E',\mathbf{x}',\mathbf{x}_1)2\pi i|e|\gamma^{\mu}\delta(E'-\eta-\omega)\\&\times\frac{i}{2\pi}S(\eta,\mathbf{x}_1,\mathbf{x}_2)2\pi i|e|\gamma^{\nu}\delta(\eta+\omega-E)\\&\times\frac{i}{2\pi}S(E,\mathbf{x}_2,\mathbf{x})\frac{i}{2\pi}D_{\mu\nu}^{\mathrm{NP}}(\omega,\mathbf{x}_1,\mathbf{x}_2),\end{aligned} \tag{4.24}$$

where $\mathbf{x}_1$ and $\mathbf{x}_2$ denote the vertices in the coordinate space, η and ω are the

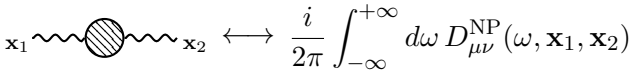

$$\longleftrightarrow \frac{i}{2\pi}\int_{-\infty}^{+\infty} d\omega\, D^{\mathrm{NP}}_{\mu\nu}(\omega,\mathbf{x}_1,\mathbf{x}_2)$$

Figure 4.2.: The additional Feynman rule for evaluating the NP correction to the photon propagator.

energies of the virtual fermion and photon, respectively, and S is the bound-fermion propagator. After integrating over η, Eq. (4.24) can be simplified to

$$\begin{aligned} G((E',\mathbf{x}');(E,\mathbf{x})) = \left(\frac{ie}{2\pi}\right)^2 \int d^3x_1 d^3x_2 d\omega\, S(E',\mathbf{x}',\mathbf{x}_1)\gamma^\mu S(E'-\omega,\mathbf{x}_1,\mathbf{x}_2) \\ \times\gamma^\nu S(E,\mathbf{x}_2,\mathbf{x}) D^{\mathrm{NP}}_{\mu\nu}(\omega,\mathbf{x}_1,\mathbf{x}_2)\delta(E-E'). \end{aligned} \tag{4.25}$$

In order to calculate the corresponding energy shift of a bound-fermion state $|i\rangle$, one needs the function $\Delta g_{ii}(E)$:

$$\begin{aligned} \Delta g^{(1)}_{ii}(E)\delta(E-E') = \frac{2\pi}{i}\langle i|G(E',E)\gamma^0|i\rangle = \frac{ie^2}{2\pi}\int d^3x d^3x' d^3x_1 d^3x_2 d\omega \\ \times\psi_i^\dagger(\mathbf{x}')\sum_{n_1}\frac{\psi_{n_1}(\mathbf{x}')\bar\psi_{n_1}(\mathbf{x}_1)}{E'-\varepsilon_{n_1}(1-i0)}\gamma^\mu\sum_{n_2}\frac{\psi_{n_2}(\mathbf{x}_1)\bar\psi_{n_2}(\mathbf{x}_2)}{E'-\omega-\varepsilon_{n_2}(1-i0)} \\ \times\gamma^\nu\sum_{n_3}\frac{\psi_{n_3}(\mathbf{x}_2)\bar\psi_{n_3}(\mathbf{x})}{E-\varepsilon_{n_3}(1-i0)}\gamma^0\psi_i(\mathbf{x})D^{\mathrm{NP}}_{\mu\nu}(\omega,\mathbf{x}_1,\mathbf{x}_2)\delta(E-E'), \end{aligned} \tag{4.26}$$

which simplifies due to the orthogonality condition for the fermion wave functions ψ as follows:

$$\begin{aligned} \Delta g^{(1)}_{ii}(E) = \frac{ie^2}{2\pi}\frac{1}{(E-\varepsilon_i)^2}\sum_{n_2}\int d^3x_1 d^3x_2 d\omega \\ \times\frac{\bar\psi_i(\mathbf{x}_1)\gamma^\mu\psi_{n_2}(\mathbf{x}_1)\bar\psi_{n_2}(\mathbf{x}_2)\gamma^\nu\psi_i(\mathbf{x}_2)}{E-\omega-\varepsilon_{n_2}(1-i0)}D^{\mathrm{NP}}_{\mu\nu}(\omega,\mathbf{x}_1,\mathbf{x}_2). \end{aligned} \tag{4.27}$$

After renaming the dummy index n_2 to i' and using Eq. (1.31), we obtain for the NP energy shift:

$$\begin{aligned} \Delta E^{(1)}_{i,\mathrm{NP}} &= \frac{1}{2\pi i}\oint_\Gamma dE\,(E-\varepsilon_i)\Delta g^{(1)}_{ii}(E) \\ &= \frac{ie^2}{2\pi}\sum_{i'}\int d^3x_1 d^3x_2 d\omega\,\frac{\bar\psi_i(\mathbf{x}_1)\gamma^\mu\psi_{i'}(\mathbf{x}_1)\bar\psi_{i'}(\mathbf{x}_2)\gamma^\nu\psi_i(\mathbf{x}_2)}{\varepsilon_i-\omega-\varepsilon_{i'}(1-i0)}D^{\mathrm{NP}}_{\mu\nu}(\omega,\mathbf{x}_1,\mathbf{x}_2), \end{aligned} \tag{4.28}$$

where, similar to the nuclear excitation energies ω_{N}, one can define for the bound fermion: $\omega_{\mathrm{f}} = \varepsilon_{i'} - \varepsilon_i$. In addition, one also recognizes in the numerator of Eq. (4.28) matrix elements of the Dirac four-current operator

$$\hat j^\mu_{\mathrm{f}}(\mathbf{x}) = -|e|\,\delta^{(3)}(\mathbf{x}-\mathbf{x}_{\mathrm{f}})\alpha^\mu, \quad \alpha^\mu = (\mathbb{1}_4,\boldsymbol{\alpha}) = \gamma^0\gamma^\mu. \tag{4.29}$$

Finally, it is convenient to split the total correction $\Delta E^{(1)}_{i,\mathrm{NP}}$ into three separate contributions corresponding to the two terms coming from Eq. (4.19) and the seagull term. In this way, the effective self-energy diagram can be equivalently expressed as a sum of the ladder (L), cross (X) and seagull (SG) diagrams shown in Fig. 4.3:

$$\Delta E^{(1)}_{i,\mathrm{NP}} = \Delta E^{\mathrm{L}}_{i,\mathrm{NP}} + \Delta E^{\mathrm{X}}_{i,\mathrm{NP}} + \Delta E^{\mathrm{SG}}_{i,\mathrm{NP}}, \tag{4.30}$$

where

$$\begin{aligned}\Delta E^{\mathrm{L}}_{i,\mathrm{NP}} = -\frac{i}{2\pi}\sum_{i'I'}\int d^3x_1 d^3x_2 d^3x_3 d^3x_4 d\omega\, D_{\mu\xi}(\omega,\mathbf{x}_1-\mathbf{x}_3)D_{\zeta\nu}(\omega,\mathbf{x}_4-\mathbf{x}_2)\\ \times\frac{\langle i|\hat{j}^{\mu}_{\mathrm{f}}(\mathbf{x}_1)|i'\rangle\langle i'|\hat{j}^{\nu}_{\mathrm{f}}(\mathbf{x}_2)|i\rangle}{\omega+\omega_{\mathrm{f}}-i\varepsilon_{i'}0}\,\frac{\langle I|\hat{J}^{\xi}_{\mathrm{N}}(\mathbf{x}_3)\,|I'\rangle\langle I'|\hat{J}^{\zeta}_{\mathrm{N}}(\mathbf{x}_4)\,|I\rangle}{\omega-\omega_{\mathrm{N}}+i0},\end{aligned} \tag{4.31}$$

$$\begin{aligned}\Delta E^{\mathrm{X}}_{i,\mathrm{NP}} = +\frac{i}{2\pi}\sum_{i'I'}\int d^3x_1 d^3x_2 d^3x_3 d^3x_4 d\omega\, D_{\mu\xi}(\omega,\mathbf{x}_1-\mathbf{x}_3)D_{\zeta\nu}(\omega,\mathbf{x}_4-\mathbf{x}_2)\\ \times\frac{\langle i|\hat{j}^{\mu}_{\mathrm{f}}(\mathbf{x}_1)|i'\rangle\langle i'|\hat{j}^{\nu}_{\mathrm{f}}(\mathbf{x}_2)|i\rangle}{\omega+\omega_{\mathrm{f}}-i\varepsilon_{i'}0}\,\frac{\langle I'|\hat{J}^{\xi}_{\mathrm{N}}(\mathbf{x}_3)\,|I\rangle\langle I|\hat{J}^{\zeta}_{\mathrm{N}}(\mathbf{x}_4)\,|I'\rangle}{\omega+\omega_{\mathrm{N}}-i0},\end{aligned} \tag{4.32}$$

$$\begin{aligned}\Delta E^{\mathrm{SG}}_{i,\mathrm{NP}} = -\frac{i}{2\pi}\sum_{i'}\int d^3x_1 d^3x_2 d^3x_3 d\omega\, D_{\mu\xi}(\omega,\mathbf{x}_1-\mathbf{x}_3)D_{\zeta\nu}(\omega,\mathbf{x}_3-\mathbf{x}_2)\\ \times\frac{\langle i|\hat{j}^{\mu}_{\mathrm{f}}(\mathbf{x}_1)|i'\rangle\langle i'|\hat{j}^{\nu}_{\mathrm{f}}(\mathbf{x}_2)|i\rangle}{\omega+\omega_{\mathrm{f}}-i\varepsilon_{i'}0}\,\frac{|e|\langle I|\hat{\rho}_{\mathrm{N}}(\mathbf{x}_3)|I\rangle}{M_{\mathrm{p}}}\delta^{\xi\zeta}.\end{aligned} \tag{4.33}$$

The ladder and cross diagrams represent a standard two-photon exchange between a bound fermion and a nucleus, while the seagull term can be depicted as coupling to the nucleus at the same point.

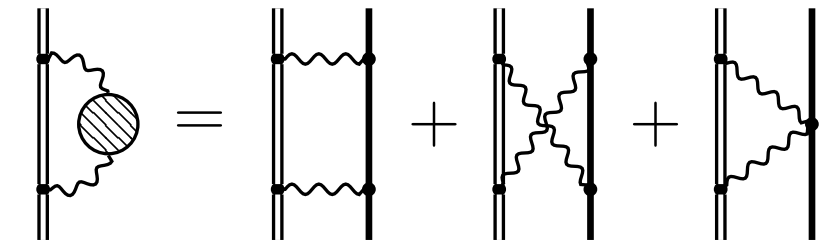

Figure 4.3.: Total NP as a sum of the ladder (L), cross (X) and seagull (SG) diagrams representing a two-photon (the wavy lines) exchange. A bound fermion is denoted by a double line, while a nucleus is denoted by a single solid line. The shaded blob represents the NP insertion.

Alternatively, by using the Fourier transforms of the type

$$D_{\mu\xi}\left(\omega,\mathbf{x}_1-\mathbf{x}_3\right)=\int\frac{d^3q}{(2\pi)^3}\,e^{i\mathbf{q}(\mathbf{x}_1-\mathbf{x}_3)}D_{\mu\xi}\left(\omega,\mathbf{q}\right), \tag{4.34}$$

$$\hat{j}^{\mu}_{\mathrm{f}}(\mathbf{q})=\int d^3x_1\,e^{-i\mathbf{q}\mathbf{x}_1}\hat{j}^{\mu}_{\mathrm{f}}(\mathbf{x}_1), \tag{4.35}$$

one can also rewrite Eqs. (4.31)–(4.33) in the momentum representation:

$$\begin{aligned}\Delta E^{\mathrm{L}}_{i,\mathrm{NP}}=-i\sum_{i'I'}\int\frac{d^3q\,d^3q'}{(2\pi)^6}\frac{d\omega}{2\pi}\,D_{\mu\xi}(\omega,\mathbf{q})D_{\zeta\nu}(\omega,\mathbf{q}')\\ \times\frac{\langle i|\hat{j}^{\mu}_{\mathrm{f}}(-\mathbf{q})|i'\rangle\langle i'|\hat{j}^{\nu}_{\mathrm{f}}(\mathbf{q}')|i\rangle}{\omega+\omega_{\mathrm{f}}-i\varepsilon_{i'}0}\,\frac{\langle I|\hat{J}^{\xi}_{\mathrm{N}}\left(\mathbf{q}\right)|I'\rangle\langle I'|\hat{J}^{\zeta}_{\mathrm{N}}\left(-\mathbf{q}'\right)|I\rangle}{\omega-\omega_{\mathrm{N}}+i0},\end{aligned} \tag{4.36}$$

$$\begin{aligned}\Delta E^{\mathrm{X}}_{i,\mathrm{NP}}=+i\sum_{i'I'}\int\frac{d^3q\,d^3q'}{(2\pi)^6}\frac{d\omega}{2\pi}\,D_{\mu\xi}(\omega,\mathbf{q})D_{\zeta\nu}(\omega,\mathbf{q}')\\ \times\frac{\langle i|\hat{j}^{\mu}_{\mathrm{f}}(-\mathbf{q})|i'\rangle\langle i'|\hat{j}^{\nu}_{\mathrm{f}}(\mathbf{q}')|i\rangle}{\omega+\omega_{\mathrm{f}}-i\varepsilon_{i'}0}\,\frac{\langle I'|\hat{J}^{\xi}_{\mathrm{N}}\left(\mathbf{q}\right)|I\rangle\langle I|\hat{J}^{\zeta}_{\mathrm{N}}\left(-\mathbf{q}'\right)|I'\rangle}{\omega+\omega_{\mathrm{N}}-i0},\end{aligned} \tag{4.37}$$

$$\begin{aligned}\Delta E^{\mathrm{SG}}_{i,\mathrm{NP}}=-i\sum_{i'}\int\frac{d^3q\,d^3q'}{(2\pi)^6}\frac{d\omega}{2\pi}\,D_{\mu\xi}(\omega,\mathbf{q})D_{\zeta\nu}(\omega,\mathbf{q}')\\ \times\frac{\langle i|\hat{j}^{\mu}_{\mathrm{f}}(-\mathbf{q})|i'\rangle\langle i'|\hat{j}^{\nu}_{\mathrm{f}}(\mathbf{q}')|i\rangle}{\omega+\omega_{\mathrm{f}}-i\varepsilon_{i'}0}\,\frac{|e|\langle I|\hat{\rho}_{\mathrm{N}}(\mathbf{q}-\mathbf{q}')|I\rangle}{M_{\mathrm{p}}}\delta^{\xi\zeta}.\end{aligned} \tag{4.38}$$

4.1.3. Feynman gauge

In order to proceed with the formulas (4.36)–(4.38) further, one has to specify a gauge and thereby an explicit expression for the photon propagator $D_{\mu\xi}$. Perhaps, the most convenient choice is the Feynman gauge, where this expression takes on a very simple form

$$D^{\mathrm{F}}_{\mu\xi}(\omega,\mathbf{q})=-\frac{\eta_{\mu\xi}}{\omega^2-\mathbf{q}^2+i0}. \tag{4.39}$$

Then, for instance, the formula for the ladder term becomes

$$\begin{aligned}\Delta E^{\mathrm{L}}_{i,\mathrm{NP}}=-i\sum_{i'I'}\int\frac{\mathrm{q}^2d\mathrm{q}d\Omega_{\mathbf{q}}\,\mathrm{q}'^2d\mathrm{q}'d\Omega_{\mathbf{q}'}}{(2\pi)^6}\frac{d\omega}{2\pi}\\ \times\frac{\langle i|\hat{j}^{\mu}_{\mathrm{f}}(-\mathbf{q})|i'\rangle\langle I|\hat{J}_{\mathrm{N},\mu}\left(\mathbf{q}\right)|I'\rangle\times\langle i'|\hat{j}^{\nu}_{\mathrm{f}}(\mathbf{q}')|i\rangle\langle I'|\hat{J}_{\mathrm{N},\nu}\left(-\mathbf{q}'\right)|I\rangle}{(\omega^2-\mathrm{q}^2+i0)(\omega^2-\mathrm{q}'^2+i0)(\omega+\omega_{\mathrm{f}}-i\varepsilon_{i'}0)(\omega-\omega_{\mathrm{N}}+i0)}.\end{aligned} \tag{4.40}$$

First, we perform the integration in ω, where we define for the ladder and cross diagrams

$$I_{\pm}(\mathrm{q},\mathrm{q}')\coloneqq i\int\frac{d\omega}{2\pi}\frac{\mathrm{q}^2\mathrm{q}'^2}{(\omega^2-\mathrm{q}^2+i0)(\omega^2-\mathrm{q}'^2+i0)(\omega+\omega_{\mathrm{f}}-i\varepsilon_{i'}0)(\omega\mp\omega_{\mathrm{N}}\pm i0)}. \tag{4.41}$$

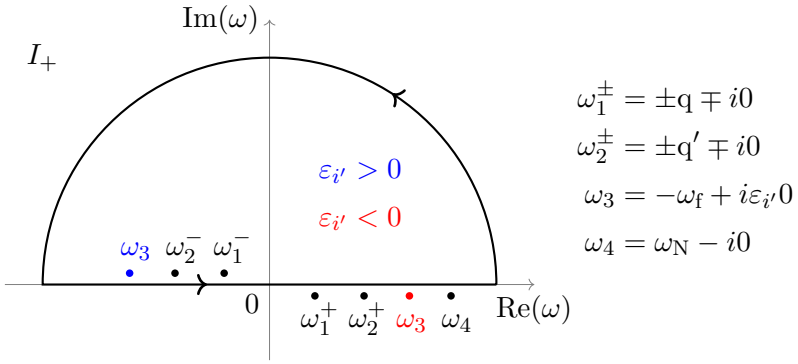

Figure 4.4.: The poles of the integrand in Eq. (4.41) for I_+ in the complex ω-plane as well as one possible choice of the integration contour. For $\varepsilon_{i'} > 0$, the case of $\omega_\mathrm{f} > 0$ is shown.

The poles of the integrand for I_+ are shown in Fig. 4.4. The integral in Eq. (4.41) can be evaluated via the residue theorem by choosing the integration contour as an infinite semicircle lying either in the upper or in the lower half-plane. For example, considering the case of $\varepsilon_{i'} < 0$ and integrating over the contour shown in Fig. 4.4, one obtains

$$I_+(\mathrm{q},\mathrm{q}';\varepsilon_{i'}<0) = \frac{i}{2\pi} 2\pi i \times \mathrm{q}^2\mathrm{q}'^2 \left[\frac{1}{-2\mathrm{q}(\mathrm{q}^2-\mathrm{q}'^2)(-\mathrm{q}+\omega_\mathrm{f})(-\mathrm{q}-\omega_\mathrm{N})} + \frac{1}{-2\mathrm{q}'(\mathrm{q}'^2-\mathrm{q}^2)(-\mathrm{q}'+\omega_\mathrm{f})(-\mathrm{q}'-\omega_\mathrm{N})}\right], \tag{4.42}$$

which can be simplified to

$$I_+(\mathrm{q},\mathrm{q}';\varepsilon_{i'}<0) = \frac{\mathrm{q}\mathrm{q}'}{2(\mathrm{q}-\omega_\mathrm{f})(\mathrm{q}'-\omega_\mathrm{f})(\mathrm{q}+\omega_\mathrm{N})(\mathrm{q}'+\omega_\mathrm{N})} \times \left[\frac{\omega_\mathrm{f}\omega_\mathrm{N}+\mathrm{q}\mathrm{q}'}{\mathrm{q}+\mathrm{q}'} + \omega_\mathrm{f} - \omega_\mathrm{N} - \mathrm{q} - \mathrm{q}'\right]. \tag{4.43}$$

Analogous integrations and algebraic manipulations for all the other cases ultimately lead to the following combined formula:

$$I_\pm(\mathrm{q},\mathrm{q}') = \frac{\mathrm{q}\mathrm{q}'}{2(\mathrm{q}+\widetilde{\omega}_\mathrm{f})(\mathrm{q}'+\widetilde{\omega}_\mathrm{f})(\mathrm{q}+\omega_\mathrm{N})(\mathrm{q}'+\omega_\mathrm{N})} \times \left\{\frac{\omega_\mathrm{f}\omega_\mathrm{N} \pm \mathrm{q}\mathrm{q}'}{\mathrm{q}+\mathrm{q}'} + \omega_\mathrm{f} + \mathrm{sgn}(\varepsilon_{i'})\left[\omega_\mathrm{N}+\mathrm{q}+\mathrm{q}'\right] \pm \theta(\pm\varepsilon_{i'})\frac{2\mathrm{q}\mathrm{q}'}{\omega_\mathrm{N}+\widetilde{\omega}_\mathrm{f}}\right\}, \tag{4.44}$$

where $\widetilde{\omega}_\mathrm{f} \coloneqq \mathrm{sgn}(\varepsilon_{i'})\omega_\mathrm{f}$. Thus, after the integration in ω, Eq. (4.40) reduces to

$$\Delta E^\mathrm{L}_{i,\mathrm{NP}} = -\sum_{i'I'} \int \frac{d\mathrm{q} d\Omega_\mathbf{q}\, d\mathrm{q}' d\Omega_{\mathbf{q}'}}{(2\pi)^6} I_+(\mathrm{q},\mathrm{q}') \times \langle i|\hat{j}^\mu_\mathrm{f}(-\mathbf{q})|i'\rangle\langle I|\hat{J}_{\mathrm{N},\mu}(\mathbf{q})\,|I'\rangle \times \langle i'|\hat{j}^\nu_\mathrm{f}(\mathbf{q}')|i\rangle\langle I'|\hat{J}_{\mathrm{N},\nu}(-\mathbf{q}')\,|I\rangle. \tag{4.45}$$

Next, with the help of multipole expansions, the angular integrations in Eq. (4.45) can also be performed analytically. We start with the Fourier transforms of the transition matrix elements of the charge density operators:

$$\langle i|\hat{\rho}_{\mathrm{f}}(-\mathbf{q})|i'\rangle = \int d^3x\, \langle i|\hat{\rho}_{\mathrm{f}}(\mathbf{x})|i'\rangle e^{i\mathbf{qx}}, \tag{4.46}$$

$$\langle I|\hat{\rho}_{\mathrm{N}}(\mathbf{q})|I'\rangle = \int d^3x\, \langle I|\hat{\rho}_{\mathrm{N}}(\mathbf{x})|I'\rangle e^{-i\mathbf{qx}}. \tag{4.47}$$

Similar to Ref. [113], we use the well-known expansion of a plane wave:

$$e^{\pm i\mathbf{qx}} = 4\pi \sum_{JM} (\pm i)^J j_J(\mathrm{qx}) Y_{JM}(\Omega_{\mathbf{x}}) Y^*_{JM}(\Omega_{\mathbf{q}}), \tag{4.48}$$

and define

$$\hat{m}_{JM}(\mathrm{q}) \coloneqq \int d^3x\, j_J(\mathrm{qx}) Y_{JM}(\Omega_{\mathbf{x}}) \hat{\rho}_{\mathrm{f}}(\mathbf{x}), \tag{4.49}$$

$$\hat{M}_{JM}(\mathrm{q}) \coloneqq \int d^3x\, j_J(\mathrm{qx}) Y_{JM}(\Omega_{\mathbf{x}}) \hat{\rho}_{\mathrm{N}}(\mathbf{x}). \tag{4.50}$$

Since $\hat{m}_{JM}(\mathrm{q})$ and $\hat{M}_{JM}(\mathrm{q})$ are irreducible tensor operators of rank J, we can apply the Wigner-Eckart theorem. For example, the multipole expansion of the fermionic matrix element (4.46) reads

$$\langle i|\hat{\rho}_{\mathrm{f}}(-\mathbf{q})|i'\rangle = 4\pi \sum_{J_1 M_1} i^{J_1} Y^*_{J_1 M_1}(\Omega_{\mathbf{q}}) (-1)^{j-m} \begin{pmatrix} j & J_1 & j' \\ -m & M_1 & m' \end{pmatrix} \langle i||\hat{m}_{J_1}(\mathrm{q})||i'\rangle. \tag{4.51}$$

In this thesis, we restrict ourselves to the common case $J = 0$ for the nuclear ground state. As a result, the multipole expansion of Eq. (4.47) simplifies considerably:

$$\langle I|\hat{\rho}_{\mathrm{N}}(\mathbf{q})|I'\rangle = 4\pi \sum_{J_2 M_2} (-i)^{J_2} Y^*_{J_2 M_2}(\Omega_{\mathbf{q}}) \begin{pmatrix} 0 & J_2 & J' \\ 0 & M_2 & M' \end{pmatrix} \langle I||\hat{M}_{J_2}(\mathrm{q})||I'\rangle, \tag{4.52}$$

since the corresponding $3j$-symbol is given by

$$\begin{pmatrix} 0 & J_2 & J' \\ 0 & M_2 & M' \end{pmatrix} = (-1)^{J'+M'} \frac{\delta_{J_2 J'} \delta_{M_2(-M')}}{\sqrt{2J'+1}}. \tag{4.53}$$

In the case of the current densities:

$$\langle i|\,\hat{\mathbf{j}}_{\mathrm{f}}(-\mathbf{q})|i'\rangle = \int d^3x\, \langle i|\,\hat{\mathbf{j}}_{\mathrm{f}}(\mathbf{x})|i'\rangle e^{i\mathbf{qx}}, \tag{4.54}$$

$$\langle I|\,\hat{\mathbf{J}}_{\mathrm{N}}(\mathbf{q})|I'\rangle = \int d^3x\, \langle I|\,\hat{\mathbf{J}}_{\mathrm{N}}(\mathbf{x})|I'\rangle e^{-i\mathbf{qx}}, \tag{4.55}$$

we employ the following expansion in terms of the vector spherical harmonics for a general three-vector $\mathbf{v}(\mathbf{x})$ (see, e.g., Ref. [68]):

$$\mathbf{v}(\mathbf{x})e^{\pm i\mathbf{qx}} = 4\pi \sum_{JLM} (\pm i)^L (\mathbf{Y}_{JLM}(\Omega_\mathbf{x}) \cdot \mathbf{v}(\mathbf{x})) j_L(\mathrm{qx}) \mathbf{Y}^*_{JLM}(\Omega_\mathbf{q}), \tag{4.56}$$

where the vector spherical harmonics are defined as

$$\mathbf{Y}_{JLM}(\Omega) \coloneqq \sum_\sigma C^{JM}_{L(M-\sigma),1\sigma} Y_{L(M-\sigma)}(\Omega) \boldsymbol{\xi}_\sigma, \tag{4.57}$$

with the spherical basis vectors

$$\boldsymbol{\xi}_1 = -\frac{1}{\sqrt{2}} \begin{pmatrix} 1 \\ i \\ 0 \end{pmatrix}, \quad \boldsymbol{\xi}_0 = \begin{pmatrix} 0 \\ 0 \\ 1 \end{pmatrix}, \quad \boldsymbol{\xi}_{-1} = \frac{1}{\sqrt{2}} \begin{pmatrix} 1 \\ -i \\ 0 \end{pmatrix}. \tag{4.58}$$

Therefore, we define the multipole operators for the current densities as follows:

$$\hat{t}_{JLM}(\mathrm{q}) \coloneqq \int d^3x \, j_L(\mathrm{qx}) \left(\mathbf{Y}_{JLM}(\Omega_\mathbf{x}) \cdot \hat{\mathbf{j}}_\mathrm{f}(\mathbf{x}) \right), \tag{4.59}$$

$$\hat{T}_{JLM}(\mathrm{q}) \coloneqq \int d^3x \, j_L(\mathrm{qx}) \left(\mathbf{Y}_{JLM}(\Omega_\mathbf{x}) \cdot \hat{\mathbf{J}}_\mathrm{N}(\mathbf{x}) \right), \tag{4.60}$$

and express the quantities in Eqs. (4.54) and (4.55) in terms of the reduced matrix elements of $\hat{t}_{JLM}(\mathrm{q})$ and $\hat{T}_{JLM}(\mathrm{q})$, respectively.

At this point, the angular integrations in Eq. (4.45) can be readily performed due to the orthogonality property of the spherical harmonics:

$$\int d\Omega \, Y^*_{J_1M_1}(\Omega) Y_{J_2M_2}(\Omega) = \delta_{J_1J_2}\delta_{M_1M_2}, \tag{4.61}$$

as well as the similar relation for the vector spherical harmonics:

$$\int d\Omega \, \mathbf{Y}^*_{J_1L_1M_1}(\Omega) \cdot \mathbf{Y}_{J_2L_2M_2}(\Omega) = \delta_{J_1J_2}\delta_{L_1L_2}\delta_{M_1M_2}, \tag{4.62}$$

with the complex conjugates given by

$$Y^*_{JM}(\Omega) = (-1)^M Y_{J(-M)}(\Omega) \tag{4.63}$$

and

$$\begin{aligned} \mathbf{Y}^*_{JLM}(\Omega) &= \sum_\sigma C^{JM}_{L(M-\sigma),1\sigma} Y^*_{L(M-\sigma)}(\Omega) \boldsymbol{\xi}^*_\sigma \\ &= \sum_\sigma (-1)^{J-L-1} C^{J(-M)}_{L(\sigma-M),1(-\sigma)} (-1)^{M-\sigma} Y_{L(\sigma-M)}(\Omega) (-1)^\sigma \boldsymbol{\xi}_{-\sigma} \\ &= (-1)^{J-L-1+M} \mathbf{Y}_{JL(-M)}(\Omega). \end{aligned} \tag{4.64}$$

Furthermore, we can also sum over the angular projections m' and M' of the intermediate fermionic and nuclear states, respectively, by making use of the orthogonality relation for the $3j$-symbols:

$$\sum_{m_1,m_2} \begin{pmatrix} j_1 & j_2 & j_3 \\ m_1 & m_2 & m_3 \end{pmatrix} \begin{pmatrix} j_1 & j_2 & j_3' \\ m_1 & m_2 & m_3' \end{pmatrix} = \frac{1}{2j_3+1}\delta_{j_3 j_3'}\delta_{m_3 m_3'}, \tag{4.65}$$

such that we finally obtain

$$\begin{aligned}\Delta E^{\mathrm{L}}_{i,\mathrm{NP}} = -\frac{1}{2j+1}\left(\frac{2}{\pi}\right)^2 \sum_{n'\kappa' N' J'\pi'} \frac{1}{2J'+1} \\ \times \int_0^\infty \int_0^\infty d\mathrm{q} d\mathrm{q}'\, I_+(\mathrm{q},\mathrm{q}')\, \mathcal{W}^{\mathrm{L}}_{\mathrm{F}}(\mathrm{q})\, \mathcal{W}^{\mathrm{L}}_{\mathrm{F}}(\mathrm{q}'),\end{aligned} \tag{4.66}$$

$$\begin{aligned}\Delta E^{\mathrm{X}}_{i,\mathrm{NP}} = -\frac{1}{2j+1}\left(\frac{2}{\pi}\right)^2 \sum_{n'\kappa' N' J'\pi'} \frac{1}{2J'+1} \\ \times \int_0^\infty \int_0^\infty d\mathrm{q} d\mathrm{q}'\, I_-(\mathrm{q},\mathrm{q}')\, \mathcal{W}^{\mathrm{X}}_{\mathrm{F}}(\mathrm{q})\, \mathcal{W}^{\mathrm{X}}_{\mathrm{F}}(\mathrm{q}'),\end{aligned} \tag{4.67}$$

where

$$\begin{aligned}\mathcal{W}^{\mathrm{L}}_{\mathrm{F}}(\mathrm{q}) = \Bigg[&\langle i'||\hat{m}_{J'}(\mathrm{q})||i\rangle\langle I'||\hat{M}_{J'}(\mathrm{q})||I\rangle \\ &- \sum_{L=J'-1}^{J'+1} (-1)^{J'-L-1}\langle i'||\hat{t}_{J'L}(\mathrm{q})||i\rangle\langle I'||\hat{T}_{J'L}(\mathrm{q})||I\rangle\Bigg],\end{aligned} \tag{4.68}$$

$$\begin{aligned}\mathcal{W}^{\mathrm{X}}_{\mathrm{F}}(\mathrm{q}) = \Bigg[&\langle i'||\hat{m}_{J'}(\mathrm{q})||i\rangle\langle I'||\hat{M}_{J'}(\mathrm{q})||I\rangle \\ &+ \sum_{L=J'-1}^{J'+1} \langle i'||\hat{t}_{J'L}(\mathrm{q})||i\rangle\langle I'||\hat{T}_{J'L}(\mathrm{q})||I\rangle\Bigg].\end{aligned} \tag{4.69}$$

A similar calculation for the seagull term yields

$$\Delta E^{\mathrm{SG}}_{i,\mathrm{NP}} = -\frac{1}{2j+1}\left(\frac{2}{\pi}\right)^2 \sum_{n'\kappa' J'\pi'} \int_0^\infty \int_0^\infty d\mathrm{q} d\mathrm{q}'\, I_{\mathrm{SG}}(\mathrm{q},\mathrm{q}')\, \mathcal{W}^{\mathrm{SG}}_{\mathrm{F}}(\mathrm{q},\mathrm{q}'), \tag{4.70}$$

where

$$I_{\mathrm{SG}}(\mathrm{q},\mathrm{q}') = \mathrm{sgn}(\varepsilon_{i'})\frac{|e|}{2M_{\mathrm{p}}}\frac{\mathrm{q}\mathrm{q}'(\widetilde{\omega}_{\mathrm{f}}+\mathrm{q}+\mathrm{q}')}{(\mathrm{q}+\mathrm{q}')(\mathrm{q}+\widetilde{\omega}_{\mathrm{f}})(\mathrm{q}'+\widetilde{\omega}_{\mathrm{f}})}, \tag{4.71}$$

$$\mathcal{W}^{\mathrm{SG}}_{\mathrm{F}}(\mathrm{q},\mathrm{q}') = \sum_{L=J'-1}^{J'+1}\Big[\langle i'||\hat{t}_{J'L}(\mathrm{q})||i\rangle\langle i'||\hat{t}_{J'L}(\mathrm{q}')||i\rangle M^{\mathrm{SG}}_L(\mathrm{q},\mathrm{q}')\Big], \tag{4.72}$$

$$M^{\mathrm{SG}}_L(\mathrm{q},\mathrm{q}') = \int_0^\infty \mathrm{x}^2 d\mathrm{x}\, \langle I|\hat{\rho}_{\mathrm{N}}(\mathrm{x})|I\rangle j_L(\mathrm{q}\mathrm{x}) j_L(\mathrm{q}'\mathrm{x}). \tag{4.73}$$

In the above formulas, n' stands for the principal quantum number of intermediate fermionic states with the relativistic angular momentum κ', while N' enumerates nuclear excitations with the total angular momentum J' and the parity π'. The expressions for the atomic and nuclear reduced matrix elements are presented in Appendices A and B, respectively. We note that the seagull term obtained by using Eq. (4.73) contains a contribution coming from the center-of-mass motion, which must be eliminated by using the effective proton charge $e_\mathrm{p} = |e|N/A$ instead of $e_\mathrm{p} = |e|$, where A is the mass number, and N is the neutron number [107].

We would also like to point out a subtlety with regard to calculating NP corrections to excited atomic states. In performing the ω-integration above, we have omitted the terms $i0$ in the denominators of the final expressions for simplicity. However, in the case of excited atomic states, this cannot always be done, and one encounters integrals of the following form:

$$\Delta E = \int_0^\infty \int_0^\infty \frac{f(\mathrm{q},\mathrm{q}')\,d\mathrm{q}\,d\mathrm{q}'}{(\mathrm{q}-a-i0)(\mathrm{q}'-b-i0)}, \tag{4.74}$$

where $a > 0$ and $b > 0$. In evaluating such two-dimensional integrals, due to the Poincaré-Bertrand theorem, there is an additional term as compared to simply applying the Sokhotski-Plemelj formula twice [114]:

$$\begin{aligned}\frac{1}{\mathrm{q}-a-i0}\frac{1}{\mathrm{q}'-b-i0} = \left[\frac{\mathcal{P}}{\mathrm{q}-a} + i\pi\delta(\mathrm{q}-a)\right]\left[\frac{\mathcal{P}}{\mathrm{q}'-b} + i\pi\delta(\mathrm{q}'-b)\right] \\ +\pi^2\delta(\mathrm{q}-a)\delta(\mathrm{q}'-b),\end{aligned} \tag{4.75}$$

such that the products of the delta-functions cancel each other, resulting in

$$\mathrm{Re}(\Delta E) = \mathcal{P}\int_0^\infty \mathcal{P}\int_0^\infty \frac{f(\mathrm{q},\mathrm{q}')\,d\mathrm{q}\,d\mathrm{q}'}{(\mathrm{q}-a)(\mathrm{q}'-b)}, \tag{4.76}$$

where $\mathcal{P}$ denotes the Cauchy principal value. Here, the real part of ΔE is the physical energy shift of an excited atomic state, while the imaginary part corresponds to the decay rate. In other words, any improper integrals arising from our final formulas should be simply understood in the Cauchy principal value sense.

In addition, the results of similar derivations for the Coulomb gauge are given in Appendix C.

4.1.4. Longitudinal approximation

An obvious advantage of the formalism presented so far is that it allows to take into account the full interaction between a bound fermion and a nucleus in the most complete and accurate way. This is especially important for muonic atoms, where the overlap between muonic and nuclear wave functions is substantial. However,

the associated calculations are computationally expensive, and they require detailed knowledge of the nuclear transition charge and current densities. For electronic atoms, a fairly reasonable approximation can be obtained by neglecting the contributions from the vector current $\hat{\mathbf{J}}_{\mathrm{N,\,fluc}}$ since the velocities associated with nuclear dynamics are mainly non-relativistic [104]. Moreover, once $\hat{\mathbf{J}}_{\mathrm{N,\,fluc}}$ is neglected, it is also possible to simplify the calculations even further and express the NP correction in terms of the experimentally measurable nuclear transition probabilities. These simplifications will be especially useful in Section 4.3 for extending the formalism to the case of the bound-electron g factor. In this subsection, we will first establish the foundations of such an approach and then show how it works for the simpler calculations of the NP energy shifts.

We will call the following framework the "longitudinal approximation" since, by neglecting the nuclear vector current, we keep only the longitudinal component D_{00}^{NP} of the NP correction to the photon propagator, which is obtained most conveniently in the Coulomb gauge:

$$D_{00}^{\mathrm{NP}}(\omega,\mathbf{x}_1,\mathbf{x}_2)=\int d^3x_3 d^3x_4\,\frac{1}{4\pi|\mathbf{x}_1-\mathbf{x}_3|}\Pi_{\mathrm{N}}^{00}(\omega,\mathbf{x}_3,\mathbf{x}_4)\frac{1}{4\pi|\mathbf{x}_4-\mathbf{x}_2|}, \tag{4.77}$$

where the Π_{N}^{00} component of the NP tensor is given by

$$\begin{aligned}\Pi_{\mathrm{N}}^{00}(\omega,\mathbf{x}_3,\mathbf{x}_4)=\sum_{I'}\Bigg(&\frac{\langle I|\hat{\rho}_{\mathrm{N,\,fluc}}(\mathbf{x}_3)|I'\rangle\langle I'|\hat{\rho}_{\mathrm{N,\,fluc}}(\mathbf{x}_4)|I\rangle}{\omega-\omega_{\mathrm{N}}+i0}\\&-\frac{\langle I'|\hat{\rho}_{\mathrm{N,\,fluc}}(\mathbf{x}_3)|I\rangle\langle I|\hat{\rho}_{\mathrm{N,\,fluc}}(\mathbf{x}_4)|I'\rangle}{\omega+\omega_{\mathrm{N}}-i0}\Bigg).\end{aligned} \tag{4.78}$$

In order to proceed further, we assume that the nuclear charge density operator can be decomposed in terms of electric multipoles as follows:

$$\hat{\rho}_{\mathrm{N,\,fluc}}(\mathbf{x})=\sum_{JM}\mathcal{R}_J(\mathrm{x})Y_{JM}^*(\Omega_{\mathbf{x}})\hat{Q}_{JM}, \tag{4.79}$$

where the electric multipole operators $\hat{Q}_{JM}$ are given by the standard definition

$$\hat{Q}_{JM}=\int d^3x\,\mathrm{x}^J Y_{JM}(\Omega_{\mathbf{x}})\hat{\rho}_{\mathrm{N,\,fluc}}(\mathbf{x}),\quad \hat{Q}_{JM}^\dagger=(-1)^M\hat{Q}_{J-M}, \tag{4.80}$$

such that the following condition on the radial functions $\mathcal{R}_J$ must hold:

$$\int_0^\infty d\mathrm{x}\,\mathrm{x}^{J+2}\mathcal{R}_J(\mathrm{x})=1. \tag{4.81}$$

Substituting the expansion from Eq. (4.79) into the expression for the NP tensor in Eq. (4.78), we obtain

$$\begin{aligned}\Pi_{\mathrm{N}}^{00}(\omega,\mathbf{x}_3,\mathbf{x}_4)=\sum_{I'}\sum_{J_1M_1,J_2M_2}&\mathcal{R}_{J_1}(\mathrm{x}_3)\mathcal{R}_{J_2}(\mathrm{x}_4)Y_{J_1M_1}^*(\Omega_{\mathbf{x}_3})Y_{J_2M_2}(\Omega_{\mathbf{x}_4})\\&\times\left(\frac{\langle I|\hat{Q}_{J_1M_1}|I'\rangle\langle I'|\hat{Q}_{J_2M_2}^\dagger|I\rangle}{\omega-\omega_{\mathrm{N}}+i0}-\frac{\langle I|\hat{Q}_{J_2M_2}^\dagger|I'\rangle\langle I'|\hat{Q}_{J_1M_1}|I\rangle}{\omega+\omega_{\mathrm{N}}-i0}\right).\end{aligned} \tag{4.82}$$

Then, after using the Wigner-Eckart theorem:

$$\begin{aligned}\langle I|\hat{Q}_{J_1M_1}|I'\rangle &= \begin{pmatrix} 0 & J_1 & J' \\ 0 & M_1 & M' \end{pmatrix} \langle I||\hat{Q}_J||J'\rangle \\ &= \delta_{J_1J'}\delta_{M_1(-M')}\frac{(-1)^{J'+M'}}{\sqrt{2J'+1}}\langle I||\hat{Q}_{J_1}||I'\rangle,\end{aligned} \tag{4.83}$$

and introducing the reduced transition probabilities as

$$B(EJ'[N'], J' \to 0) \coloneqq \frac{\left|\langle I||\hat{Q}_{J'}||I'\rangle\right|^2}{2J'+1} \ (\coloneqq B(EJ'[N']) \text{ for brevity}), \tag{4.84}$$

one can simplify Eq. (4.82) to

$$\begin{aligned}\Pi_{\mathrm{N}}^{00}(\omega, \mathbf{x}_3, \mathbf{x}_4) = \sum_{J'M'N'} &\mathcal{R}_{J'}(\mathrm{x}_3)\mathcal{R}_{J'}(\mathrm{x}_4)Y_{J'M'}(\Omega_{\mathbf{x}_3})Y^*_{J'M'}(\Omega_{\mathbf{x}_4}) \\ &\times \frac{2\omega_{\mathrm{N}}}{\omega^2-\omega_{\mathrm{N}}^2+i0}B(EJ'[N']),\end{aligned} \tag{4.85}$$

where, as in the previous subsection, N' enumerates nuclear excited states with the total angular momentum J'. Going back to Eq. (4.77), we are now ready to evaluate D_{00}^{NP}. With the aid of the well-known expansion of the Coulomb potential:

$$\frac{1}{4\pi|\mathbf{x}_1-\mathbf{x}_3|} = \sum_{l=0}^{\infty}\frac{1}{2l+1}\frac{\mathrm{x}_<^l}{\mathrm{x}_>^{l+1}}\sum_{m=-l}^{l}Y_{lm}(\Omega_{\mathbf{x}_1})Y^*_{lm}(\Omega_{\mathbf{x}_3}), \tag{4.86}$$

the integrations in Eq. (4.77) can be easily performed leading to

$$\begin{aligned}D_{00}^{\mathrm{NP}}(\omega, \mathbf{x}_1, \mathbf{x}_2) = \sum_{J'M'N'} &F_{J'}(\mathrm{x}_1)F_{J'}(\mathrm{x}_2)Y_{J'M'}(\Omega_{\mathbf{x}_1})Y^*_{J'M'}(\Omega_{\mathbf{x}_2}) \\ &\times \frac{2\omega_{\mathrm{N}}}{\omega^2-\omega_{\mathrm{N}}^2+i0}B(EJ'[N']),\end{aligned} \tag{4.87}$$

where

$$F_{J'}(\mathrm{x}) = \frac{1}{2J'+1}\left[\frac{1}{\mathrm{x}^{J'+1}}\int_0^{\mathrm{x}}d\mathrm{y}\,\mathrm{y}^{J'+2}\mathcal{R}_{J'}(\mathrm{y}) + \mathrm{x}^{J'}\int_{\mathrm{x}}^{\infty}d\mathrm{y}\,\frac{1}{\mathrm{y}^{J'-1}}\mathcal{R}_{J'}(\mathrm{y})\right]. \tag{4.88}$$

The radial functions $\mathcal{R}_{J'}$ take on the simplest form for collective nuclear surface vibrations in the sharp-surface approximation [105]:

$$\mathcal{R}_{J'}(\mathrm{y}) = R_0^{-(J'+2)}\delta(\mathrm{y}-R_0), \quad J' \geq 2, \tag{4.89}$$

where R_0 denotes the radius of a homogeneously charged sphere characterizing the nuclear ground state. Correspondingly, for the functions $F_{J'}$ we have

$$F_{J'}(\mathrm{x}) = \frac{1}{2J'+1}\left[\frac{1}{\mathrm{x}^{J'+1}}\theta(\mathrm{x}-R_0) + \frac{\mathrm{x}^{J'}}{R_0^{2J'+1}}\theta(R_0-\mathrm{x})\right], \quad J' \geq 2. \tag{4.90}$$

In the case of other types of nuclear excitations, such as rotational modes and giant resonances, somewhat different expressions of $F_{J'}$ are obtained [105]. However, for electronic atoms, the details of the radial dependence of $D_{00}^{\rm NP}$ turn out to be of minor importance. Therefore, Eq. (4.90) can be used with a reasonable accuracy for the other excitation modes and even be extended to $J' = 1$ [115].

For the special case of collective monopole excitations (nuclear breathing modes), it can be shown that [105]

$$F_0(\mathrm{x}) \propto \left[1 - \left(\frac{\mathrm{x}}{R_0}\right)^2\right] \theta(R_0 - \mathrm{x}), \tag{4.91}$$

where the proportionality coefficient depends on the normalization convention for the reduced transition probabilities $B(E0)$.

The input parameters $\omega_{\rm N}$ and $B(EJ')$ for low-lying nuclear states are available for many nuclei from experiments and tabulated in Nuclear Data Sheets (see, e.g., Ref. [116]). On the other hand, the $B(EJ')$ values for giant resonances can be estimated by means of the following phenomenological energy-weighted sum rules [115]:

$$\begin{aligned}
\langle\omega_{\rm N}(J'\tau')\rangle B(E0) &= \frac{25Ze^2}{4\pi M_{\rm p}}\langle \mathrm{r}_{\rm p}^2\rangle \left(\frac{Z}{A}(1-\tau') + \frac{N}{A}\tau'\right), \quad J' = 0, \\
\langle\omega_{\rm N}(J'\tau')\rangle B(EJ') &= \frac{J'(2J'+1)Ze^2}{8\pi M_{\rm p}}\langle \mathrm{r}_{\rm p}^{2J'-2}\rangle \left(\frac{Z}{A}(1-\tau') + \frac{N}{A}\tau'\right), \quad J' \geq 1,
\end{aligned} \tag{4.92}$$

where $M_{\rm p}$ is the proton mass, τ' is the isospin of an excitation, and the expectation value for protons in the initial state is estimated as $\langle \mathrm{r}_{\rm p}^{2J'-2}\rangle = 3R_0^{2J'-2}/(2J'+1)$. Here, the giant resonances are assumed to be concentrated in a single state for each $(J'\tau')$ with excitation energies (in MeV) given by

$$\begin{aligned}
\langle\omega_{\rm N}(J'\tau')\rangle &= [100(1-\tau') + 200\tau'](1 - A^{-1/3})A^{-1/3}, \quad J' = 0, \\
&= 95(1 - A^{-1/3})A^{-1/3}, \quad J' = 1, \\
&= [75(1-\tau') + 160\tau'](1 - A^{-1/3})A^{-1/3}, \quad J' \geq 2.
\end{aligned} \tag{4.93}$$

With the normalization convention given by Eqs. (4.92), the radial function F_0 reads

$$F_0(\mathrm{x}) = \frac{5}{8\sqrt{\pi}R_0^3}\left[1 - \left(\frac{\mathrm{x}}{R_0}\right)^2\right]\theta(R_0 - \mathrm{x}). \tag{4.94}$$

We note that our expressions of the functions $F_{J'}$ differ from those in Ref. [115] by a factor of 4π because we use the units $e^2 = 4\pi\alpha$, which leads to the factors of 4π in the denominators of the photon propagators in Eq. (4.77).

Finally, according to Eq. (4.28), the NP energy shift of an electron state $|i\rangle$ is obtained in the longitudinal approximation as

$$\Delta E^{(1)}_{i,\mathrm{NP}} = -\frac{ie^2}{2\pi}\sum_{i'}\int d^3x_1 d^3x_2 d\omega\,\frac{\psi^\dagger_i(\mathbf{x}_1)\psi_{i'}(\mathbf{x}_1)\psi^\dagger_{i'}(\mathbf{x}_2)\psi_i(\mathbf{x}_2)}{\omega+\omega_\mathrm{f}-i\varepsilon_{i'}0} \times \sum_{J'M'N'} F_{J'}(\mathrm{x}_1)F_{J'}(\mathrm{x}_2)Y_{J'M'}(\Omega_{\mathbf{x}_1})Y^*_{J'M'}(\Omega_{\mathbf{x}_2})\frac{2\omega_\mathrm{N}}{\omega^2-\omega^2_\mathrm{N}+i0}B(EJ'[N']). \tag{4.95}$$

Similar to the previous subsection, we first perform the contour integration in ω:

$$i\int\frac{d\omega}{2\pi}\frac{2\omega_\mathrm{N}}{(\omega+\omega_\mathrm{f}-i\varepsilon_{i'}0)(\omega^2-\omega^2_\mathrm{N}+i0)} = \frac{1}{\omega_\mathrm{f}+\mathrm{sgn}(\varepsilon_{i'})\omega_\mathrm{N}}, \tag{4.96}$$

and then apply the Wigner-Eckart theorem:

$$\int d^3x_1\,\psi^\dagger_i(\mathbf{x}_1)F_{J'}(\mathrm{x}_1)Y_{J'M'}(\Omega_{\mathbf{x}_1})\psi_{i'}(\mathbf{x}_1) = (-1)^{j-m}\begin{pmatrix} j & J' & j' \\ -m & M' & m'\end{pmatrix} \times\langle n\kappa||F_{J'}Y_{J'}||n'\kappa'\rangle, \tag{4.97}$$

where the reduced matrix element is given by [117]

$$\langle n\kappa||F_{J'}Y_{J'}||n'\kappa'\rangle = \sqrt{\frac{2J'+1}{4\pi}}C_{J'}(\kappa,\kappa')\times\langle n\kappa|F_{J'}|n'\kappa'\rangle, \tag{4.98}$$

with

$$C_J(\kappa_1,\kappa_2) = (-1)^{j_1+\frac{1}{2}}\sqrt{(2j_1+1)(2j_2+1)}\begin{pmatrix} j_2 & J & j_1 \\ \frac{1}{2} & 0 & -\frac{1}{2}\end{pmatrix}\Pi(l_2,l_1,J), \tag{4.99}$$

$$\langle n\kappa|F_{J'}|n'\kappa'\rangle = \int_0^\infty d\mathrm{x}\,F_{J'}(\mathrm{x})\left[G_{n\kappa}(\mathrm{x})G_{n'\kappa'}(\mathrm{x})+F_{n\kappa}(\mathrm{x})F_{n'\kappa'}(\mathrm{x})\right]. \tag{4.100}$$

The parity factor $\Pi(l_2,l_1,J)$ is equal to 1 if the value l_2+l_1+J is even, and vanishes otherwise. After combining everything together and employing the orthogonality property of the $3j$-symbols for summing over the angular projections m' and M', we obtain a simple and efficient formula

$$\Delta E^{(1)}_{i,\mathrm{NP}} = -\frac{e^2}{4\pi}\sum_{J'N'}(2J'+1)B(EJ'[N'])\sum_{n'\kappa'}\frac{1}{\omega_\mathrm{f}+\mathrm{sgn}(\varepsilon_{i'})\omega_\mathrm{N}} \times(2j'+1)\langle n\kappa|F_{J'}|n'\kappa'\rangle^2\begin{pmatrix} j' & J' & j \\ \frac{1}{2} & 0 & -\frac{1}{2}\end{pmatrix}^2\Pi(l',l,J'). \tag{4.101}$$

4.2. Muonic fine-structure anomalies

The formalism developed in the previous section can be applied to a wide range of problems, but perhaps the most intriguing one resides in the realm of muonic atoms. For more than 40 years there has been a perplexing discrepancy between theory and experiment with respect to the fine-structure splittings between the muonic $np_{1/2}$ and $np_{3/2}$ energy levels ($n = 2, 3$). In simple terms, the origin of the puzzle can be described as follows. When X-ray spectra of the muonic cascade are analyzed with the goal of determining nuclear radii, a multitude of effects have to be taken into account, including finite nuclear size, QED corrections, electron screening, relativistic recoil, static nuclear moments and dynamical muon-nucleus interactions [37]. Under the assumption that all effects except NP have been correctly taken into account, the remaining difference between theory and experiment is typically ascribed to the "experimentally measured" NP correction. However, in some cases, the NP energy shifts extracted in this way turned out to be in striking disagreement with theoretical predictions. For instance, the experiments suggest that $|\Delta E^{\mathrm{NP}}_{2p_{3/2}}| > |\Delta E^{\mathrm{NP}}_{2p_{1/2}}|$ for muonic ^{208}Pb [48, 49], ^{90}Zr [50] and $^{112-124}$Sn [51]. At first glance, these results seem to be counterintuitive by the simple argument that the $2p_{1/2}$ orbital is closer to the nucleus and thus should be affected more strongly by nuclear dynamics. In addition, a strong anomaly of the same kind was also observed for the $\Delta 3p$ splitting in μ-^{208}Pb [49].

The most notable theoretical efforts to explain these anomalies were performed in Refs. [118–121], where, unlike previous attempts, the transverse part of the electromagnetic muon-nucleus interaction was taken into account. While the longitudinal, or Coulomb, part always leads to $|\Delta E^{\mathrm{NP}}_{2p_{3/2}}| < |\Delta E^{\mathrm{NP}}_{2p_{1/2}}|$ as expected, the transverse part was shown to give rise to an additional NP contribution with the opposite muon-spin dependence [118]. According to Ref. [119], the transverse interaction accounted for about half of the $\Delta 2p$ anomaly and one-fourth of the $\Delta 3p$ one in μ-^{208}Pb. Nevertheless, significant portions of the discrepancies persisted, with $|\Delta E^{\mathrm{NP}}_{2p_{1/2}}|$ still being slightly larger than $|\Delta E^{\mathrm{NP}}_{2p_{3/2}}|$. It was later suggested in Ref. [120] that the effect of the transverse interaction could be enhanced by treating the nucleus in the relativistic mean-field approximation, providing a glimpse of a possible resolution to the $\Delta 2p$ anomaly in μ-^{208}Pb. However, the authors themselves stressed the large uncertainties associated with the nuclear spectrum obtained in this way, and explaining the $\Delta 3p$ splitting still remained a challenge. In another attempt, an enhancement factor for NP contributions from giant resonances was proposed for both muonic ^{208}Pb and ^{90}Zr [121]. Nonetheless, the experimental data could not be reproduced reasonably well, and the anomalies continued to be unresolved.

4. Nuclear-polarization effect

In this section, we present our analysis of the fine-structure anomalies in muonic atoms based on our NP calculations within the formalism from Sections 4.1.1–4.1.3. These results were published in Ref. [2], and the text is to a large extent verbatim. The motivation behind this work is to take into account both muonic and nuclear spectra in the most complete to date manner by bringing together state-of-the-art techniques from both atomic and nuclear physics. The spectrum of a bound muon is calculated by means of the methods described in Chapter 1 for solving the Dirac equation in a potential of an extended nucleus. Similar to Chapter 3, we found that it is sufficient to use the simple Fermi charge distribution $\rho(\mathrm{r}) = N\{1+\exp[(\mathrm{r}-c)/a]\}^{-1}$ with the standard value of the diffuseness parameter $a = 2.3/[4\ln(3)]\,\mathrm{fm}$ and adjust the half-density radius c such that the current tabulated value of the RMS nuclear radius [99] is reproduced. As for the nuclear spectrum, we employ the random-phase approximation (RPA) with a full self-consistency between the Hartree-Fock mean field and the RPA excitations, as described in Chapter 2. Non-relativistic charge-current operators (see Appendix B) are used for calculating the nuclear matrix elements for the 0^+, 1^-, 2^+, 3^-, 4^+, 5^- and 1^+ excitation modes. The cutoff energy of unoccupied single-nucleon states in the RPA model space is chosen to be 60 MeV, which corresponds, for example, to around 1500 RPA excitations for the 3^- mode in ^{208}Pb. A strong quantitative test for completeness of the obtained spectra is the exhaustion of the double-commutator energy-weighted sum rule (EWSR) [91]. In our calculations the EWSR is fulfilled at the level of at least 99%, being above 99.8% in most cases. Finally, parallel computing on a cluster is employed to facilitate such combined muon-nuclear computations.

The main limitation of any NP calculation is that nuclear transition matrix elements cannot be calculated from first principles, and an effective nuclear model has to be applied instead. Hence, another and equally important goal of our study is to analyze the nuclear model dependence, which represents the largest source of the theoretical uncertainty. To this end, we performed the computations for 9 different Skyrme parametrizations, namely, KDE0 [122], SKX [123], SLy5 [90], BSk14 [124], SAMi [125], NRAPR [126], SkP [98], SkM* [127] and SGII [128]. These Skyrme interactions were chosen with the aim to cover a wide but physically relevant range in the parameter space. This can be achieved by examining the corresponding macroscopic properties that characterize the nuclear equation of state in the vicinity of the saturation density (0.16 fm^{-3}). The sensitivity of the saturation properties on some key nuclear observables have been studied in detail, and plausible ranges have been given in the literature [129]. In selecting the aforementioned set of parametrizations, we ensured that they span significant portions of rather conservative constraints on various saturation properties so that our model space is large enough to cover all possible realistic results.

In Table 4.1 we present our results for the NP corrections to the states $1s_{1/2}$, $2p_{1/2}$ and $2p_{3/2}$ in muonic ^{90}Zr, ^{120}Sn and ^{208}Pb. In the case of μ-^{208}Pb the states $3p_{1/2}$ and $3p_{3/2}$ are also considered. The quantities of main interest are the corresponding NP contributions to the fine-structure splittings $\Delta 2p^{\mathrm{NP}} = |\Delta E^{\mathrm{NP}}_{2p_{1/2}}| - |\Delta E^{\mathrm{NP}}_{2p_{3/2}}|$ and $\Delta 3p^{\mathrm{NP}} = |\Delta E^{\mathrm{NP}}_{3p_{1/2}}| - |\Delta E^{\mathrm{NP}}_{3p_{3/2}}|$. Our calculations in the Feynman and Coulomb gauges agree within 0.1–0.3% demonstrating an excellent fulfillment of gauge invariance; therefore, only the results in the Feynman gauge are shown.

We start our analysis with μ-^{90}Zr. To put the effect of the nuclear model dependence into the context of the $\Delta 2p$ anomaly, we show our results in Fig. 4.5 in relation to the experimentally allowed region for $|\Delta E^{\mathrm{NP}}_{1s_{1/2}}|$ and $\Delta 2p^{\mathrm{NP}}$, which was obtained in Ref. [50] by fitting calculated muonic transition energies to measured ones. Notably, the results for different nuclear models are simply spread along a line almost parallel to the allowed region such that the distance of around 15 eV between theory and experiment for $\Delta 2p^{\mathrm{NP}}$ remains practically constant. Taking the spread of our results as the theoretical uncertainty $\sigma_{\mathrm{th}}[\Delta 2p^{\mathrm{NP}}] = 0.7$ eV and combining it with the experimental $\sigma_{\mathrm{exp}}[\Delta 2p^{\mathrm{NP}}] = 3$ eV [50], we obtain a discrepancy of almost 5 standard deviations.

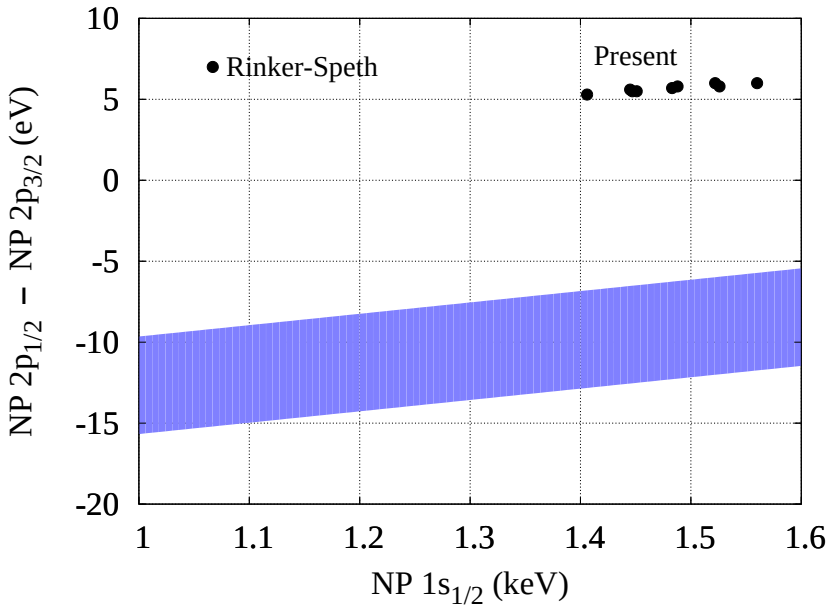

Figure 4.5.: Theoretical values of the NP corrections for μ-^{90}Zr in relation to the experimentally allowed range for $\Delta 2p^{\mathrm{NP}}$ as a function of $|\Delta E^{\mathrm{NP}}_{1s_{1/2}}|$. The graph was adapted from Ref. [50].

As for tin isotopes, the authors of Ref. [51] do not provide experimentally allowed ranges for $\Delta 2p^{\mathrm{NP}}$. Nevertheless, according to their analysis, the theoretical values of the $\Delta 2p$ fine-structure splittings are consistently too high by about 150 eV, and it is necessary to have $\Delta 2p^{\mathrm{NP}} < 0$ in order to obtain better agreement with experiment. However, the authors estimate $\Delta 2p^{\mathrm{NP}}$ as 29 eV and 28 eV for muonic ^{112}Sn and ^{124}Sn, respectively. Our results for μ-^{120}Sn in Table 4.1 demonstrate again that the nuclear model uncertainty does not offer an explanation for the anomalies, with $\Delta 2p^{\mathrm{NP}}$ being persistently positive and around 20 eV for all the Skyrme parametrizations used.

In the case of μ-^{208}Pb the situation is more subtle since, in principle, some 1^- nuclear excitations in the regions 5.5–6.5 MeV and 8–9 MeV [116] may come close in energy to the $2p \to 1s$ and $3p \to 1s$ muonic transitions, respectively. Effects coming from quasi-degeneracy in the combined muon-nuclear basis are referred to as muon-nuclear resonances. As discussed in Ref. [130], due to the long range of the dipole NP potential, 1^- nuclear levels can resonate significantly with the $np \to 1s$ muonic transitions even when the associated energy denominators in a second-order perturbation calculation are hundreds of keV. The corresponding contributions to $\Delta E^{\mathrm{NP}}_{np_{1/2}}$ and $\Delta E^{\mathrm{NP}}_{np_{3/2}}$ can be negligible for the $np \to 1s$ transition energies, but critical for the more precisely measured Δnp splittings, with one of the $np_{1/2}$ and $np_{3/2}$ levels being affected by a resonance much more strongly than the other. The net effect is highly sensitive not only to the exact relative positions of the muonic and nuclear levels involved but also to the shapes of the corresponding nuclear transition charge and current densities [121].

In our calculated spectra for ^{208}Pb we encounter a number of 1^- excitations in both aforementioned regions. Although RPA is an excellent tool for describing integral properties of a nuclear spectrum as a whole, the accuracy for individual energy levels is by no means high enough to reliably predict such resonant phenomena. Therefore, similar to Ref. [130], we simply eliminate any accidental muon-nuclear resonances by discarding 1^- RPA excitations that come closer than 0.3 MeV to the $2p \to 1s$ or $3p \to 1s$ muonic transitions. However, this does not significantly affect the overall completeness of the spectra, since the total contributions of the discarded RPA states to the EWSR are always less than 1%. Fig. 4.6 shows the resulting NP correlations between $|\Delta E^{\mathrm{NP}}_{1s_{1/2}}|$ and both $\Delta 2p^{\mathrm{NP}}$ (a) and $\Delta 3p^{\mathrm{NP}}$ (b) in relation to the experimentally allowed regions [49]. It can be seen that, in the absence of muon-nuclear resonances, the model uncertainties $\sigma_{\mathrm{th}}[\Delta 2p^{\mathrm{NP}}] = 21.2$ eV and $\sigma_{\mathrm{th}}[\Delta 3p^{\mathrm{NP}}] = 14.6$ eV, considered together with $\sigma_{\mathrm{exp}}[\Delta 2p^{\mathrm{NP}}] = 54$ eV and $\sigma_{\mathrm{exp}}[\Delta 3p^{\mathrm{NP}}] = 103$ eV [49], are once again much smaller than the gaps between theory and experiment amounting to about 4 and 3 standard deviations, respectively. We emphasize that due to the extremely high intrinsic uncertainties associated with muon-nuclear resonances, they should be regarded as a measure of last resort in explaining the fine-structure anomalies. Because of these possible complications in the special case of μ-^{208}Pb, we

suggest that the less intricate cases of muonic ^{90}Zr and $^{112-124}$Sn should be tackled first.

Thus, in the quest to explain the persisting fine-structure anomalies in muonic atoms, we have found that the tension between theory and experiment remains high even in light of the dominant nuclear model uncertainty. We note that the non-relativistic nuclear treatment in our calculations is justified by the agreement between the non-relativistic seagull term and antinucleon NP contributions in light muonic atoms [131]. In addition, there is a general consistency between relativistic and non-relativistic approaches for a variety of nuclear phenomena [89, 129, 132]. However, in the special case of NP, a possible non-negligible role of relativistic nuclear effects in heavy systems may still deserve further investigation, as proposed in Refs. [120, 131].

For the most part, however, we deem the NP effect unlikely to be responsible for the anomalies, implying that the solution is presumably rooted in refined QED calculations. In particular, the self-energy correction in muonic atoms, despite being comparable to the NP shifts [121], has only been estimated using rather simple prescriptions [37]. Therefore, a rigorous treatment of this effect developed in the field of highly-charged ions (see, e.g., Refs. [133–135]) could shed some light on the anomalies [136]. Lastly, some other exotic effects, such as the anomalous spin-dependent interaction mentioned in Ref. [137], might also play a role in explaining the discrepancies, although it is far less likely. Overall, we conclude that more attention to other effects beyond NP is required in order to finally resolve this tantalizing and long-standing puzzle.

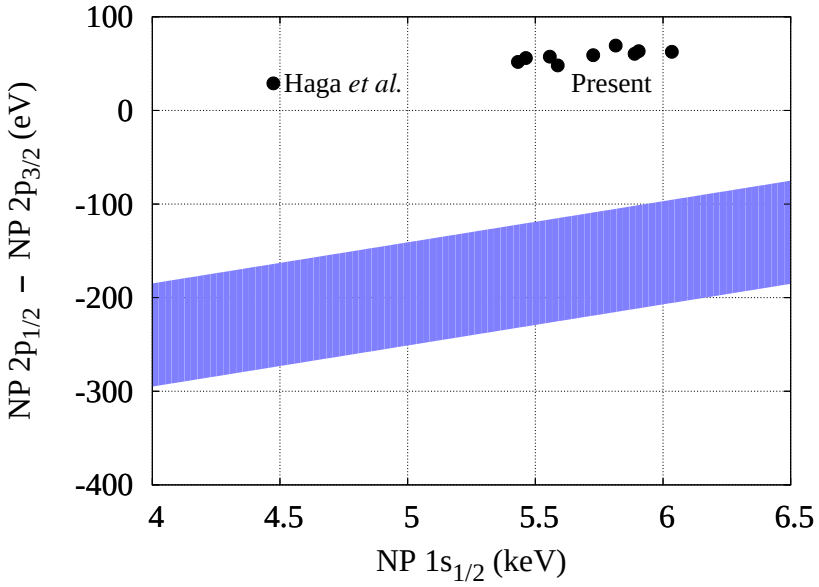

(a)

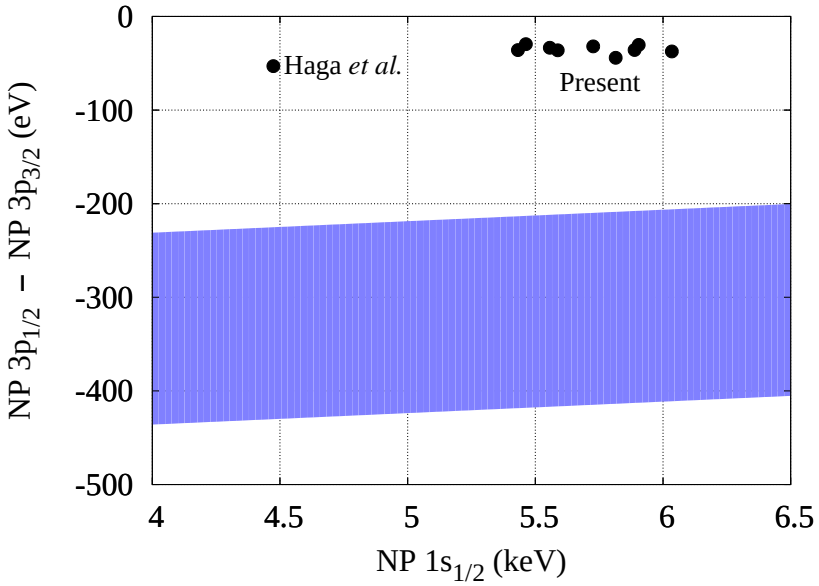

(b)

Figure 4.6.: Theoretical values of the NP corrections for μ-^{208}Pb in relation to the experimentally allowed ranges for $\Delta 2p^{\mathrm{NP}}$ (a) and $\Delta 3p^{\mathrm{NP}}$ (b) as functions of $|\Delta E^{\mathrm{NP}}_{1s_{1/2}}|$. The graphs were adapted from Refs. [49, 119].

Table 4.1.: NP corrections (absolute values $|\Delta E^{\mathrm{NP}}| = -\Delta E^{\mathrm{NP}}$, in eV) to the states $1s_{1/2}$, $2p_{1/2}$ and $2p_{3/2}$ in muonic ^{90}Zr, ^{120}Sn and ^{208}Pb. In the case of μ-^{208}Pb the states $3p_{1/2}$ and $3p_{3/2}$ are also considered. The quantities $\Delta 2p^{\mathrm{NP}} = |\Delta E^{\mathrm{NP}}_{2p_{1/2}}| - |\Delta E^{\mathrm{NP}}_{2p_{3/2}}|$ and $\Delta 3p^{\mathrm{NP}} = |\Delta E^{\mathrm{NP}}_{3p_{1/2}}| - |\Delta E^{\mathrm{NP}}_{3p_{3/2}}|$ are the corresponding NP contributions to the fine-structure splittings. The Skyrme parametrizations are ordered in increasing values of $|\Delta E^{\mathrm{NP}}_{1s_{1/2}}|$ in μ-^{90}Zr.

		KDE0	SKX	SLy5	BSk14	SAMi	NRAPR	SkP	SkM*	SGII
μ-^{90}Zr	$1s_{1/2}$	1406	1445	1447	1451	1483	1488	1522	1526	1560
	$2p_{1/2}$	65.9	70.3	69.5	70.0	72.5	71.7	73.9	74.4	75.7
	$2p_{3/2}$	60.6	64.7	64.0	64.5	66.8	65.9	67.9	68.6	69.7
	$\Delta 2p^{\mathrm{NP}}$	5.3	5.6	5.5	5.5	5.7	5.8	6.0	5.8	6.0
μ-^{120}Sn	$1s_{1/2}$	2564	2510	2481	2425	2530	2531	2570	2567	2744
	$2p_{1/2}$	247	248	236	231	246	245	247	247	269
	$2p_{3/2}$	228	229	218	214	228	226	227	228	248
	$\Delta 2p^{\mathrm{NP}}$	19.9	19.6	18.0	17.0	18.7	18.7	19.2	18.9	21.1
μ-^{208}Pb	$1s_{1/2}$	5463	5432	5557	5588	5727	5889	5815	5905	6035
	$2p_{1/2}$	1781	1850	1834	1900	1937	1997	1955	2005	2044
	$2p_{3/2}$	1725	1798	1776	1852	1877	1936	1886	1942	1981
	$3p_{1/2}$	529	576	556	566	616	540	628	614	627
	$3p_{3/2}$	559	612	589	602	648	576	672	645	664
	$\Delta 2p^{\mathrm{NP}}$	56.0	51.8	57.5	48.1	59.1	60.5	69.3	63.3	62.7
	$\Delta 3p^{\mathrm{NP}}$	-29.5	-35.9	-33.4	-36.1	-31.9	-35.8	-44.1	-30.3	-37.3

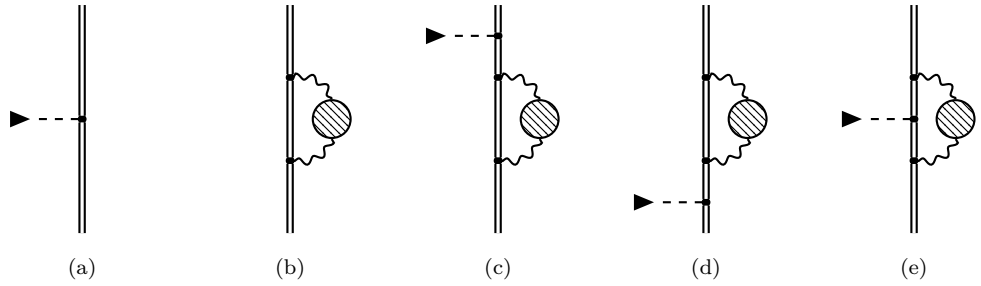

Figure 4.7.: Feynman diagrams representing: (a) the interaction of a bound electron with an external magnetic field, (b) NP as effective self-energy, and (c, d, e) three possible combinations corresponding to the NP correction to the Zeeman interaction. A bound electron and a photon are indicated by the double and wavy lines, respectively. The external potential is denoted by the black triangles, and the shaded blobs represent the NP insertion.

4.3. g factor of hydrogenlike ions

In this section, we extend the NP formalism to the case of the bound-electron g factor of H-like ions, following the ideas from Ref. [138]. First, we recall that the Zeeman splitting in an external magnetic field $\mathbf{B} = (0, 0, B^{\mathcal{3}})$ is described within the first-order perturbation theory by the following potential (see Eq. (1.67)):

$$\delta V(\mathbf{x}) = \frac{|e|}{2} B^{\mathcal{3}} \left[\mathbf{x} \times \boldsymbol{\alpha}\right]^{\mathcal{3}} . \tag{4.102}$$

The interaction between a bound electron and the potential $\delta V(\mathbf{x})$ is shown diagramatically in Fig. 4.7(a). The leading-order NP correction to the Zeeman interaction comes from the effective self-energy depicted in Fig. 4.7(b), which leads to the three possible combined diagrams shown in Figs. 4.7(c, d, e).

The Green's function G for the diagram (c) reads

$$\begin{aligned} G^{(\mathrm{c})}((E', \mathbf{x}'); (E, \mathbf{x})) = \int d^3x_1 d^3x_2 d^3x_3 d\eta d\omega \, \frac{i}{2\pi} S(E', \mathbf{x}', \mathbf{x}_1)(-2\pi i)\gamma^0 \delta V(\mathbf{x}_1) \\ \times \frac{i}{2\pi} S(E', \mathbf{x}_1, \mathbf{x}_2) 2\pi i |e| \gamma^\mu \delta(E' - \eta - \omega) \\ \times \frac{i}{2\pi} S(\eta, \mathbf{x}_2, \mathbf{x}_3) 2\pi i |e| \gamma^\nu \delta(\eta + \omega - E) \\ \times \frac{i}{2\pi} S(E, \mathbf{x}_3, \mathbf{x}) \frac{i}{2\pi} D^{\mathrm{NP}}_{\mu\nu}(\omega, \mathbf{x}_2, \mathbf{x}_3), \end{aligned} \tag{4.103}$$

which, after performing the integration in η, simplifies to

$$\begin{aligned} G^{(\mathrm{c})}((E',\mathbf{x}');(E,\mathbf{x})) = \left(\frac{ie}{2\pi}\right)^2 \int d^3x_1 d^3x_2 d^3x_3 d\omega\, S(E',\mathbf{x}',\mathbf{x}_1)\gamma^0 \delta V(\mathbf{x}_1) \\ \times S(E',\mathbf{x}_1,\mathbf{x}_2)\gamma^\mu S(E-\omega,\mathbf{x}_2,\mathbf{x}_3)\gamma^\nu \\ \times S(E,\mathbf{x}_3,\mathbf{x}) D^{\mathrm{NP}}_{\mu\nu}(\omega,\mathbf{x}_2,\mathbf{x}_3)\delta(E-E'). \end{aligned} \tag{4.104}$$

In this section, we will restrict ourselves to the longitudinal approximation such that only the D^{NP}_{00} component of the NP correction to the photon propagator in the form (4.87) will be taken into account. After plugging the expression (1.15) for the dressed electron propagator S into Eq. (4.104), using Eq. (1.22) and taking advantage of the orthogonality condition for the electron wave functions, one obtains the function $\Delta g^{(2,\mathrm{c})}_{ii}(E)$ in the following form:

$$\begin{aligned} \Delta g^{(2,\mathrm{c})}_{ii}(E) = \frac{ie^2}{(E-\varepsilon_i)^2} \sum_{J'M'N'} \int \frac{d\omega}{2\pi} \frac{2\omega_{\mathrm{N}}}{\omega^2-\omega_{\mathrm{N}}^2+i0} B(EJ'[N']) \\ \times \sum_{i_1,i_2} \frac{\langle i|\delta V|i_1\rangle\langle i_1|F_{J'}Y_{J'M'}|i_2\rangle\langle i_2|F_{J'}Y^*_{J'M'}|i\rangle}{[E-\varepsilon_{i_1}][E-\omega-\varepsilon_{i_2}(1-i0)]}. \end{aligned} \tag{4.105}$$

The contribution from the diagram (c) in Fig. 4.7 can be conveniently divided into the so-called irreducible ($\varepsilon_{i_1} \neq \varepsilon_i$) and reducible ($\varepsilon_{i_1} = \varepsilon_i$) parts. The first term in Eq. (1.32) for the irreducible part then becomes

$$\begin{aligned} \Delta E^{(2,\mathrm{c,irr})}_{i,\mathrm{NP}} &= \frac{1}{2\pi i} \oint_\Gamma dE\,(E-\varepsilon_i)\, \Delta g^{(2,\mathrm{c})}_{ii}(E)\Big|_{\varepsilon_{i_1}\neq\varepsilon_i} \\ &= ie^2 \sum_{J'M'N'} \int \frac{d\omega}{2\pi} \frac{2\omega_{\mathrm{N}}}{\omega^2-\omega_{\mathrm{N}}^2+i0} B(EJ'[N']) \\ &\times \sum_{i_1,i_2}^{i_1\neq i} \frac{\langle i|\delta V|i_1\rangle\langle i_1|F_{J'}Y_{J'M'}|i_2\rangle\langle i_2|F_{J'}Y^*_{J'M'}|i\rangle}{[\varepsilon_i-\varepsilon_{i_1}][\varepsilon_i-\omega-\varepsilon_{i_2}(1-i0)]}. \end{aligned} \tag{4.106}$$

As in Section 4.1, the integration in ω can be easily performed using the contour method:

$$i\int \frac{d\omega}{2\pi} \frac{2\omega_{\mathrm{N}}}{(\omega^2-\omega_{\mathrm{N}}^2+i0)(\varepsilon_i-\varepsilon_{i_2}-\omega+i\varepsilon_{i_2}0)} = \frac{1}{\varepsilon_i-\varepsilon_{i_2}-\mathrm{sgn}(\varepsilon_{i_2})\omega_{\mathrm{N}}}. \tag{4.107}$$

All three matrix elements in Eq. (4.106) are then evaluated via the Wigner-Eckart theorem as follows:

$$\langle i|\delta V|i_1\rangle = \frac{|e|}{2} B^{\mathcal{J}} (-1)^{j_i-m_i} \begin{pmatrix} j_i & 1 & j_1 \\ -m_i & 0 & m_1 \end{pmatrix} \langle i||\mathrm{x}[\mathbf{n}\times\boldsymbol{\alpha}]^{\mathcal{J}}||i_1\rangle, \tag{4.108}$$

$$\langle i_1|F_{J'}Y_{J'M'}|i_2\rangle = (-1)^{j_1-m_1} \begin{pmatrix} j_1 & J' & j_2 \\ -m_1 & M' & m_2 \end{pmatrix} \langle i_1||F_{J'}Y_{J'}||i_2\rangle, \tag{4.109}$$

$$\langle i_2|F_{J'}Y^*_{J'M'}|i\rangle = \langle i|F_{J'}Y_{J'M'}|i_2\rangle = (-1)^{j_i-m_i}\begin{pmatrix} j_i & J' & j_2 \\ -m_i & M' & m_2 \end{pmatrix}\langle i||F_{J'}Y_{J'}||i_2\rangle, \tag{4.110}$$

where $\mathbf{n} = \mathbf{x}/\mathrm{x}$. Due to the orthogonality property of the $3j$-symbols from Eqs. (4.109) and (4.110), the summations over M' and m_2 lead to the conditions $j_1 = j_i$ and $m_1 = m_i$. Then the $3j$-symbol in Eq. (4.110) becomes [139]

$$\begin{pmatrix} j_i & 1 & j_i \\ -m_i & 0 & m_i \end{pmatrix} = (-1)^{j_i-m_i}\frac{m_i}{\sqrt{(2j_i+1)(j_i+1)j_i}}, \tag{4.111}$$

and Eq. (4.106) can be rewritten as

$$\begin{aligned}\Delta E^{(2,\mathrm{c,irr})}_{i,\mathrm{NP}} = {}& \frac{|e|^3}{2}B^{\mathcal{J}}\frac{m_i}{\sqrt{(2j_i+1)(j_i+1)j_i}}\frac{1}{2j_i+1}\sum_{J'N'}B(EJ'[N']) \\ & \times \sum_{\substack{i_1,i_2 \\ j_1=j_i}}^{i_1\neq i}\frac{\langle i||\mathrm{x}[\mathbf{n}\times\boldsymbol{\alpha}]^{\mathcal{J}}||i_1\rangle\langle i_1||F_{J'}Y_{J'}||i_2\rangle\langle i||F_{J'}Y_{J'}||i_2\rangle}{[\varepsilon_i-\varepsilon_{i_1}][\varepsilon_i-\varepsilon_{i_2}-\mathrm{sgn}(\varepsilon_{i_2})\omega_{\mathrm{N}}]}.\end{aligned} \tag{4.112}$$

The reduced matrix element from Eq. (4.108) in general reads [140]

$$\begin{aligned}\langle i||\mathrm{x}[\mathbf{n}\times\boldsymbol{\alpha}]^{\mathcal{J}}||i_1\rangle = {}& (-1)^{l_i}\sqrt{2(2j_i+1)(2j_1+1)}\begin{pmatrix} j_i & j_1 & 1 \\ \frac{1}{2} & \frac{1}{2} & -1 \end{pmatrix}\Pi(l_i+l_1) \\ & \times\int_0^\infty d\mathrm{x}\,\mathrm{x}\Big[G_{n_i\kappa_i}(\mathrm{x})F_{n_1\kappa_1}(\mathrm{x})\triangle(l_i,\tilde{l}_1,1)+F_{n_i\kappa_i}(\mathrm{x})G_{n_1\kappa_1}(\mathrm{x})\triangle(\tilde{l}_i,l_1,1)\Big],\end{aligned} \tag{4.113}$$

where

$$\triangle(l_1,l_2,l_3) = \begin{cases}1 \text{ if } |l_1-l_2|\leq l_3\leq l_1+l_2, \\ 0 \text{ otherwise,}\end{cases} \tag{4.114}$$

$$\tilde{l}(\kappa) \coloneqq l(-\kappa) = l(\kappa)-\mathrm{sgn}(\kappa), \quad l(\kappa) = |\kappa|+\frac{\mathrm{sgn}(\kappa)-1}{2}. \tag{4.115}$$

From the condition $j_1 = j_i$, together with the parity factor $\Pi(l_1+l_i)$ in Eq. (4.113), it follows that $\kappa_1 = \kappa_i$ and $l_1 = l_i$. Thus, with the help of the equality [139]

$$\begin{pmatrix} j_i & j_i & 1 \\ \frac{1}{2} & \frac{1}{2} & -1 \end{pmatrix} = (-1)^{2j_i+1}(-1)^{j_i+\frac{1}{2}}\frac{j_i+\frac{1}{2}}{\sqrt{2j_i(j_i+1)(2j_i+1)}}, \tag{4.116}$$

the expression in Eq. (4.113) is simplified to

$$\langle i||\mathrm{x}[\mathbf{n}\times\boldsymbol{\alpha}]^{\mathcal{J}}||i_1\rangle\Big|_{j_1=j_i} = \kappa_i\sqrt{\frac{2j_i+1}{j_i(j_i+1)}}\,\langle n_i\kappa_i|\mathrm{x}\sigma^1|n_1\kappa_i\rangle, \tag{4.117}$$

with

$$\langle n_1\kappa_1|\mathrm{x}\sigma^1|n_2\kappa_2\rangle \coloneqq \int_0^\infty d\mathrm{x}\,\mathrm{x}\begin{pmatrix}G_{n_1\kappa_1}(\mathrm{x})\\F_{n_1\kappa_1}(\mathrm{x})\end{pmatrix}\begin{pmatrix}0&1\\1&0\end{pmatrix}\begin{pmatrix}G_{n_2\kappa_2}(\mathrm{x})\\F_{n_2\kappa_2}(\mathrm{x})\end{pmatrix}. \tag{4.118}$$

The reduced matrix elements in Eqs. (4.109) and (4.110) are given by Eq. (4.98). Taking into account that $\Delta E^{(2,\mathrm{d,irr})}_{i,\mathrm{NP}} = \left[\Delta E^{(2,\mathrm{c,irr})}_{i,\mathrm{NP}}\right]^* = \Delta E^{(2,\mathrm{c,irr})}_{i,\mathrm{NP}}$, we obtain the following final expression for the total irreducible contribution from the diagrams (c) and (d) in Fig. 4.7:

$$\begin{aligned}\Delta E^{(2,\mathrm{c+d,irr})}_{i,\mathrm{NP}} &= \frac{|e|B^3 m_i}{2}\frac{e^2}{2\pi}\frac{\kappa_i}{j_i(j_i+1)(2j_i+1)}\sum_{J'N'}(2J'+1)B(EJ'[N'])\\ &\times\sum_{n_1,n_2\kappa_2}^{n_1\neq n_i} C^2_{J'}(\kappa_i,\kappa_2)\frac{\langle n_i\kappa_i|\mathrm{x}\sigma^1|n_1\kappa_i\rangle\langle n_1\kappa_i|F_{J'}|n_2\kappa_2\rangle\langle n_2\kappa_2|F_{J'}|n_i\kappa_i\rangle}{[\varepsilon_{n_i\kappa_i}-\varepsilon_{n_1\kappa_i}][\varepsilon_{n_i\kappa_i}-\varepsilon_{n_2\kappa_2}-\mathrm{sgn}(\varepsilon_{n_2\kappa_2})\omega_\mathrm{N}]}.\end{aligned} \tag{4.119}$$

Next, in the reducible contribution from the diagrams (c) and (d) we include both terms from Eq. (1.32):

$$\begin{aligned}\Delta E^{(2,\mathrm{c+d,red})}_{i,\mathrm{NP}} &= 2\times\frac{1}{2\pi i}\oint_\Gamma dE\,(E-\varepsilon_i)\,\Delta g^{(2,\mathrm{c})}_{ii}(E)\Big|_{\varepsilon_{i_1}=\varepsilon_i}\\ &-\left(\frac{1}{2\pi i}\oint_\Gamma dE\,(E-\varepsilon_i)\Delta g^{(1,\mathrm{a})}_{ii}(E)\right)\left(\frac{1}{2\pi i}\oint_\Gamma dE\,\Delta g^{(1,\mathrm{b})}_{ii}(E)\right).\end{aligned} \tag{4.120}$$

It can be easily shown that

$$\Delta g^{(1,\mathrm{a})}_{ii}(E) = \frac{\langle i|\delta V|i\rangle}{(E-\varepsilon_i)^2}, \tag{4.121}$$

and by applying the longitudinal approximation to Eq. (4.27) we also have

$$\begin{aligned}\Delta g^{(1,\mathrm{b})}_{ii}(E) &= \frac{ie^2}{(E-\varepsilon_i)^2}\sum_{J'M'N'}\int\frac{d\omega}{2\pi}\frac{2\omega_\mathrm{N}}{\omega^2-\omega_\mathrm{N}^2+i0}B(EJ'[N'])\\ &\times\sum_{i_2}\frac{\langle i|F_{J'}Y_{J'M'}|i_2\rangle\langle i_2|F_{J'}Y^*_{J'M'}|i\rangle}{\varepsilon_i-\omega-\varepsilon_{i_2}(1-i0)},\end{aligned} \tag{4.122}$$

which leads to the total reducible contribution

$$\begin{aligned}\Delta E^{(2,\mathrm{c+d,red})}_{i,\mathrm{NP}} &= -ie^2\langle i|\delta V|i\rangle\sum_{J'M'N'}\int\frac{d\omega}{2\pi}\frac{2\omega_\mathrm{N}}{\omega^2-\omega_\mathrm{N}^2+i0}B(EJ'[N'])\\ &\times\sum_{i_2}\frac{\langle i|F_{J'}Y_{J'M'}|i_2\rangle\langle i_2|F_{J'}Y^*_{J'M'}|i\rangle}{[\varepsilon_i-\omega-\varepsilon_{i_2}(1-i0)]^2}.\end{aligned} \tag{4.123}$$

After integrating in ω, applying the Wigner-Eckart theorem and summing over the angular projections, we obtain that

$$\begin{aligned}\Delta E^{(2,\mathrm{c+d,red})}_{i,\mathrm{NP}} &= -\frac{|e|B^3 m_i}{2}\frac{e^2}{4\pi}\frac{\kappa_i}{j_i(j_i+1)(2j_i+1)}\langle n_i\kappa_i|\mathrm{x}\sigma^1|n_i\kappa_i\rangle\\ &\times\sum_{J'N'}(2J'+1)B(EJ'[N'])\sum_{n_2,\kappa_2}C^2_{J'}(\kappa_i,\kappa_2)\frac{\langle n_i\kappa_i|F_{J'}|n_2\kappa_2\rangle^2}{[\varepsilon_{n_i\kappa_i}-\varepsilon_{n_2\kappa_2}-\mathrm{sgn}(\varepsilon_{n_2\kappa_2})\omega_\mathrm{N}]^2}.\end{aligned} \tag{4.124}$$

We now turn to the last diagram (e) in Fig. 4.7. The corresponding NP correction is called the vertex contribution, and its Green's function G reads

$$G^{(\mathrm{e})}((E',\mathbf{x}');(E,\mathbf{x})) = \left(\frac{ie}{2\pi}\right)^2 \int d^3x_1 d^3x_2 d^3x_3 d\omega\, S(E',\mathbf{x}',\mathbf{x}_1)\gamma^\mu S(E'-\omega,\mathbf{x}_1,\mathbf{x}_2) \times \gamma^0 \delta V(\mathbf{x}_2) S(E'-\omega,\mathbf{x}_2,\mathbf{x}_3)\gamma^\nu S(E,\mathbf{x}_3,\mathbf{x}) \times D^{\mathrm{NP}}_{\mu\nu}(\omega,\mathbf{x}_1,\mathbf{x}_3)\delta(E-E'). \tag{4.125}$$

The energy correction due to the diagram (e) is then expressed as

$$\Delta E^{(2,\mathrm{e})}_{i,\mathrm{NP}} = ie^2 \sum_{J'M'N'} \int \frac{d\omega}{2\pi} \frac{2\omega_{\mathrm{N}}}{\omega^2-\omega_{\mathrm{N}}^2+i0} B(EJ'[N']) \times \sum_{i_1,i_2} \frac{\langle i|F_{J'}Y_{J'M'}|i_1\rangle\langle i_1|\delta V|i_2\rangle\langle i_2|F_{J'}Y^*_{J'M'}|i\rangle}{[\varepsilon_i-\omega-\varepsilon_{i_1}(1-i0)][\varepsilon_i-\omega-\varepsilon_{i_2}(1-i0)]}. \tag{4.126}$$

We call the term with $\varepsilon_{i_1} = \varepsilon_{i_2}$ the pole contribution, in which case the integration in ω is done as follows:

$$i\int \frac{d\omega}{2\pi} \frac{2\omega_{\mathrm{N}}}{[\omega^2-\omega_{\mathrm{N}}^2+i0][\varepsilon_i-\varepsilon_{i_1}-\omega+i\varepsilon_{i_1}0]^2} = \frac{1}{[\varepsilon_i-\varepsilon_{i_1}-\mathrm{sgn}(\varepsilon_{i_1})\omega_{\mathrm{N}}]^2}. \tag{4.127}$$

In order to perform the integration in ω for the rest of the sum in Eq. (4.126) (the so-called residual contribution, $\varepsilon_{i_1} \neq \varepsilon_{i_2}$), we make use of the following equality:

$$\frac{1}{(\varepsilon_i-\varepsilon_{i_1}-\omega)(\varepsilon_i-\varepsilon_{i_2}-\omega)} = \frac{1}{\varepsilon_{i_1}-\varepsilon_{i_2}}\left[\frac{1}{(\varepsilon_i-\varepsilon_{i_1}-\omega)} - \frac{1}{(\varepsilon_i-\varepsilon_{i_2}-\omega)}\right], \tag{4.128}$$

such that

$$i\int \frac{d\omega}{2\pi} \frac{2\omega_{\mathrm{N}}}{(\omega^2-\omega_{\mathrm{N}}^2+i0)(\varepsilon_i-\varepsilon_{i_1}-\omega+i\varepsilon_{i_1}0)(\varepsilon_i-\varepsilon_{i_2}-\omega+i\varepsilon_{i_2}0)} = \frac{1}{\varepsilon_{i_1}-\varepsilon_{i_2}}\left[\frac{1}{\varepsilon_i-\varepsilon_{i_1}-\mathrm{sgn}(\varepsilon_{i_1})\omega_{\mathrm{N}}} - \frac{1}{\varepsilon_i-\varepsilon_{i_2}-\mathrm{sgn}(\varepsilon_{i_2})\omega_{\mathrm{N}}}\right]. \tag{4.129}$$

Using the fact that $\left[\Delta E^{(2,\mathrm{e})}_{i,\mathrm{NP}}\right]^* = \Delta E^{(2,\mathrm{e})}_{i,\mathrm{NP}}$, it can be easily seen that the two terms on the right-hand side of Eq. (4.129) lead to identical contributions. Then, after applying the Wigner-Eckart theorem, summing over the projections of the angular momenta and making use of the following identity [139]:

$$\sum_{\mu_1\mu_2\mu_3} (-1)^{l_1+l_2+l_3+\mu_1+\mu_2+\mu_3} \begin{pmatrix} j_1 & l_2 & l_3 \\ m_1 & \mu_2 & -\mu_3 \end{pmatrix} \begin{pmatrix} l_1 & j_2 & l_3 \\ -\mu_1 & m_2 & \mu_3 \end{pmatrix} \times \begin{pmatrix} l_1 & l_2 & j_3 \\ \mu_1 & -\mu_2 & m_3 \end{pmatrix} = \begin{pmatrix} j_1 & j_2 & j_3 \\ m_1 & m_2 & m_3 \end{pmatrix} \begin{Bmatrix} j_1 & j_2 & j_3 \\ l_1 & l_2 & l_3 \end{Bmatrix}, \tag{4.130}$$

as well as employing Eq. (4.111), the expression for the residual contribution from the diagram (e) in Fig. 4.7 becomes

$$\begin{aligned}\Delta E^{(2,\mathrm{e,res})}_{i,\mathrm{NP}} &= 2\times\frac{|e|^3}{2}B^{\prime}\frac{m_i}{\sqrt{j_i(j_i+1)(2j_i+1)}}\sum_{J'N'}B(EJ'[N'])\\ &\times\sum_{i_1,i_2}^{i_1\neq i_2}(-1)^{j_1+j_2+1+J'}\left\{\begin{array}{ccc} j_i & 1 & j_i\\ j_2 & J' & j_1\end{array}\right\}\\ &\times\frac{\langle i||F_{J'}Y_{J'}||i_1\rangle\langle i_1||\mathrm{x}[\mathbf{n}\times\boldsymbol{\alpha}]^{\prime}||i_2\rangle\langle i_2||F_{J'}Y_{J'}||i\rangle}{[\varepsilon_{i_1}-\varepsilon_{i_2}][\varepsilon_i-\varepsilon_{i_1}-\mathrm{sgn}(\varepsilon_{i_1})\omega_{\mathrm{N}}]},\end{aligned}\tag{4.131}$$

or, after writing out the expressions for the reduced matrix elements:

$$\begin{aligned}\Delta E^{(2,\mathrm{e,res})}_{i,\mathrm{NP}} &= \frac{|e|B^{\prime}m_i}{2}\frac{e^2}{2\pi}\frac{1}{\sqrt{j_i(j_i+1)(2j_i+1)}}\sum_{J'N'}(-1)^{J'}(2J'+1)B(EJ'[N'])\\ &\times\sum_{n_1\kappa_1,n_2\kappa_2}^{n_1\neq n_2}\left\{\begin{array}{ccc} j_i & 1 & j_i\\ j_2 & J' & j_1\end{array}\right\}\left(\begin{array}{ccc} j_1 & j_2 & 1\\ \frac{1}{2} & \frac{1}{2} & -1\end{array}\right)(-1)^{j_1+j_2+1+l_1}\sqrt{2(2j_1+1)(2j_2+1)}\\ &\times C_{J'}(\kappa_i,\kappa_1)C_{J'}(\kappa_2,\kappa_i)\Pi(l_1+l_2)\frac{\langle n_i\kappa_i|F_{J'}|n_1\kappa_1\rangle\langle n_1\kappa_1|\mathrm{x}\sigma^1|n_2\kappa_2\rangle\langle n_2\kappa_2|F_{J'}|n_i\kappa_i\rangle}{[\varepsilon_{n_1\kappa_1}-\varepsilon_{n_2\kappa_2}][\varepsilon_{n_i\kappa_i}-\varepsilon_{n_1\kappa_1}-\mathrm{sgn}(\varepsilon_{n_1\kappa_1})\omega_{\mathrm{N}}]}.\end{aligned}\tag{4.132}$$

In a similar manner, one also obtains for the pole contribution

$$\begin{aligned}\Delta E^{(2,\mathrm{e,pol})}_{i,\mathrm{NP}} &= \frac{|e|B^{\prime}m_i}{2}\frac{e^2}{4\pi}\frac{1}{\sqrt{j_i(j_i+1)(2j_i+1)}}\sum_{J'N'}(-1)^{J'}(2J'+1)B(EJ'[N'])\\ &\times\sum_{n_1\kappa_1}\left\{\begin{array}{ccc} j_i & 1 & j_i\\ j_1 & J' & j_1\end{array}\right\}\kappa_1\sqrt{\frac{2j_1+1}{j_1(j_1+1)}}C_{J'}(\kappa_i,\kappa_1)C_{J'}(\kappa_1,\kappa_i)\\ &\times\frac{\langle n_i\kappa_i|F_{J'}|n_1\kappa_1\rangle^2\langle n_1\kappa_1|\mathrm{x}\sigma^1|n_1\kappa_1\rangle}{[\varepsilon_{n_i\kappa_i}-\varepsilon_{n_1\kappa_1}-\mathrm{sgn}(\varepsilon_{n_1\kappa_1})\omega_{\mathrm{N}}]^2}.\end{aligned}\tag{4.133}$$

Finally, the corresponding NP correction to the g factor is simply given by

$$\Delta g^{\mathrm{total}}_{i,\mathrm{NP}} = \Delta E^{(2,\mathrm{c+d+e})}_{i,\mathrm{NP}}\times\left[\frac{|e|B^{\prime}m_i}{2}\right]^{-1}.\tag{4.134}$$

We note that the derivations presented in this section can be readily adapted to other forms of the external potential $\delta V(\mathbf{x})$, e.g., in calculations of the NP correction to the hyperfine structure [3, 141].

4.4. Reduced g factor

In Chapter 3, we examined the suppression of the FNS effect in the specific differences of g factors. Originally, the introduction of these quantities was partly motivated by the possibility of using them to extract the fine-structure constant α with an improved level of precision. However, since the specific differences g'_s and g'_p involve the ground-state g factors of Li- and B-like ions, respectively, a successful implementation of these ideas requires significant developments in the many-electron QED theory, which still needs to be improved by orders of magnitude for this purpose (see, e.g. Ref. [25]). Therefore, in Ref. [4] another weighted difference for determining the fine-structure constant was put forward, which relies only on the properties of H-like systems. An obvious advantage of such a scheme is that the theory of one-electron ions is substantially more advanced than that of Li- and B-systems, as it is completely free from the complications associated with many-electron effects.

In the following, we first show the main idea behind the new weighted difference. We first recall that, according to Ref. [82], the bound-electron g factor in the case of an extended nucleus can be expressed in terms of the electron energy as follows:

$$g_{\rm ext}[n\kappa] = \frac{\kappa}{j(j+1)}\left(\kappa\frac{\partial E_{\rm ext}[n\kappa]}{\partial m_{\rm e}} - \frac{1}{2}\right), \tag{4.135}$$

which for the ground state $1s_{1/2}$ ($\kappa = -1,\ j = 1/2$) becomes

$$g_{\rm ext}[1s_{1/2}] = \frac{4}{3}\left(\frac{\partial E_{\rm ext}[1s_{1/2}]}{\partial m_{\rm e}} + \frac{1}{2}\right). \tag{4.136}$$

On the other hand, it was shown in Ref. [100] that to a good level of approximation

$$\Delta E_{\rm FNS}[1s_{1/2}] \backsimeq m_{\rm e}^{2\gamma+1}, \quad \gamma = \sqrt{1-(Z\alpha)^2}\,, \tag{4.137}$$

from which it readily follows that

$$\Delta g_{\rm FNS}[1s_{1/2}] \approx \frac{4}{3}\,(2\gamma+1)\,\frac{\Delta E_{\rm FNS}[1s_{1/2}]}{m_{\rm e}}. \tag{4.138}$$

Thus, Eq. (4.138) motivates the introduction of the following difference in order to cancel out the FNS effect:

$$\widetilde{g} \coloneqq g - x\frac{E}{m_{\rm e}}, \tag{4.139}$$

with the weight

$$x = \frac{4}{3}\left(2\sqrt{1-(Z\alpha)^2}+1\right). \tag{4.140}$$

The quantity $\widetilde{g}$ was named in Ref. [4] as the reduced g factor. It can be shown that, apart from taking advantage of the property (4.138), $\widetilde{g}$ also exhibits a somewhat

enhanced sensitivity to a variation of the fine-structure constant $\delta\alpha$ as compared to g. This favors the new proposed scheme for extracting α over those employing the specific differences, where the sensitivity to $\delta\alpha$ is slightly reduced.

The expected high degree of cancellation of the FNS effect in $\widetilde{g}$ was confirmed by using the methods similar to those presented in Chapter 3. However, it is not obvious to what extent this kind of suppression may occur for more complicated nuclear-structure effects, such as nuclear polarization. To answer this question, we performed NP calculations for a wide range of H-like ions by means of the formalism developed in the previous section. For consistency, the longitudinal approximation was used for both the g factor and the electron energy. In Table 4.4 we present the results for the NP corrections to the ground-state energy, g factor and reduced g factor of H-like ions ranging from $^{22}_{10}\mathrm{Ne}^{9+}$ to $^{238}_{92}\mathrm{U}^{91+}$. The parameters ω_{N} and $B(EJ')$ for low-lying nuclear states were taken from Refs. [116, 142–154], while the contributions from giant resonances were estimated by means of the sum rules in Eqs. (4.92) and (4.93). Our results demonstrate that a significant cancellation of the NP effect indeed takes place in the reduced g factor. Moreover, we have found that the calculation uncertainty of $\Delta\widetilde{g}_{\mathrm{NP}}$ was also suppressed compared to the uncertainties of ΔE_{NP} and Δg_{NP}, which is crucial for an improved extraction of α from $\widetilde{g}$. For example, assuming a 5% theoretical uncertainty for $\Delta\widetilde{g}_{\mathrm{NP}}$, one obtains that it is of the same order of magnitude as the uncertainty of the FNS effect. We compare the nuclear-structure uncertainties of $\widetilde{g}$ with the one due to the absolute uncertainty of the fine-structure constant $\delta\alpha = 1.1 \cdot 10^{-12}$ [8] in Fig. 4.8 [4]. As it can be seen, there is a broad range of elements with $Z < 50$ suitable for an improved determination of α from the reduced g factor.

In addition, it has been recently demonstrated that the reduced g factor is also a promising quantity to search for physics beyond the Standard Model. While the detrimental uncertainties from nuclear-structure effects in this weighted difference are strongly suppressed, it was shown that hypothetical contributions from possible new interactions are well preserved [155]. As a result, the current best atomic limits on a hypothetical fifth force can be improved by at least an order of magnitude, if the isotope shift of the ground-state energy can be measured with five to six digits of relative precision. From the experimental point of view, it has been already demonstrated that such measurements are feasible at the required level of precision [156].

Table 4.2.: NP corrections to the ground-state energy, g factor and reduced g factor of H-like ions. The corresponding root-mean-square nuclear charge radii are also listed. The numbers in brackets indicate powers of 10.

Ion	$\sqrt{\langle r^2 \rangle}$ (fm)	ΔE_{NP} (meV)	Δg_{NP}	$\Delta \widetilde{g}_{\mathrm{NP}}$
$^{22}_{10}\mathrm{Ne}^{9+}$	2.9525	-0.00024	-2.10[-12]	-2.39[-13]
$^{28}_{14}\mathrm{Si}^{13+}$	3.1224	-0.00105	-9.07[-12]	-8.77[-13]
$^{40}_{20}\mathrm{Ca}^{19+}$	3.4776	-0.00607	-5.11[-11]	-3.95[-12]
$^{64}_{30}\mathrm{Zn}^{29+}$	3.9283	-0.0545	-4.45[-10]	-2.56[-11]
$^{84}_{36}\mathrm{Kr}^{35+}$	4.1884	-0.144	-1.15[-9]	-5.87[-11]
$^{102}_{44}\mathrm{Ru}^{43+}$	4.4809	-0.541	-4.25[-9]	-1.66[-10]
$^{112}_{48}\mathrm{Cd}^{47+}$	4.5944	-0.857	-6.66[-9]	-2.34[-10]
$^{142}_{60}\mathrm{Nd}^{59+}$	4.9123	-2.96	-2.22[-8]	-5.53[-10]
$^{158}_{64}\mathrm{Gd}^{63+}$	5.1569	-10.4	-7.69[-8]	-1.62[-9]
$^{162}_{66}\mathrm{Dy}^{65+}$	5.2074	-12.9	-9.47[-8]	-1.86[-9]
$^{174}_{70}\mathrm{Yb}^{69+}$	5.3108	-18.9	-1.37[-7]	-2.32[-9]
$^{196}_{78}\mathrm{Pt}^{77+}$	5.4307	-22.6	-1.57[-7]	-1.74[-9]
$^{208}_{82}\mathrm{Pb}^{81+}$	5.5012	-28.9	-1.98[-7]	-1.54[-9]
$^{238}_{92}\mathrm{U}^{91+}$	5.5817	-196.5	-1.27[-6]	-2.09[-9]

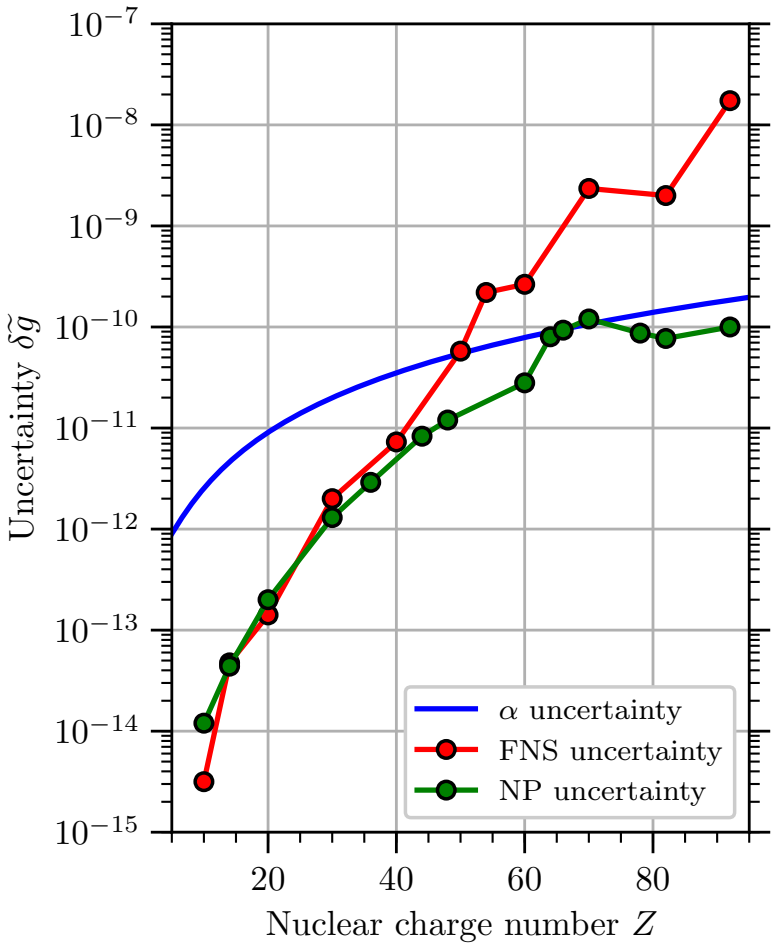

Figure 4.8.: Comparison of the nuclear-structure uncertainties of the reduced g factor with the one due to the absolute uncertainty of the fine-structure constant $\delta\alpha = 1.1 \cdot 10^{-12}$ [8]. The figure was taken from Ref. [4].

Summary and Outlook

Since the first formulations of the "planetary" model of the atom, there has been a tremendous progress in understanding both the structure of the atomic nucleus and the arrangement of electrons around it. As a result, atomic and nuclear physics have grown to become more and more specialized and somewhat separate fields. Yet, the atom itself remains a single whole. In this thesis, we have explored the intersection of modern atomic and nuclear physics with the aim to move one step closer to a truly holistic description of this fundamental building block of matter. Our point of view is to investigate how atomic properties are influenced by fine details of nuclear structure. To describe the latter, we use the Skyrme-Hartree-Fock mean-field approach to construct the nuclear ground state and the random-phase approximation (RPA) to build up the complete spectrum of nuclear excitations. At the same time, the interplay between atomic and nuclear degrees of freedom is put into a relativistic field-theoretical framework. An overview of all the tools necessary for such calculations is presented in Chapters 1 and 2.

We start with the ground-state nuclear properties in Chapter 3, where we consider the finite-nuclear-size (FNS) effect from the microscopic point of view. There, we employ nuclear charge distributions obtained by the Skyrme-Hartree-Fock procedure in order to calculate the FNS corrections to atomic energy levels and the bound-electron g-factor in H-like ions. We have demonstrated that such theoretical charge densities are in good agreement with the ones obtained from electron-scattering experiments. We have found, however, that an accurate shape of a charge distribution is not nearly enough and that the value of the nuclear charge radius is an absolutely crucial input parameter for FNS calculations. Based on that observation, we have proposed a scheme of slightly adjusting a single parameter of the Skyrme force in order to reproduce the current tabulated values of the root-mean-square nuclear radii, while keeping the shapes of the charge distributions intact. This procedure allows to effectively suppress the ambiguity in the choice of a Skyrme parametrization, and it can also be used to translate the error bars of nuclear radii into the calculation uncertainties of the FNS corrections. In addition, we have studied the suppression of the FNS effect in the weighted differences of g factors, and we have shown that in the high-Z regime a direct numerical evaluation of the weights is preferable over using analytical perturbation-theory expressions.

Even though we have found that the FNS corrections for the microscopic description and the simple two-parameter Fermi model agree within the current error bars of nuclear radii, we expect the details of nuclear charge distributions to become increasingly important in the future when the nuclear radii are known to a higher level of precision. Furthermore, our approach can be readily extended to other, perhaps more sensitive, quantities, such as the magnetic-dipole and electric-quadrupole hyperfine-splitting constants. The microscopic nuclear description may also be used to obtain nuclear magnetization distributions, which are crucial for evaluation of the Bohr-Weisskopf effect and an accurate description of the hyperfine splitting.

In Chapter 4, nuclear excitations are brought into the picture resulting in dynamic electron- or muon-nucleus interactions, known as nuclear polarization (NP). First, we present a field-theoretical treatment of the NP correction to atomic energies, where the photon propagator gets modified by the NP insertion. The insertion, in turn, is built out of the nuclear excited states obtained within the RPA method. This approach allows to describe NP on the same footing as the QED effects so that the methods from Chapter 1 can be utilized in a systematic way.

Next, these developments are applied to the long-standing problem of the fine-structure anomalies in heavy muonic atoms, where the theoretical predictions for the NP energy shifts are generally considered to be responsible for the persisting discrepancies between theory and experiment for the $\Delta 2p$ splitting in muonic ^{90}Zr, $^{112-124}$Sn and ^{208}Pb as well as the $\Delta 3p$ splitting in μ-^{208}Pb. In this context, we have pursued two goals. The first is to provide the most complete to date NP calculations in these systems, while the second is to analyze the dominant calculation uncertainty coming from the nuclear model dependence. To achieve the latter and cover all possible realistic results, we have selected nine different parametrizations of the effective Skyrme force spanning a wide range in the parameter space. We have found that the tension between theory and experiment remains high in all cases even in light of the nuclear model uncertainty. Thus, these findings constitute evidence against the prevalent hypothesis that the NP effect is the source of the anomalies. Regarding possible resolutions to this intriguing puzzle, on the one hand, there are still some open questions on the NP side, such as the role of relativistic nuclear effects in heavy muonic atoms or potential muon-nuclear resonances in ^{208}Pb. On the other hand, we believe that it is worthwhile to look beyond NP. It may well be that the solution is to be found in refined QED corrections or even some exotic and previously unaccounted-for effects.

Another part of Chapter 4 is devoted to extending the NP formalism to the bound-electron g factor in H-like ions. The derivations are performed in the longitudinal (or Coulomb) approximation, which is justified by the smaller overlap between the electronic and nuclear wave functions as compared to the case of muonic atoms. The resulting formulas have been used to investigate the degree of cancellation of

the NP effect in the weighted difference of the ground-state g factor and the total dimensionless ground-state energy $E_{1s_{1/2}}/m_{\mathrm{e}}$ in H-like ions. This quantity was put forward in our research group, and it was named the reduced g factor. With the motivation of extracting the fine-structure constant α from high-precision spectroscopic experiments, the reduced g factor was designed in such a way as to cancel out the leading FNS effect. It was not obvious, however, to what degree such a cancellation would hold in the case of the NP correction. By performing NP calculations for the reduced g factor, we have shown that a significant suppression of the NP correction indeed takes place in this weighted difference. Furthermore, the theoretical uncertainty of the NP contribution to the reduced g factor turned out to be of the same order of magnitude as that of the FNS effect. Thus, it has been demonstrated that the reduced g factor is indeed a very promising tool for determining the fine-structure constant with an improved precision in the foreseeable future. We note that it has been recently shown that comparing theoretical predictions and experimental results via the reduced g factor is also a competitive way to search for physics beyond the Standard Model.

Overall, it can be clearly seen that there is no lack of motivation for advancing our understanding of nuclear-structure effects in atomic systems. There already exists an overwhelming variety of systems, phenomena and ideas where a firm grasp of the interplay between atomic and nuclear physics has become indispensable. As the experimental precision is being continuously pushed forward, this demand for detailed knowledge of nuclear structure in the context of atomic properties can only be expected to grow even more. For these purposes, a unified and fully microscopic approach is the only way to truly gain a deeper insight into the inner workings of the atom as a single, *indivisible* entity.

A. Atomic reduced matrix elements

The explicit expressions of the Dirac charge and current density operators from Eq. (4.29) are

$$\hat{\rho}_{\mathrm{f}}(\mathbf{x}) = -|e| \begin{pmatrix} \mathbb{1}_2 & 0 \\ 0 & \mathbb{1}_2 \end{pmatrix} \delta^{(3)}(\mathbf{x} - \mathbf{x}_{\mathrm{f}}), \quad \hat{\mathbf{j}}_{\mathrm{f}}(\mathbf{x}) = -|e| \begin{pmatrix} 0 & \boldsymbol{\sigma} \\ \boldsymbol{\sigma} & 0 \end{pmatrix} \delta^{(3)}(\mathbf{x} - \mathbf{x}_{\mathrm{f}}), \tag{A.1}$$

where $\mathbf{x}_{\mathrm{f}}$ denotes the coordinates of a bound fermion, and $\boldsymbol{\sigma} = (\sigma^1, \sigma^2, \sigma^3)$ are the Pauli matrices.

In order to calculate the reduced matrix elements of the atomic multipole operators $\hat{m}_{JM}$ and $\hat{t}_{JLM}$, we make use of the following relations [117]:

$$\langle \kappa' m' | Y_{J'M'} | \kappa m \rangle = (-1)^{j'-m'} \begin{pmatrix} j' & J' & j \\ -m' & M' & m \end{pmatrix} \sqrt{\frac{2J'+1}{4\pi}} C_{J'}(\kappa', \kappa), \tag{A.2}$$

where

$$C_{J'}(\kappa', \kappa) = (-1)^{j'+\frac{1}{2}} \sqrt{(2j'+1)(2j+1)} \begin{pmatrix} j & J' & j' \\ \frac{1}{2} & 0 & -\frac{1}{2} \end{pmatrix} \Pi(l, l', J'), \tag{A.3}$$

and

$$\langle \kappa' m' | \boldsymbol{\sigma} \cdot \mathbf{Y}_{J'L'M'} | \kappa m \rangle = (-1)^{j'-m'} \begin{pmatrix} j' & J' & j \\ -m' & M' & m \end{pmatrix} \sqrt{\frac{2J'+1}{4\pi}} S_{J'L'}(\kappa, \kappa'), \tag{A.4}$$

where

$$S_{J'(J'+1)}(\kappa, \kappa') = \sqrt{\frac{J'+1}{2J'+1}} \left(1 + \frac{\kappa + \kappa'}{J'+1}\right) C_{J'}(-\kappa', \kappa), \tag{A.5}$$

$$S_{J'J'}(\kappa, \kappa') = \frac{\kappa - \kappa'}{\sqrt{J'(J'+1)}} C_{J'}(\kappa', \kappa), \tag{A.6}$$

$$S_{J'(J'-1)}(\kappa, \kappa') = \sqrt{\frac{J'}{2J'+1}} \left(-1 + \frac{\kappa + \kappa'}{J'}\right) C_{J'}(-\kappa', \kappa). \tag{A.7}$$

Then for the bound-fermion wave functions of the form

$$\psi_{n\kappa m}(\mathbf{x}) = \frac{1}{\mathrm{x}} \begin{pmatrix} G_{n\kappa}(\mathrm{x}) \Omega_{\kappa m}(\Omega_{\mathbf{x}}) \\ i F_{n\kappa}(\mathrm{x}) \Omega_{-\kappa m}(\Omega_{\mathbf{x}}) \end{pmatrix}, \tag{A.8}$$

it immediately follows that

$$\begin{aligned}\langle i'||\hat{m}_{J'}(\mathrm{q})||i\rangle = &-|e|\sqrt{\frac{2J'+1}{4\pi}}C_{J'}(\kappa',\kappa)\\ &\times\int_0^\infty d\mathrm{x}\, j_{J'}(\mathrm{qx})\left[G_{n'\kappa'}(\mathrm{x})G_{n\kappa}(\mathrm{x})+F_{n'\kappa'}(\mathrm{x})F_{n\kappa}(\mathrm{x})\right],\end{aligned} \tag{A.9}$$

$$\begin{aligned}\langle i'||\hat{t}_{J'L}(\mathrm{q})||i\rangle = -i|e|\sqrt{\frac{2J'+1}{4\pi}}\int_0^\infty d\mathrm{x}\, j_L(\mathrm{qx})[&G_{n'\kappa'}(\mathrm{x})F_{n\kappa}(\mathrm{x})S_{J'L}(-\kappa,\kappa')\\ &-F_{n'\kappa'}(\mathrm{x})G_{n\kappa}(\mathrm{x})S_{J'L}(\kappa,-\kappa')].\end{aligned} \tag{A.10}$$

B. Nuclear reduced matrix elements

In this thesis, we employ the non-relativistic nuclear charge-current density operators given by [118]

$$\hat{\rho}_{\mathrm{N}}(\mathbf{x}) = \sum_{i}^{A} |e|\, \delta^{(3)}(\mathbf{x} - \mathbf{x}_i) \frac{1 - \tau_{3,i}}{2}, \tag{B.1}$$

$$\hat{\mathbf{J}}_{\mathrm{N}}(\mathbf{x}) = \hat{\mathbf{J}}_{\mathrm{N,c}}(\mathbf{x}) + \hat{\mathbf{J}}_{\mathrm{N,m}}(\mathbf{x}), \tag{B.2}$$

$$\hat{\mathbf{J}}_{\mathrm{N,c}}(\mathbf{x}) = \sum_{i}^{A} |e|\, \delta^{(3)}(\mathbf{x} - \mathbf{x}_i) \frac{1 - \tau_{3,i}}{2} \frac{\overrightarrow{\nabla}_{\mathbf{x}_i} - \overleftarrow{\nabla}_{\mathbf{x}_i}}{2Mi}, \tag{B.3}$$

$$\hat{\mathbf{J}}_{\mathrm{N,m}}(\mathbf{x}) = \hat{\mathbf{J}}^{\mathrm{p}}_{\mathrm{N,m}}(\mathbf{x}) + \hat{\mathbf{J}}^{\mathrm{n}}_{\mathrm{N,m}}(\mathbf{x}) = \nabla \times \hat{\boldsymbol{\mu}}(\mathbf{x}), \tag{B.4}$$

$$\hat{\boldsymbol{\mu}}(\mathbf{x}) = \sum_{i}^{A} \delta^{(3)}(\mathbf{x} - \mathbf{x}_i) \frac{|e|}{2M} \left(\frac{1 - \tau_{3,i}}{2} \mu_{\mathrm{p}} + \frac{1 + \tau_{3,i}}{2} \mu_{\mathrm{n}} \right) \boldsymbol{\sigma}_i, \tag{B.5}$$

where the sums run over all nucleons with $\tau_{3,i} = -1$ for protons and $\tau_{3,i} = 1$ for neutrons, $\boldsymbol{\sigma}_i$ are the Pauli matrices acting on the ith nucleon, M is the nucleon mass, and $\mu_{\mathrm{p}} \approx 2.793$ and $\mu_{\mathrm{n}} \approx -1.913$ are the magnetic moments (in nuclear magnetons) of a proton and a neutron, respectively [8]. $\hat{\mathbf{J}}_{\mathrm{N,c}}$ is the convection current due to the motion of individual nucleons within the nucleus, while $\hat{\mathbf{J}}_{\mathrm{N,m}}$ is the magnetization current generated by the magnetic moments of the nucleons.

The reduced matrix elements of the nuclear multipole operators $\hat{M}_{JM}$ and $\hat{T}_{JLM}$ read

$$\langle I' || \hat{M}_{J'}(\mathrm{q}) || I \rangle = \int_0^\infty d\mathrm{x}\, \mathrm{x}^2 j_{J'}(\mathrm{qx}) \varrho^{I'I}_{J'}(\mathrm{x}), \tag{B.6}$$

$$\langle I' || \hat{T}_{J'L}(\mathrm{q}) || I \rangle = \int_0^\infty d\mathrm{x}\, \mathrm{x}^2 j_{L}(\mathrm{qx}) \mathcal{J}^{I'I}_{J'L}(\mathrm{x}), \tag{B.7}$$

where in the RPA formalism [118]

$$\begin{aligned} \varrho^{I'I}_{J'}(\mathrm{x}) &= \langle I' || \int d\Omega_{\mathbf{x}}\, Y_{J'}(\Omega_{\mathbf{x}}) \hat{\rho}_{\mathrm{N}}(\mathbf{x}) || I \rangle \\ &= \sum_{j_1 j_2} \left[X^{(I')}_{j_1 j_2} + (-1)^{J'} Y^{(I')}_{j_1 j_2} \right] \langle j_2 || \int d\Omega_{\mathbf{x}}\, Y_{J'}(\Omega_{\mathbf{x}}) \hat{\rho}_{\mathrm{N}}(\mathbf{x}) || j_1 \rangle, \end{aligned} \tag{B.8}$$

$$\begin{aligned} \mathcal{J}^{I'I}_{J'L}(\mathrm{x}) = \langle I' || \int d\Omega_{\mathbf{x}}\, \mathbf{Y}_{J'L}(\Omega_{\mathbf{x}}) \cdot \hat{\mathbf{J}}_{\mathrm{N}}(\mathbf{x}) || I \rangle &= \sum_{j_1 j_2} \left[X^{(I')}_{j_1 j_2} + (-1)^{L} Y^{(I')}_{j_1 j_2} \right] \\ &\times \langle j_2 || \int d\Omega_{\mathbf{x}} \left(\mathbf{Y}_{J'L}(\Omega_{\mathbf{x}}) \cdot \left[\hat{\mathbf{J}}_{\mathrm{N,c}}(\mathbf{x}) + \hat{\mathbf{J}}_{\mathrm{N,m}}(\mathbf{x}) \right] \right) || j_1 \rangle. \end{aligned} \tag{B.9}$$

The particle-hole reduced matrix elements between single-nucleon states ($|j\rangle \equiv |njl\rangle$) for the charge density are written as [118]

$$\begin{aligned}\langle j_2||\int d\Omega_{\mathbf{x}}\, Y_{J'}(\Omega_{\mathbf{x}})\hat{\rho}_{\mathrm{N}}(\mathbf{x})||j_1\rangle = \frac{|e|}{2}\left[1+(-1)^{l_1+l_2+J'}\right](-1)^{j_1-j_2+J'} \\ \times\sqrt{\frac{(2j_1+1)(2J'+1)}{4\pi}}C^{j_2\frac{1}{2}}_{j_1\frac{1}{2},J'0}R_1(\mathrm{x})R_2(\mathrm{x}),\end{aligned} \tag{B.10}$$

where $R_1(\mathrm{x})$ and $R_2(\mathrm{x})$ denote single-nucleon radial wave functions.

Next, with the use of the definition

$$\varepsilon = (-1)^{l+\frac{1}{2}-j}\left(j+\frac{1}{2}\right), \tag{B.11}$$

the matrix elements for the convection current can be expressed as [118]

$$\begin{aligned}&\langle j_2||\int d\Omega_{\mathbf{x}}\,\left(\mathbf{Y}_{J'(J'+1)}(\Omega_{\mathbf{x}})\cdot\hat{\mathbf{J}}_{\mathrm{N,c}}(\mathbf{x})\right)||j_1\rangle \\ &=\frac{|e|}{2Mi}\frac{1+(-1)^{l_1+l_2+J'}}{2}(-1)^{j_1+j_2+J'}\sqrt{\frac{(J'+1)(2j_1+1)}{4\pi}}C^{j_2\frac{1}{2}}_{j_1\frac{1}{2},J'0} \\ &\times\left\{R_2(\mathrm{x})\frac{d}{d\mathrm{x}}R_1(\mathrm{x})-R_1(\mathrm{x})\frac{d}{d\mathrm{x}}R_2(\mathrm{x})-\frac{l_1(l_1+1)-l_2(l_2+1)}{J'+1}\frac{R_1(\mathrm{x})R_2(\mathrm{x})}{\mathrm{x}}\right\},\end{aligned} \tag{B.12}$$

$$\begin{aligned}&\langle j_2||\int d\Omega_{\mathbf{x}}\,\left(\mathbf{Y}_{J'J'}(\Omega_{\mathbf{x}})\cdot\hat{\mathbf{J}}_{\mathrm{N,c}}(\mathbf{x})\right)||j_1\rangle \\ &=-\frac{|e|}{2Mi}\frac{1+(-1)^{l_1+l_2+J'+1}}{2}(-1)^{j_1+j_2+J'}\sqrt{\frac{(2J'+1)(2j_1+1)}{4\pi J'(J'+1)}}C^{j_2\frac{1}{2}}_{j_1\frac{1}{2},J'0} \\ &\times\left[(\varepsilon_1+\varepsilon_2)^2-(\varepsilon_1+\varepsilon_2)-J'(J'+1)\right]\frac{R_1(\mathrm{x})R_2(\mathrm{x})}{\mathrm{x}},\end{aligned} \tag{B.13}$$

$$\begin{aligned}&\langle j_2||\int d\Omega_{\mathbf{x}}\,\left(\mathbf{Y}_{J'(J'-1)}(\Omega_{\mathbf{x}})\cdot\hat{\mathbf{J}}_{\mathrm{N,c}}(\mathbf{x})\right)||j_1\rangle \\ &=-\frac{|e|}{2Mi}\frac{1+(-1)^{l_1+l_2+J'}}{2}(-1)^{j_1+j_2+J'}\sqrt{\frac{J'(2j_1+1)}{4\pi}}C^{j_2\frac{1}{2}}_{j_1\frac{1}{2},J'0} \\ &\times\left\{R_2(\mathrm{x})\frac{d}{d\mathrm{x}}R_1(\mathrm{x})-R_1(\mathrm{x})\frac{d}{d\mathrm{x}}R_2(\mathrm{x})+\frac{l_1(l_1+1)-l_2(l_2+1)}{J'}\frac{R_1(\mathrm{x})R_2(\mathrm{x})}{\mathrm{x}}\right\},\end{aligned} \tag{B.14}$$

whereas for the magnetization current [118]

$$\begin{aligned}&\langle j_2||\int d\Omega_{\mathbf{x}}\,\left(\mathbf{Y}_{J'(J'+1)}(\Omega_{\mathbf{x}})\cdot\hat{\mathbf{J}}^{q}_{\mathrm{N,m}}(\mathbf{x})\right)||j_1\rangle \\ &=\frac{|e|}{2Mi}\mu_q\frac{1+(-1)^{l_1+l_2+J'}}{2}(-1)^{j_1+j_2+J'}\sqrt{\frac{(2j_1+1)}{4\pi(J'+1)}}C^{j_2\frac{1}{2}}_{j_1\frac{1}{2},J'0} \\ &\times(\varepsilon_1-\varepsilon_2)\left(\frac{d}{d\mathrm{x}}-\frac{J'}{\mathrm{x}}\right)R_1(\mathrm{x})R_2(\mathrm{x}),\end{aligned} \tag{B.15}$$

$$\langle j_2||\int d\Omega_{\mathbf{x}}\,\left(\mathbf{Y}_{J'J'}(\Omega_{\mathbf{x}})\cdot\hat{\mathbf{J}}^q_{\mathrm{N,m}}(\mathbf{x})\right)||j_1\rangle$$
$$=\frac{|e|}{2Mi}\mu_q\frac{1+(-1)^{l_1+l_2+J'+1}}{2}(-1)^{j_1+j_2+J'}\sqrt{\frac{(2J'+1)(2j_1+1)}{4\pi J'(J'+1)}}C^{j_2\frac{1}{2}}_{j_1\frac{1}{2},J'0} \tag{B.16}$$
$$\times\left[(\varepsilon_1+\varepsilon_2)\left(\frac{d}{d\mathrm{x}}+\frac{1}{\mathrm{x}}\right)-\frac{J'(J'+1)}{\mathrm{x}}\right]R_1(\mathrm{x})R_2(\mathrm{x}),$$

$$\langle j_2||\int d\Omega_{\mathbf{x}}\,\left(\mathbf{Y}_{J'(J'-1)}(\Omega_{\mathbf{x}})\cdot\hat{\mathbf{J}}^q_{\mathrm{N,m}}(\mathbf{x})\right)||j_1\rangle$$
$$=\frac{|e|}{2Mi}\mu_q\frac{1+(-1)^{l_1+l_2+J'}}{2}(-1)^{j_1+j_2+J'}\sqrt{\frac{(2j_1+1)}{4\pi J'}}C^{j_2\frac{1}{2}}_{j_1\frac{1}{2},J'0} \tag{B.17}$$
$$\times(\varepsilon_1-\varepsilon_2)\left(\frac{d}{d\mathrm{x}}+\frac{J'+1}{\mathrm{x}}\right)R_1(\mathrm{x})R_2(\mathrm{x}).$$

We note that care must be taken with respect to different phase conventions used in the literature. For instance, if the phase convention for single-nucleon wave functions differs from that of Eq. (2.14) by the factor of i^l, then the relative sign between the $X^{(I')}_{j_1j_2}$ and $Y^{(I')}_{j_1j_2}$ RPA amplitudes in Eqs. (B.8) and (B.9) changes as

$$\left[X^{(I')}_{j_1j_2}+(-1)^{J'}Y^{(I')}_{j_1j_2}\right]\rightarrow\left[X^{(I')}_{j_1j_2}+Y^{(I')}_{j_1j_2}\right]\ \text{for the charge density} \tag{B.18}$$

and

$$\left[X^{(I')}_{j_1j_2}+(-1)^{L}Y^{(I')}_{j_1j_2}\right]\rightarrow\left[X^{(I')}_{j_1j_2}-Y^{(I')}_{j_1j_2}\right]\ \text{for the current density.} \tag{B.19}$$

C. Nuclear polarization in the Coulomb gauge

The photon propagator in the Coulomb gauge reads

$$D^{\rm C}_{\mu\nu}(\omega,\mathbf{q}) = \begin{bmatrix} \dfrac{1}{\mathbf{q}^2+i0} & 0 \\ 0 & \dfrac{\delta^{\rm T}_{ij}}{q^2+i0} \end{bmatrix}, \quad \delta^{\rm T}_{ij} = \delta_{ij} - \frac{q_i q_j}{\mathbf{q}^2}, \tag{C.1}$$

where $\delta^{\rm T}_{ij}$ projects out the transverse parts of the fermionic and nuclear currents.

The corresponding NP energy shifts due to the ladder, cross and seagull diagrams are given by [107]

$$\Delta E^{\rm L}_{i,{\rm NP}} = -\frac{1}{2j+1}\sum_{n'\kappa'N'J'\pi'}\frac{1}{2J'+1}\int_0^\infty\!\!\int_0^\infty d{\rm q}d{\rm q}'\left[\frac{\theta(\varepsilon_{i'})}{\widetilde{\omega}_{\rm f}+\omega_{\rm N}}\mathcal{W}^{\rm L}_{\rm C}({\rm q})\mathcal{W}^{\rm L}_{\rm C}({\rm q}') + I_+({\rm q},{\rm q}')\mathcal{W}^{\rm T}_{\rm C}({\rm q})\mathcal{W}^{\rm T}_{\rm C}({\rm q}') + I^{\rm LT}_+({\rm q}')\mathcal{W}^{\rm L}_{\rm C}({\rm q})\mathcal{W}^{\rm T}_{\rm C}({\rm q}')\right], \tag{C.2}$$

$$\Delta E^{\rm X}_{i,{\rm NP}} = -\frac{1}{2j+1}\sum_{n'\kappa'N'J'\pi'}\frac{1}{2J'+1}\int_0^\infty\!\!\int_0^\infty d{\rm q}d{\rm q}'\left[-\frac{\theta(-\varepsilon_{i'})}{\widetilde{\omega}_{\rm f}+\omega_{\rm N}}\mathcal{W}^{\rm L}_{\rm C}({\rm q})\mathcal{W}^{\rm L}_{\rm C}({\rm q}') + I_-({\rm q},{\rm q}')\mathcal{W}^{\rm T}_{\rm C}({\rm q})\mathcal{W}^{\rm T}_{\rm C}({\rm q}') + I^{\rm LT}_-({\rm q}')\mathcal{W}^{\rm L}_{\rm C}({\rm q})\mathcal{W}^{\rm T}_{\rm C}({\rm q}')\right], \tag{C.3}$$

$$\Delta E^{\rm SG}_{i,{\rm NP}} = -\frac{1}{2j+1}\left(\frac{2}{\pi}\right)^2\sum_{n'\kappa'J'^{\pi'}}\int_0^\infty\!\!\int_0^\infty d{\rm q}d{\rm q}'\, I_{\rm SG}({\rm q},{\rm q}')\,\mathcal{W}^{\rm SG}_{\rm C}({\rm q},{\rm q}'), \tag{C.4}$$

where

$$I^{\rm LT}_\pm({\rm q}') = \pm\frac{{\rm sgn}(\varepsilon_{i'}){\rm q}'(\widetilde{\omega}_{\rm f}+\omega_{\rm N}) \pm \theta(\pm\varepsilon_{i'})2{\rm q}'^2}{({\rm q}'+\widetilde{\omega}_{\rm f})({\rm q}'+\omega_{\rm N})(\widetilde{\omega}_{\rm f}+\omega_{\rm N})}, \tag{C.5}$$

$$\mathcal{W}^{\rm L}_{\rm C}({\rm q}) = \langle i'||\hat{m}_{J'}({\rm q})||i\rangle\langle I'||\hat{M}_{J'}({\rm q})||I\rangle, \tag{C.6}$$

$$\mathcal{W}^{\rm T}_{\rm C}({\rm q}) = -\left[\frac{\omega_{\rm f}\omega_{\rm N}}{{\rm q}^2}\mathcal{W}^{\rm L}_{\rm C}({\rm q}) + \sum_{L=J'-1}^{J'+1}\langle i'||\hat{t}_{J'L}({\rm q})||i\rangle\langle I'||\hat{T}_{J'L}({\rm q})||I\rangle\right], \tag{C.7}$$

$$\mathcal{W}^{\rm SG}_{\rm C}({\rm q},{\rm q}') = \sum_{L=J'\pm1}\left[\langle i'||\hat{u}_{J'L}({\rm q})||i\rangle\langle i'||\hat{u}_{J'L}({\rm q}')||i\rangle M^{\rm SG}_L({\rm q},{\rm q}')\right] + \langle i'||\hat{t}_{J'J'}({\rm q})||i\rangle\langle i'||\hat{t}_{J'J'}({\rm q}')||i\rangle M^{\rm SG}_{J'}({\rm q},{\rm q}'), \tag{C.8}$$

with

$$\langle i'||\hat{u}_{J'(J'-1)}(\mathrm{q})||i\rangle = \langle i'||\hat{t}_{J'(J'-1)}(\mathrm{q})||i\rangle - i\sqrt{\frac{J'}{2J'+1}}\frac{\omega_\mathrm{f}}{\mathrm{q}}\langle i'||\hat{m}_{J'}(\mathrm{q})||i\rangle, \tag{C.9}$$

$$\langle i'||\hat{u}_{J'(J'+1)}(\mathrm{q})||i\rangle = \langle i'||\hat{t}_{J'(J'+1)}(\mathrm{q})||i\rangle - i\sqrt{\frac{J'+1}{2J'+1}}\frac{\omega_\mathrm{f}}{\mathrm{q}}\langle i'||\hat{m}_{J'}(\mathrm{q})||i\rangle. \tag{C.10}$$

We note that the terms containing $I_\pm^{\mathrm{LT}}(\mathrm{q}')$ in Eqs. (C.2) and (C.3) describe the interference between the longitudinal and transverse contributions. The expressions for $I_\pm(\mathrm{q},\mathrm{q}')$, $I_{\mathrm{SG}}(\mathrm{q},\mathrm{q}')$ and $M_L^{\mathrm{SG}}(\mathrm{q},\mathrm{q}')$ are the same as given by Eqs. (4.44), (4.71) and (4.73), respectively.

Bibliography

[1] I. A. Valuev, Z. Harman, C. H. Keitel, and N. S. Oreshkina, Phys. Rev. A **101**, 062502 (2020).

[2] I. A. Valuev, G. Colò, X. Roca-Maza, C. H. Keitel, and N. S. Oreshkina, Phys. Rev. Lett. **128**, 203001 (2022).

[3] A. Schneider, B. Sikora, S. Dickopf, M. Müller, N. S. Oreshkina, A. Rischka, I. A. Valuev, S. Ulmer, J. Walz, Z. Harman, C. H. Keitel, A. Mooser, and K. Blaum, Nature **606**, 878 (2022).

[4] H. Cakir, N. S. Oreshkina, I. A. Valuev, V. Debierre, V. A. Yerokhin, C. H. Keitel, and Z. Harman, submitted, arxiv:2006.14261 [physics.atom-ph] (2020).

[5] V. Debierre, N. S. Oreshkina, I. A. Valuev, Z. Harman, and C. H. Keitel, submitted, arxiv:2207.04868 [physics.atom-ph] (2022).

[6] H. Schüler and J. E. Keyston, Z. Phys. **70**, 1 (1931).

[7] D. J. Griffiths and D. F. Schroeter, *Introduction to Quantum Mechanics* (Cambridge University Press, 2018).

[8] E. Tiesinga, P. J. Mohr, D. B. Newell, and B. N. Taylor, J. Phys. Chem. Ref. Data **50**, 033105 (2021).

[9] V. M. Shabaev, A. I. Bondarev, D. A. Glazov, M. Y. Kaygorodov, Y. S. Kozhedub, I. A. Maltsev, A. V. Malyshev, R. V. Popov, I. I. Tupitsyn, and N. A. Zubova, Hyperfine Interact. **239**, 1 (2018).

[10] N. Hell, P. Beiersdorfer, G. V. Brown, M. E. Eckart, R. L. Kelley, C. A. Kilbourne, M. A. Leutenegger, T. E. Lockard, F. S. Porter, and J. Wilms, X-Ray Spectrom. **49**, 218 (2020).

[11] K. Blaum, S. Eliseev, and S. Sturm, Quantum Sci. Technol. **6**, 014002 (2021).

[12] A. Gumberidze, T. Stöhlker, D. Banaś, K. Beckert, P. Beller, H. F. Beyer, F. Bosch, S. Hagmann, C. Kozhuharov, D. Liesen, F. Nolden, X. Ma, P. H. Mokler, M. Steck, D. Sierpowski, and S. Tashenov, Phys. Rev. Lett. **94**, 223001 (2005).

[13] V. A. Yerokhin and V. M. Shabaev, Phys. Rev. A **64**, 062507 (2001).

[14] V. A. Yerokhin, P. Indelicato, and V. M. Shabaev, Phys. Rev. Lett. **91**, 073001 (2003).

[15] S. Schiller, Phys. Rev. Lett. **98**, 180801 (2007).

[16] P. Indelicato, J. Phys. B: At. Mol. Opt. Phys. **52**, 232001 (2019).

[17] V. M. Shabaev, A. N. Artemyev, V. A. Yerokhin, O. M. Zherebtsov, and G. Soff, Phys. Rev. Lett. **86**, 3959 (2001).

[18] H. Häffner, T. Beier, N. Hermanspahn, H.-J. Kluge, W. Quint, S. Stahl, J. Verdú, and G. Werth, Phys. Rev. Lett. **85**, 5308 (2000).

[19] S. Sturm, F. Köhler, J. Zatorski, A. Wagner, Z. Harman, G. Werth, W. Quint, C. H. Keitel, and K. Blaum, Nature **506**, 467 (2014).

[20] J. Verdú, S. Djekić, S. Stahl, T. Valenzuela, M. Vogel, G. Werth, T. Beier, H.-J. Kluge, and W. Quint, Phys. Rev. Lett. **92**, 093002 (2004).

[21] S. Sturm, A. Wagner, B. Schabinger, J. Zatorski, Z. Harman, W. Quint, G. Werth, C. H. Keitel, and K. Blaum, Phys. Rev. Lett. **107**, 023002 (2011).

[22] S. Sturm, A. Wagner, M. Kretzschmar, W. Quint, G. Werth, and K. Blaum, Phys. Rev. A **87**, 030501(R) (2013).

[23] A. Wagner, S. Sturm, F. Köhler, D. A. Glazov, A. V. Volotka, G. Plunien, W. Quint, G. Werth, V. M. Shabaev, and K. Blaum, Phys. Rev. Lett. **110**, 033003 (2013).

[24] F. Köhler, K. Blaum, M. Block, S. Chenmarev, S. Eliseev, D. A. Glazov, M. Goncharov, J. Hou, A. Kracke, D. A. Nesterenko, Y. N. Novikov, W. Quint, E. Minaya Ramirez, V. M. Shabaev, S. Sturm, A. V. Volotka, and G. Werth, Nat. Commun. **7**, 1 (2016).

[25] I. Arapoglou, A. Egl, M. Höcker, T. Sailer, B. Tu, A. Weigel, R. Wolf, H. Cakir, V. A. Yerokhin, N. S. Oreshkina, V. A. Agababaev, A. V. Volotka, D. V. Zinenko, D. A. Glazov, Z. Harman, C. H. Keitel, S. Sturm, and K. Blaum, Phys. Rev. Lett. **122**, 253001 (2019).

[26] S. Sturm, I. Arapoglou, A. Egl, M. Höcker, S. Kraemer, T. Sailer, B. Tu, A. Weigel, R. Wolf, J. C. López-Urrutia, and K. Blaum, Eur. Phys. J. Spec. Top. **227**, 1425 (2019).

[27] V. M. Shabaev, D. A. Glazov, N. S. Oreshkina, A. V. Volotka, G. Plunien, H.-J. Kluge, and W. Quint, Phys. Rev. Lett. **96**, 253002 (2006).

[28] V. A. Yerokhin, E. Berseneva, Z. Harman, I. I. Tupitsyn, and C. H. Keitel, Phys. Rev. Lett. **116**, 100801 (2016).

[29] O. Y. Andreev, L. N. Labzowsky, G. Plunien, and G. Soff, Phys. Rev. Lett. **94**, 243002 (2005).

[30] J. C. Berengut, V. A. Dzuba, and V. V. Flambaum, Phys. Rev. Lett. **105**, 120801 (2010).

[31] A. Windberger, J. R. Crespo López-Urrutia, H. Bekker, N. S. Oreshkina, J. C. Berengut, V. Bock, A. Borschevsky, V. A. Dzuba, E. Eliav, Z. Harman, U. Kaldor, S. Kaul, U. I. Safronova, V. V. Flambaum, C. H. Keitel, P. O. Schmidt, J. Ullrich, and O. O. Versolato, Phys. Rev. Lett. **114**, 150801 (2015).

[32] N. S. Oreshkina, S. M. Cavaletto, N. Michel, Z. Harman, and C. H. Keitel, Phys. Rev. A **96**, 030501(R) (2017).

[33] H. Bekker, A. Borschevsky, Z. Harman, C. H. Keitel, T. Pfeifer, P. O. Schmidt, J. R. C. López-Urrutia, and J. C. Berengut, Nature Commun. **10**, 5651 (2019).

[34] V. Debierre, C. H. Keitel, and Z. Harman, Phys. Lett. B **807**, 135527 (2020).

[35] V. M. Shabaev, D. A. Glazov, M. B. Shabaeva, V. A. Yerokhin, G. Plunien, and G. Soff, Phys. Rev. A **65**, 062104 (2002).

[36] R. L. Workman *et al.* (Particle Data Group), Prog. Theor. Exp. Phys. **2022**, 083C01 (2022).

[37] E. Borie and G. A. Rinker, Rev. Mod. Phys. **54**, 67 (1982).

[38] T. Yamazaki, K. Nagamine, S. Nagamiya, O. Hashimoto, K. Sugimoto, K. Nakai, and S. Kobayashi, Phys. Scr. **11**, 133 (1975).

[39] A. Knecht, A. Skawran, and S. M. Vogiatzi, Eur. Phys. J. Plus **135**, 1 (2020).

[40] G. Fricke, C. Bernhardt, K. Heilig, L. Schaller, L. Schellenberg, E. Shera, and C. Dejager, At. Data Nucl. Data Tables **60**, 177 (1995).

[41] Y. Tanaka, R. M. Steffen, E. B. Shera, W. Reuter, M. V. Hoehn, and J. D. Zumbro, Phys. Rev. Lett. **51**, 1633 (1983).

[42] A. Antognini, N. Berger, T. E. Cocolios, R. Dressler, R. Eichler, A. Eggenberger, P. Indelicato, K. Jungmann, C. H. Keitel, K. Kirch, A. Knecht, N. Michel, J. Nuber, N. S. Oreshkina, A. Ouf, A. Papa, R. Pohl, M. Pospelov, E. Rapisarda, N. Ritjoho, S. Roccia, N. Severijns, A. Skawran, S. M. Vogiatzi, F. Wauters, and L. Willmann, Phys. Rev. C **101**, 054313 (2020).

[43] V. L. Fitch and J. Rainwater, Phys. Rev. **92**, 789 (1953).

[44] R. Pohl, A. Antognini, F. Nez, F. D. Amaro, F. Biraben, J. M. R. Cardoso, D. S. Covita, A. Dax, S. Dhawan, L. M. P. Fernandes, A. Giesen, T. Graf, T. W. Hänsch, P. Indelicato, L. Julien, C.-Y. Kao, P. Knowles, E.-O. Le Bigot, Y.-W. Liu, J. A. M. Lopes, L. Ludhova, C. M. B. Monteiro, F. Mulhauser, T. Nebel, P. Rabinowitz, J. M. F. dos Santos, L. A. Schaller, K. Schuhmann, C. Schwob, D. Taqqu, J. F. C. A. Veloso, and F. Kottmann, Nature **466**, 213 (2010).

[45] A. Antognini, F. Nez, K. Schuhmann, F. D. Amaro, F. Biraben, J. M. R. Cardoso, D. S. Covita, A. Dax, S. Dhawan, M. Diepold, L. M. P. Fernandes, A. Giesen, A. L. Gouvea, T. Graf, T. W. Hänsch, P. Indelicato, L. Julien, C.-Y. Kao, P. Knowles, F. Kottmann, E.-O. Le Bigot, Y.-W. Liu, J. A. M. Lopes, L. Ludhova, C. M. B. Monteiro, F. Mulhauser, T. Nebel, P. Rabinowitz, J. M. F. dos Santos, L. A. Schaller, C. Schwob, D. Taqqu, J. F. C. A. Veloso, J. Vogelsang, and R. Pohl, Science **339**, 417 (2013).

[46] N. Bezginov, T. Valdez, M. Horbatsch, A. Marsman, A. C. Vutha, and E. A. Hessels, Science **365**, 1007 (2019).

[47] Y.-H. Lin, H.-W. Hammer, and U.-G. Meißner, Phys. Rev. Lett. **128**, 052002 (2022).

[48] Y. Yamazaki, H. D. Wohlfahrt, E. B. Shera, M. V. Hoehn, and R. M. Steffen, Phys. Rev. Lett. **42**, 1470 (1979).

[49] P. Bergem, G. Piller, A. Rueetschi, L. A. Schaller, L. Schellenberg, and H. Schneuwly, Phys. Rev. C **37**, 2821 (1988).

[50] T. Q. Phan, P. Bergem, A. Rüetschi, L. A. Schaller, and L. Schellenberg, Phys. Rev. C **32**, 609 (1985).

[51] C. Piller, C. Gugler, R. Jacot-Guillarmod, L. A. Schaller, L. Schellenberg, H. Schneuwly, G. Fricke, T. Hennemann, and J. Herberz, Phys. Rev. C **42**, 182 (1990).

[52] V. M. Shabaev, Phys. Rep. **356**, 119 (2002).

[53] V. M. Shabaev, I. I. Tupitsyn, V. A. Yerokhin, G. Plunien, and G. Soff, Phys. Rev. Lett. **93**, 130405 (2004).

[54] P. A. M. Dirac, Proc. R. Soc. Lond. A **117**, 610 (1928).

[55] T. Lancaster and S. J. Blundell, *Quantum Field Theory for the Gifted Amateur* (Oxford University Press, 2014).

[56] D. Hanneke, S. Fogwell, and G. Gabrielse, Phys. Rev. Lett. **100**, 120801 (2008).

[57] D. Hanneke, S. Fogwell Hoogerheide, and G. Gabrielse, Phys. Rev. A **83**, 052122 (2011).

[58] T. Aoyama, M. Hayakawa, T. Kinoshita, and M. Nio, Phys. Rev. Lett. **109**, 111807 (2012).

[59] T. Aoyama, M. Hayakawa, T. Kinoshita, and M. Nio, Phys. Rev. D **91**, 033006 (2015), *erratum*: **96**, 019901 (2017).

[60] T. Aoyama, T. Kinoshita, and M. Nio, Phys. Rev. D **97**, 036001 (2018).

[61] M. E. Peskin and D. V. Schroeder, *An Introduction To Quantum Field Theory* (Addison-Wesley, 1995).

[62] W. Greiner and J. Reinhardt, *Field Quantization* (Springer Berlin, Heidelberg, 1996).

[63] S. Weinberg, *The Quantum Theory of Fields*, Vol. 1: Foundations (Cambridge University Press, 1996).

[64] V. B. Berestetskii, L. P. Pitaevskii, and E. M. Lifshitz, *Quantum Electrodynamics*, Vol. 4 of the Course of Theoretical Physics by L. D. Landau and E. M. Lifshitz (Elsevier Science, 2012).

[65] W. H. Furry, Phys. Rev. **81**, 115 (1951).

[66] H. Lehmann, K. Symanzik, and W. Zimmermann, Nuovo Cim. **1**, 205 (1955).

[67] W. Greiner, *Relativistic Quantum Mechanics. Wave Equations* (Springer Berlin, Heidelberg, 2000).

[68] W. R. Johnson, *Atomic Structure Theory* (Springer Berlin, Heidelberg, 2007).

[69] M. Blagojevic, *Gravitation and Gauge Symmetries* (CRC Press, 2001).

[70] W. R. Johnson, S. A. Blundell, and J. Sapirstein, Phys. Rev. A **37**, 307 (1988).

[71] H. Bachau, E. Cormier, P. Decleva, J. E. Hansen, and F. Martín, Rep. Prog. Phys. **64**, 1815 (2001).

[72] H. Cakir, *Quantum Electrodynamic Theory of Few-Electron Highly Charged Ions*, Ph.D. thesis, Heidelberg University (2020).

[73] J. Schwinger, Phys. Rev. **73**, 416 (1948).

[74] J. Schwinger, Phys. Rev. **76**, 790 (1949).

[75] R. H. Parker, C. Yu, W. Zhong, B. Estey, and H. Müller, Science **360**, 191 (2018).

[76] L. Morel, Z. Yao, P. Cladé, and S. Guellati-Khélifa, Nature **588**, 61 (2020).

[77] W. Greiner, *Quantum Mechanics. An Introduction* (Springer Berlin, Heidelberg, 2001).

[78] W. E. Lamb, Phys. Rev. **85**, 259 (1952).

[79] M. E. Rose, *Elementary Theory of Angular Momentum* (John Wiley & Sons, 1957).

[80] A. Landé, Z. Phys. **5**, 231 (1921).

[81] M. E. Rose, *Relativistic Electron Theory* (John Wiley & Sons, 1961).

[82] S. G. Karshenboim, R. N. Lee, and A. I. Milstein, Phys. Rev. A **72**, 042101 (2005).

[83] P. Ring and P. Schuck, *The Nuclear Many-Body Problem* (Springer Berlin, Heidelberg, 1980).

[84] T. H. R. Skyrme, Phil. Mag. **1**, 1043 (1956).

[85] T. H. R. Skyrme, Nucl. Phys. **9**, 615 (1958).

[86] D. Vautherin and D. M. Brink, Phys. Rev. C **5**, 626 (1972).

[87] J. S. Bell and T. H. R. Skyrme, Phil. Mag. **1**, 1055 (1956).

[88] E. Chabanat, P. Bonche, P. Haensel, J. Meyer, and R. Schaeffer, Nucl. Phys. A **627**, 710 (1997).

[89] M. Bender, P.-H. Heenen, and P.-G. Reinhard, Rev. Mod. Phys. **75**, 121 (2003).

[90] E. Chabanat, P. Bonche, P. Haensel, J. Meyer, and R. Schaeffer, Nucl. Phys. A **635**, 231 (1998), *erratum*: **643**, 441 (1998).

[91] G. Colò, L. Cao, N. V. Giai, and L. Capelli, Comput. Phys. Commun. **184**, 142 (2013).

[92] D. J. Rowe, *Nuclear Collective Motion: Models and Theory* (World Scientific, 2010).

[93] D. Bohm and D. Pines, Phys. Rev. **92**, 609 (1953).

[94] T. Sil, S. Shlomo, B. K. Agrawal, and P.-G. Reinhard, Phys. Rev. C **73**, 034316 (2006).

[95] T. Beier, Phys. Rep. **339**, 79 (2000).

[96] H. De Vries, C. W. De Jager, and C. De Vries, At. Data Nucl. Data Tables **36**, 495 (1987).

[97] L. G. Cao, U. Lombardo, C. W. Shen, and N. V. Giai, Phys. Rev. C **73**, 014313 (2006).

[98] J. Dobaczewski, H. Flocard, and J. Treiner, Nucl. Phys. A **422**, 103 (1984).

[99] I. Angeli and K. P. Marinova, At. Data Nucl. Data Tables **99**, 69 (2013).

[100] V. M. Shabaev, J. Phys. B **26**, 1103 (1993).

[101] D. A. Glazov and V. M. Shabaev, Phys. Lett. A **297**, 408 (2002).

[102] J. L. Friar, J. Heisenberg, and J. W. Negele, in *Proceedings of the June Workshop in Intermediate Energy Electromagnetic Interactions* (Massachusetts Institute of Technology, 1977) p. 325.

[103] H. Euteneuer, J. Friedrich, and N. Vögler, Nucl. Phys. A **298**, 452 (1978).

[104] G. Plunien, B. Müller, W. Greiner, and G. Soff, Phys. Rev. A **39**, 5428 (1989).

[105] G. Plunien, B. Müller, W. Greiner, and G. Soff, Phys. Rev. A **43**, 5853 (1991).

[106] R. K. Cole, Phys. Rev. **177**, 164 (1969).

[107] A. Haga, Y. Horikawa, and Y. Tanaka, Phys. Rev. A **65**, 052509 (2002).

[108] K. Johnson, Nucl. Phys. **25**, 431 (1961).

[109] S. L. Adler and R. F. Dashen, *Current Algebras and Applications to Particle Physics* (W. A. Benjamin, 1968).

[110] L. S. Brown, Phys. Rev. **150**, 1338 (1966).

[111] J. Schwinger, Phys. Rev. Lett. **3**, 296 (1959).

[112] S. G. Brown, Phys. Rev. **158**, 1444 (1967).

[113] T. de Forest Jr. and J. D. Walecka, Adv. Phys. **15**, 1 (1966).

[114] K. T. R. Davies, R. W. Davies, and G. D. White, J. Math. Phys. **31**, 1356 (1990).

[115] A. V. Nefiodov, L. N. Labzowsky, G. Plunien, and G. Soff, Phys. Lett. A **222**, 227 (1996).

[116] M. Martin, Nucl. Data Sheets **108**, 1583 (2007).

[117] W. R. Johnson, S. A. Blundell, and J. Sapirstein, Phys. Rev. A **37**, 2764 (1988).

[118] Y. Tanaka and Y. Horikawa, Nucl. Phys. A **580**, 291 (1994).

[119] A. Haga, Y. Horikawa, and Y. Tanaka, Phys. Rev. A **66**, 034501 (2002).

[120] A. Haga, Y. Horikawa, H. Toki, and Y. Tanaka, Nucl. Instrum. Methods Phys. Res., Sect. B **235**, 71 (2005).

[121] A. Haga, Y. Horikawa, and H. Toki, Phys. Rev. C **75**, 044315 (2007).

[122] B. K. Agrawal, S. Shlomo, and V. K. Au, Phys. Rev. C **72**, 014310 (2005).

[123] B. Alex Brown, Phys. Rev. C **58**, 220 (1998).

[124] S. Goriely, M. Samyn, and J. M. Pearson, Phys. Rev. C **75**, 064312 (2007).

[125] X. Roca-Maza, G. Colò, and H. Sagawa, Phys. Rev. C **86**, 031306(R) (2012).

[126] A. W. Steiner, M. Prakash, J. M. Lattimer, and P. J. Ellis, Phys. Rep. **411**, 325 (2005).

[127] J. Bartel, P. Quentin, M. Brack, C. Guet, and H.-B. Håkansson, Nucl. Phys. A **386**, 79 (1982).

[128] N. Van Giai and H. Sagawa, Phys. Lett. B **106**, 379 (1981).

[129] X. Roca-Maza and N. Paar, Prog. Part. Nucl. Phys. **101**, 96 (2018).

[130] G. A. Rinker and J. Speth, Nucl. Phys. A **306**, 360 (1978).

[131] A. Haga, Y. Horikawa, Y. Tanaka, and H. Toki, Phys. Rev. C **69**, 044308 (2004).

[132] N. Paar, D. Vretenar, E. Khan, and G. Colò, Rep. Prog. Phys. **70**, 691 (2007).

[133] P. Indelicato and P. J. Mohr, Phys. Rev. A **46**, 172 (1992).

[134] N. J. Snyderman, Ann. Phys. **211**, 43 (1991).

[135] V. A. Yerokhin and V. M. Shabaev, Phys. Rev. A **60**, 800 (1999).

[136] N. S. Oreshkina, submitted, arxiv:2206.01006 [physics.atom-ph] (2022).

[137] G. A. Rinker, in *Proceedings of the 15th LAMPF Users Group Meeting* (Los Alamos, 1981) pp. 69–76.

[138] A. V. Nefiodov, G. Plunien, and G. Soff, Phys. Rev. Lett. **89**, 081802 (2002).

[139] I. I. Sobel'man, *Introduction to the Theory of Atomic Spectra* (Pergamon Press, 1972).

[140] D. A. Varshalovich, A. N. Moskalev, and V. K. Khersonskii, *Quantum Theory of Angular Momentum* (World Scientific, 1988).

[141] A. V. Nefiodov, G. Plunien, and G. Soff, Phys. Lett. B **552**, 35 (2003).

[142] M. Shamsuzzoha Basunia, Nuclear Data Sheets **127**, 69 (2015).

[143] M. Shamsuzzoha Basunia, Nuclear Data Sheets **114**, 1189 (2013).

[144] J. Chen, Nuclear Data Sheets **140**, 1 (2017).

[145] B. Singh, Nuclear Data Sheets **108**, 197 (2007).

[146] D. Abriola, M. Bostan, S. Erturk, M. Fadil, M. Galan, S. Juutinen, T. Kibédi, F. Kondev, A. Luca, A. Negret, N. Nica, B. Pfeiffer, B. Singh, A. Sonzogni, J. Timar, J. Tuli, T. Venkova, and K. Zuber, Nuclear Data Sheets **110**, 2815 (2009).

[147] D. De Frenne, Nuclear Data Sheets **110**, 1745 (2009).

[148] S. Lalkovski and F. G. Kondev, Nuclear Data Sheets **124**, 157 (2015).

[149] T. D. Johnson, D. Symochko, M. Fadil, and J. K. Tuli, Nuclear Data Sheets **112**, 1949 (2011).

[150] N. Nica, Nuclear Data Sheets **141**, 1 (2017).

[151] C. W. Reich, Nuclear Data Sheets **108**, 1807 (2007).

[152] E. Browne and H. Junde, Nuclear Data Sheets **87**, 15 (1999).

[153] H. Xiaolong, Nuclear Data Sheets **108**, 1093 (2007).

[154] E. Browne and J. K. Tuli, Nuclear Data Sheets **127**, 191 (2015).

[155] V. Debierre, C. H. Keitel, and Z. Harman, submitted, arxiv:2202.01668 [physics.atom-ph] (2022).

[156] T. Sailer, V. Debierre, Z. Harman, F. Heiße, C. König, J. Morgner, B. Tu, A. V. Volotka, C. H. Keitel, K. Blaum, and S. Sturm, Nature **606**, 479 (2022).

Acknowledgments

Coming from a chemistry background, it was a big leap for me to transition directly to theoretical physics. But perhaps the biggest challenge at the beginning was not even catching up on an intimidating amount of new material but rather finding someone who would welcome and support me with such an endeavor. Therefore, I am deeply grateful to my supervisors PD Dr. Natalia S. Oreshkina and Hon.-Prof. Dr. Christoph H. Keitel as well as to PD Dr. Zoltán Harman for putting trust in me and giving me an opportunity to make my dream a reality.

Speaking of studying physics, I am greatly indebted to PD Dr. Antonino Di Piazza for his superb courses on quantum electrodynamics. Without exaggeration, those were among the most gratifying experiences in my entire PhD programme.

I consider myself lucky to be part of an amazing community of the Theory Division at the Max Planck Institute for Nuclear Physics. I would like to especially thank Halil Cakir for always being ready to help me with programming and for sharing his deep insights into physics. Special thanks also go to my office mates Kamil Dzikowski and Michael Quin for all the jokes and the positive atmosphere.

I am grateful for meeting a truly special friend during my studies here. Thank you, Laura Batini, for the deep conversations and all the fun times spent together. It is hard to imagine what my PhD adventure would be like without your support.

I thank our Italian collaborators Gianluca Colò and Xavier Roca-Maza for their dedication and patience. A big part of this thesis would not be possible without their kind help and excellent expertise.

I also extend thanks to Michael Quin, Dr. Konstantin Beyer, Dr. Bastian Sikora and PD Dr. Zoltán Harman for thoroughly proofreading my thesis and offering valuable feedback.

I wish to thank Prof. Dr. Maurits W. Haverkort for his time and efforts in being the second referee as well as Prof. Dr. Yury Litvinov and Prof. Dr. Werner Aeschbach for being part of my examination committee.

And above all, words cannot do justice to express my gratitude to my parents Tatiana Valueva and Aleksei Valuev, who always go above and beyond to support every step of my journey.